Towards Identification of Floc Compounds in Water using Multi-Frequency Fluorescence Lifetime Analysis

A thesis submitted in fulfilment
of the requirements for the degree of
Doctor of Philosophy
in Engineering
University of Waikato
by

S.A.D.A.N DISSANAYAKE

THE UNIVERSITY OF
WAIKATO
Te Whare Wānanga o Waikato

2025

Acknowledgements

First and foremost, I would like to express my deepest gratitude to my chief supervisor, Associate Professor Michael Cree, for his invaluable guidance, insightful feedback, and constant support throughout this research. His expertise has been a cornerstone in shaping the direction of this work.

I am equally grateful to Dr. Mark Lay, whose support as my supervisor and motivator made this thesis possible. Your patience, encouragement, and commitment made this journey both enlightening and fulfilling.

I would also like to thank Dr. Lee Streeter and Dr. Graeme Glasgow for their invaluable insights and guidance as my supervisors, which have greatly contributed to the improvement of my research.

My sincere appreciation goes to the University of Waikato, School of Engineering, for providing the necessary resources and a conducive environment for my research.

Special thanks to the AHEAD grant for financial support throughout this research endeavour.

I would like to express my gratitude to Professor Alistair Steyn-Ross for guiding me in improving my programming skills, and to Dr. Judith Borrows for facilitating access to the fluorescence spectrometer and other instrumentation in microbiology laboratory.

Thank you, Mr. Steven Wu, for providing your assistance and expertise in improving the procedures carried out in the environmental laboratory.

A heartfelt thank you goes to my friends and colleagues for their moral support, insightful discussions, and motivation during challenging times. You made this experience much more enjoyable.

Finally, I am forever indebted to my mother, my husband, my daughter, and my sister for their unwavering love, patience, and encouragement throughout this journey. Your belief in me has been my driving force.

This thesis would not have been possible without each of you. Thank you.

Abstract

UV disinfection is commonly used in water treatment to inactivate pathogens such as *Cryptosporidium* and viruses to prevent diseases such as cryptosporidiosis and norovirus in communities. Disinfection typically follows water treatment steps, such as coagulation, flocculation, clarification, and filtration. However, particles in water, for example, flocs 0.1 to 100 µm in diameter, made from humic and inorganic substances present in the water, surrounding a *Cryptosporidium* oocyst or virus, can protect the pathogens from UV exposure. Although water treatment steps prior to disinfection remove 99% of the particulates, particles can still be present in the 1000s to 10,000's per litre after filtration. While the chances of a floc particle carrying a virus or oocyst are typically low, in some regions, particularly during calving in the dairy industry, oocyst concentrations in the water might be high due to cryptosporidiosis in calves. Therefore, it is useful to test the properties of the floc compound for UV penetration to determine whether the disinfection method is appropriate.

In this thesis, a technique that uses multi-frequency analysis to measure the fluorescence lifetime of a fluorophore to provide information on particle composition is presented. Frequency-domain fluorescence fluorometry was used to determine the fluorescence lifetime. This was achieved using an experimental setup that used a laser diode operating at 100 mW and modulated at 10–60 MHz to excite the fluorophores, optical elements to focus and filter the light, and detectors to collect the fluorescence emission signal via a storage oscilloscope. The signals were then processed using a MATLAB program to determine the fluorescence lifetime.

Fluorescence lifetime measurements were challenged by the chemical and physical behaviour of the fluorophore and the adsorption of the fluorophore to the floc particles. Therefore, standard measurements such as turbidity, pH, particle size, and fluorescence were used to understand the absorption/adsorption of fluorescein to flocs. Fluorescence was observed at the 260–490 nm excitation wavelengths, with fluorescence emissions at approximately 510 nm. The particle

size and turbidity measurements showed that fluorescein acted as a flocculant, with the particle size increasing with increasing fluorescein concentration. Fluorescence intensity measurements from a standard fluorescence spectrophotometer were used to calculate fluorescein adsorption on humic acid and kaolin to generate adsorption isotherms. Fluorescein was bonded to kaolin 10 times more than to humic acid. Adequate flocculation required a pH of 6.5 to produce reasonably flocculated particles in the sample. Surface charge analysis showed that the use of buffer to control pH required more alum to neutralise the surface charge of humic acid and kaolin.

Multi frequency measurements and subsequent analysis showed that the fluorescence lifetime and contamination ratio were 4.2 $\pm$ 0.3 ns and 0.09 $\pm$ 0.05 for fluorescein. The fluorescence lifetime of fluorescein was compatible with the results of previous studies using different techniques. The samples with floc particles had a larger excitation light contamination ratio than those without particles; therefore, the contamination ratio could be used as a measure of particle contamination in the samples. The fluorescence lifetime of fluorescein did not change when fluorescein was attached to humic acid particles, but increased by 0.6 ns for kaolin floc particles.

Contents

List of Figures

List of Tables

Glossary

APD	Avalanche Photon Detector
AOTF	Acousto-Optic Tunable Filter
ADC	Analogue to Digital Converter
CCD	Charged Coupled Device
CEC	Cation Exchange Capacity
CMOS	Complementary Metal Oxide Semiconductor
CQD	Carbon Quantum Dot
CW	Continuous Wave
DAC	Digital to Analogue Converter
DAF	Dissolved Air Flotation
DC	Direct Current
DE	Diatomaceous Earth
DFT	Discrete Fourier Transform
DNA	Deoxyribo Nucleic Acid
EEM	Excitation Emission Matrix
FCS	Fluorescence Correlation Spectroscopy
FFT	Fast Fourier Transform
FLIM	Fluorescence Lifetime Imaging
FPGA	Field Programmable Gate Array
FRET	Fluorescence Resonance Energy Transfer
FT	Fourier Transform
GQD	Graphine Quantum Dot

GPIB	General Purpose Interface Bus
IF	Intermediate Frequency
ISI	Inter Symbol Interference
IFFT	Inverse Fast Fourier Transform
IQR	Interquartile Range
KDE	Kernel Density Estimation
LCTF	Liquid Crystal Tunable Filter
LED	Light Emitting Diode
MF	Micro-Filtration
MWCO	Molecular Weight Cut-off
NA	Not Available
ND	Neutral Density
NF	Nano-Filtration
NGS	Next Generation Sequencing
OD	Optical Density
PCD	Particle Charge Detector
PCR	Polymerase Chain Reaction
PMT	Photomultiplier Tube
QD	Quantum Dot
RNA	Ribonucleic Acid
RO	Reverse Osmosis
SAPD	Single Photon Avalanche Detector
SCPI	Standard Commands for Programmable Instrument
SERRS	Surface-Enhanced Resonance Raman Spectroscopy
SMA	Sub Miniature version A
SNR	Signal to Noise Ratio
SPR	Surface Plasmon Resonance

TAC	Time to Amplitude Converter
TCSPC	Time Correlated Single Photon Counting
TFTF	Thin-Film Tunable Filter
TOF	Time Of Flight
TSS	Total Suspended Solids
UF	Ultrafiltration
USB	Universal Serial Bus
UV	Ultra Violet
UVT	Ultra Violet Transmission
VISA	Virtual Instrument Standard Architecture

Chapter 1

Introduction

1.1 Background

Water is a basic need of living beings, and a certain quality must be maintained for the health of living beings. Water sourced from rivers, lakes, springs, and aquifers contains contaminants such as particulate matter, dissolved solids, taste and odour compounds, and microorganisms that may impact human health. Pathogens of concern include norovirus, *Campylobacter*, *Cryptosporidium*, and *Giardia* which can result in gastrointestinal complaints and diarrhoea, in some cases leading to hospitalisation for severe cases or immunocompromised patients. Therefore, water should be treated, for example, to New Zealand drinking water standards, to make it safe for drinking. Treatment involves the removal of particulate and dissolved solids using a variety of methods, such as coagulation, flocculation, clarification, filtration, and membrane treatment, removal of taste and odour compounds using activated carbon, and disinfection to inactivate protozoa, viruses, and bacteria using UV treatment and chlorine dosing. Biological agents in drinking water can survive the water treatment process and cause health problems in communities. This can occur when there is significant particulate carryover from the clarifier, when filtration systems fail, or when reservoirs containing settled sediments are stirred up during high flow, resulting in high particulate matter undergoing UV disinfection.

Cryptosporidium is a protozoan of particular interest as it causes severe illnesses to persons with an impaired immune system and because the oocysts can survive UV treatment when they are embedded in floc. There are reported outbreaks around the world, and Queenstown, New Zealand is a recent example of a *Cryptosporidium* outbreak, which can be due to inadequately treated water (Baker *et al.*, 2023). The likelihood of *Cryptosporidium* being present in water is low, but

oocyst count in raw water can increase from as low as 1 oocyst per L to 10 000 s of oocysts per L during the calving season and when infected people or animals have defaecated into or close to the water. The detection of *Cryptosporidium* in water is a time-consuming and expensive procedure (approximately $1000 per sample) that is not practical for regular performance. It involves filtering litres of water to isolate even one oocyst, identifying that oocyst, and then determining whether it is live or inactive. Therefore, the Drinking Water Standards NZ does not require water treatment plants to regularly test for *Cryptosporidium*. Instead, each unit operation in the treatment process was assumed to contribute to a particular log removal of *Cryptosporidium*, with UV treatment contributing to 3 log removal (i.e. 99.9% removal). To achieve this, the oocyst must be exposed to the equivalent of 12 mJ/cm^2 of UV light. UV penetration of floc depends on the floc material it is made up of and how strongly UV absorbing it is, therefore it is highly dependent on the water source, the type of contaminants that are present and the treatment methods used to produce the floc.

Fluorescence is a phenomenon in which a material or organic compound (fluorophore) that has absorbed light re-emits it at a lower energy and longer wavelength. Fluorophore emission behaviour, such as emission intensity and lifetime, depends on the material to which it is attached or the environment in which it is located. This behaviour can be used in sensing applications for biological and chemical analyses. Intensity-based methods are convenient to use in laboratories with controlled environments, such as controlled concentrations of reagents, biological material, temperature, and background light. However, there are practical issues related to on-site applications, as these parameters cannot be controlled. This results in variations in the fluorophore concentration and fluorescence intensity. These practical issues can be overcome by measuring the decay time of the fluorophore, known as fluorescence lifetime (FLT) measurement.

The fluorescence lifetime can be measured using time and frequency domain techniques. The time-domain method uses a narrow pulse of light to excite the sample, and fluorescence is measured over time. The measured data are plotted as a histogram to obtain the decay curve and calculate the lifetime. The frequency domain method excites the sample with intensity-modulated light which forces the emission to be at the same modulated frequency with a delay between emission and excitation, producing a phase shift that can be measured to calculate the fluorescence lifetime. Frequency-domain techniques require less costly and complex hardware, whereas time-domain methods require high-speed detectors and electronics to measure fluorescence decay.

Fluorophores that re-emit light after absorbing energy are required for fluorescence intensity and lifetime analyses. Fluorophores include organic dyes, proteins, and quantum dots. Recent developments in fluorescence spectroscopy have enabled these methods to be used to measure the chemical and biological composition of environmental samples, such as copper or nickel ion concentrations, and to detect cancers.

The aim of this study is to develop an experimental setup that uses fluorescence lifetime to estimate the properties of floc particles, such as composition (and eventually the presence of pathogens), and test it with model floc particles in suspension made from kaolin and humic acid impregnated with a fluorophore to determine the feasibility and practical issues around such a technique.

1.2 Thesis objectives

The objectives of this study are as follows:

- To develop a prototype to measure fluorescence lifetime of fluorophores contained within flocculated particles held in suspension using the frequency domain technique.

- To develop and test methods of analysis using multi-frequency measurements and non-linear regression techniques to estimate the florescence lifetime of the fluorophore used, determine the effect of light scattering, and signal acquisition parameters on florescence lifetime measurements.

- To investigate the effect of how floc particles prepared with the fluorophore contributed to changes in floc properties. This involved investigating parameters such as solution pH, turbidity, particle size, surface charge, and fluorophore concentration on floc morphology.

- To determine the extent of fluorophore adsorption to floc particles made using kaolin and humic acid as model water contaminants.

- To determine the range of wavelengths over which the fluorophores are excited and emit and emission intensity when trapped within kaolin and humic acid floc particles.

- To test the prototype on model floc particles.

1.3 Thesis outline

This thesis consists of seven chapters (including the introduction). The theory and applications related to water treatment are discussed in **Chapter 2**. This mainly focuses on providing the background of water contaminants, water treatment processes, and the drawbacks and possibilities of contaminants remaining in treated water. Furthermore, the limitations of currently used pathogen detection techniques are discussed.

In **Chapter 3**, fluorescence intensity and lifetime measurement techniques and their applications are discussed to create the background necessary to identify the technique that is suitable for the measurement of light penetration in flocs. The factors that influence the fluorescence lifetime and the changes used to identify the characteristics or properties of the samples are discussed. Furthermore, problems related to the measurements and limitations are addressed to improve instrument development. Component selection is a major contributor to the design; hence, a detailed discussion of each part associated with the fluorescence measurements, including the light sources, detectors, and optical components, is presented. Fluorophore selection is an important aspect, and thus, the types of fluorophores and their physical and chemical properties are reviewed in this chapter.

Chapter 4 discusses the development of the prototype that measures fluorescence emission of the intensity modulated signal, that is used to calculate fluorescence lifetime. In this chapter, hardware development is discussed with the selection of components and implementation, as well as the data extraction parameters. Two types of fluorophores, graphene quantum dots (GQD) and fluorescein, were investigated; however, owing to the limited availability of GQD, most of the fluorescence work in this study involved fluorescein. Two orientations of the detector were tested for the fluorescence emission detection. These are the scattered (90^0 angle) and transmission (incident beam) orientations tested, and the scattered orientation was selected. Multi-frequency measurements and non-linear regression analysis were used to observe any differences in the measurements due to the presence of floc particles in the sample.

All flocculated samples exhibited the same fluorescence lifetime values as fluorescein during the initial measurements from the prototype. Hence, this study was undertaken to understand the floc behaviour and binding properties of fluorescein with flocs. Therefore, standard instrumentation measurements were performed to identify the problems that arose with the sample measurements in the developed prototype. Hence, in **Chapter 5**, floc properties such as turbidity,

pH, particle size, zeta potential, and surface charge of particles were measured to identify the factors associated with measurement issues. Floc morphology was examined using a light microscope, and a fluorescence spectrometer was used to obtain the excitation and emission matrix, which helped identify the ratio of fluorophore requirements at different compound concentrations.

After analysing the chemical and physical properties of the fluorophores in the flocculated samples, the floc samples were tested using the developed prototype instrument to measure the fluorescence lifetime. The samples were excited at two laser power settings to observe the effect on the fluorescence lifetime measurements. The results obtained from the instrument were processed using multi-frequency analysis and are presented in **Chapter 6**. In the discussion, the ability to differentiate between samples according to compounds using the estimated fluorescence lifetime and contamination is discussed.

Finally, conclusions and recommendations from this work are presented in **Chapter 7**.

1.4 Publications arises from this thesis

1.4.1 Conferences

- Dissanayake, S.A.D.A.N., Cree, M.J., Lay, M., Streeter, L.& Glasgow D. (2023) *Using fluorescein as a fluorophore to test UV and light penetration of flocculated particles,* Water New Zealand Conference and Expo 2023, `https://www.waternz.org.nz/Article?Action=View\&Article_id=2634`.

- Dissanayake, S.A.D.A.N., Cree, M.J., Streeter, L.& Glasgow D. & Lay, M. (2021) *Work towards measuring fluorescence lifetime of quantum dots in presence of kaolin*, 3rd Annual Waikato Young Research Engineers Symposium, pp28.

1.4.2 Workshop presentation

- Dissanayake, S.A.D.A.N., Cree, M.J., Streeter, L.& Glasgow D. & Lay, M. (2022) *Multi Frequency Correct of Fluorescence Lifetime Measurement in the Presence of Excitation Signal Contamination*, NZ IEEE Instrumentation and Measurement Society, Waikato University in Hamilton.

Chapter 2

Water Contaminants and Treatment

In this chapter, the primary contaminants found in water sources are examined to identify the most pressing issues. Subsequently, treatment strategies were explored to comprehend the processes and parameters required by these methods. Subsequently, the current detection techniques for microorganisms are investigated. Finally, the potential of fluorescence sensing for the identification of *Cryptosporidium parvum* is discussed.

2.1 Water contaminants

Rivers, wells, ground wells, lakes, and springs are the main sources of water for human and animal consumption. Water sources can be classified into two primary types: surface water and groundwater. Groundwater refers to water located beneath the Earth's surface, whereas surface water refers to the visible flow of water above the Earth's surface. A contaminant is any substance or agent that is present in an atypical location or at a higher concentration than usual, resulting in a negative impact on the environment, living organisms, or human health. In general, water contaminants include organic, inorganic, and biological contaminants, as well as pathogens such as viruses, bacteria, and protozoa.

2.1.1 Pathogens in water

Pathogens are microorganisms, such as bacteria, viruses, fungi, and parasites, that can cause diseases in humans, animals, and plants. These infectious agents have the potential to disrupt normal biological functions, leading to various illnesses, such as watery diarrhoea, gastrointestinal infections, and fever. In this section, the four forms of pathogens are discussed.

Bacteria

Bacteria are single-celled microorganisms that are among the earliest forms of life on Earth and thrive in a variety of environments. They can be found virtually everywhere, including in soil, water, air, and living organisms, including humans. They are prokaryotic organisms that lack a nucleus and membrane-bound organelles. These microorganisms exhibit remarkable diversity in terms of shape, size, and metabolic activity. They can be spherical (cocci), rod-shaped (bacilli), or spiral (spirilla). Bacteria can be further classified based on their response to staining (Gram-positive or Gram-negative) and their energy sources (such as whether they are autotrophs, using inorganic substances, or heterotrophs, relying on organic compounds for energy). Despite their small size, bacteria play a vital role in ecosystems. While some bacteria are beneficial and essential for various biological processes, such as aiding digestion and participating in nutrient cycling, others can be harmful and cause diseases. Only a small fraction of bacteria are pathogenic (Cabral, 2010).

Campylobacter and Salmonella are the most common bacterial gastroenteritis-causing pathogens. Salmonella is a public health risk, even when present in water at low concentrations (Jyoti *et al.*, 2010). Campylobacter is thermophilic and is typically found in sewage sludge and surface water (Koenraad *et al.*, 1997). Shigella, Yersinia, and Vibrio cholerae are other common waterborne bacteria present in tainted water and shellfish that have been associated with outbreaks of disease (Ayres *et al.*, 2010).

Viruses

Viruses are microscopic infectious agents that exist as tiny particles consisting of genetic material (DNA or RNA) enclosed in a protein coat called a capsid. They are not considered living organisms because they lack the cellular machinery for self-reproduction and metabolism. Instead, viruses are obligate intracellular parasites, meaning they require a host cell to replicate and multiply (Forterre and Prangishvili, 2009). These entities are highly diverse in terms of size, shape, and structure. Some viruses have simple geometric shapes, whereas others possess more complex structures. Their size typically ranges from a few nanometres to several hundred nanometres. Viruses exhibit specificity toward host organisms and cells, often targeting specific cell types for infection. They infect organisms across all domains of life, including animals, plants, fungi, bacteria, and other viruses. The viral life cycle involves several stages: attachment and entry into the host cell, replication of viral genetic material, assembly of new viral components, and the release of mature viral particles. During replication, viruses use the host cell machinery to reproduce, which can lead to cell damage, alterations in cellular functions, or the initiation of immune responses.

Globally, noroviruses and related viruses are considered the primary cause of waterborne illnesses. In addition, human infections linked to water-transmitted diseases that

are commonly documented include rotavirus and adenovirus (Pinon and Vialette, 2019).

Protozoa

Protozoa are single-celled eukaryotic organisms belonging to the kingdom Protista and are known for their diverse shapes, structures, and lifestyles. They are found in various aquatic and terrestrial environments, including freshwater, marine habitats, soil, and even inside other organisms (Esteban and Fenchel, 2020). These microorganisms possess a distinct nucleus enclosed within a membrane, along with other membrane-bound organelles, such as mitochondria, and, in some cases, structures such as contractile vacuoles or specialised organelles, such as flagella, cilia, or pseudopodia, for movement. Protozoa are categorised into various groups based on their locomotion, such as amoeboid (using pseudopods), flagellar, or ciliary movement. Some well-known examples of protozoa include amoebas, paramecia, trypanosomes, and Plasmodium species (responsible for causing malaria). They play a crucial role in ecosystems, serving as primary consumers in food chains, decomposing organic matter, and contributing to nutrient cycling. However, some protozoa are parasitic and can cause disease in humans, animals, and plants. The life cycle of protozoa typically involves various stages, including trophozoites (the active feeding stage), cysts (a protective dormant stage), and stages specific to reproduction or transmission, depending on the species. Protozoa demonstrate incredible adaptability to different environmental conditions and have evolved various survival mechanisms. Some species can form cysts to withstand adverse conditions, whereas others exhibit complex life cycles involving multiple hosts (Esteban *et al.*, 2015; Jain *et al.*, 2019). Over the last 20 years, numerous epidemics, such as those caused by *Cryptosporidium, Giardia, Toxoplasma gondii, and Cyclospora cayetanensis* (Baldursson and Karanis (2011); Efstratiou *et al.* (2017)), have been documented as a result of protozoa spread through water.

2.1.2 Particle contaminants in water

Particle contaminants are solid or suspended elements present in water, including organic/biological matter, silt, sand, clay, microplastics, and other debris. (Rossi *et al.*, 2013; Droppo, 2001; Eerkes-Medrano *et al.*, 2019). These particles originate from industrial, human, and natural sources. Sand, silt, and clay are examples of sediment particles resulting from soil and rock erosion. Additionally, wet weather and climate change increase riverbed sediments, which give rise to total suspended solids (TSS) in water (Rossi *et al.*, 2013). These particles reduce light penetration and cloud water, increasing turbidity. Organic matter are contaminants from leaves, plant debris, and decomposing matter such as microorganisms, aquatic life, and discharged organic matter from municipal, industrial, and agricultural wastewater and farm runoff, which helps to create organic silt. These substances increase nutrient levels, biological oxygen demand,

and the growth of bacteria and algae (Chiou, 2002).

Industries discharge particles and suspended solids into water bodies in wastewater effluents and agricultural runoff, contributing to pollution and impairing water quality (Kordbacheh and Heidari, 2023; Vryzas, 2018). These particles can contain pollutants, heavy metals, and harmful substances, leading to health issues in people. Microplastics in water are a recent contaminant found in the past decade (Eerkes-Medrano *et al.*, 2019; Danopoulos *et al.*, 2020). These tiny plastic particles are less than 5 μm in size and originate from the breakdown of larger plastic items or from microbeads in personal care products. They can absorb and transport contaminants and pose risks to aquatic organisms and potentially human health (Blackburn and Green, 2022).

2.2 Water treatment

Water treatment plants remove contaminants from raw water abstracted from lakes, rivers, or groundwater to bring it up to drinking water standards before distribution to communities. Depending on the initial quality of the water and relevant water quality standards, a combination of different processes, such as coagulation, flocculation, sedimentation (or clarification), filtration, and UV treatment, are used to improve the water quality (WaterTreatment, 2008). Figure 2.1 shows the technologies suitable for the treatment of various particulates and biological contaminants (Gregory, 2005). Suspension, DAF (Dissolved Air Flotation), depth filtration, and sedimentation are used to separate contaminants 1 μm to 1 mm in size, and particle sizes below 1 μm require micro-filtration, colloidal, nano filtration, and ultrafiltration. Most bacteria, viruses, and clay can be removed using a combination of coagulation/flocculation and filtration techniques. An example of a water treatment plant is shown in Figure 2.1 and consists of screening for large materials such as leaves, sticks, and fish, sedimentation to remove the bulk of the settlable/coagulated/flocculated solids, sand filtration to remove the majority of the particulates that were not captured in the sedimentation stage, and granular activated carbon filters to remove taste, odour, and colour compounds. UV treatment inactivates any remaining microorganisms, such as viruses, bacteria, and protozoa. Chlorine is added to prevent subsequent microbial growth during storage or distribution, and fluoride is added to prevent tooth decay in humans.

2.2.1 Pretreatments

Pretreatment mainly changes the chemistry of water using sedimentation basins, infiltration galleries, and pre-oxidation. Sedimentation basins can be used to decrease the amount of sediment that reaches the water treatment process. Basins with large areas and low flow rates are used to provide the time necessary for the particles to settle. Particles larger than 100 μm are typically removed during this process. Infiltration

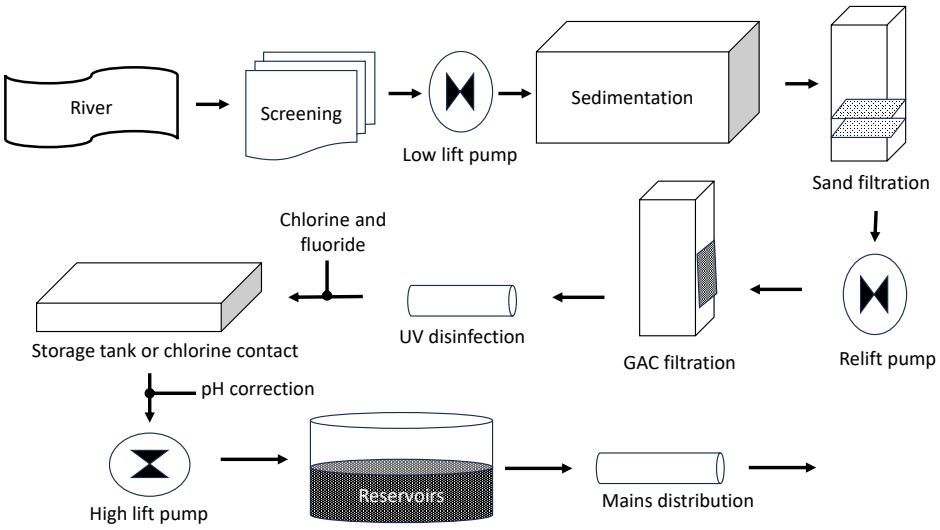

Figure 2.1: Block diagram of a typical water treatment plant.

galleries installed underground within the groundwater table are another method used to remove organic matter and microorganisms such as *Cryptosporidium* by using open-jointed or slotted pipes in the bed of the water source. Pre-oxidation using oxidising chemicals, such as chlorine, ozone, or potassium permanganate, capable of destroying cyanobacteria (blue-green algae), may also be used.

2.2.2 Coagulation,flocculation and clarification

Pretreated water was tested for pH, alkalinity, surfacecharge, and turbidity prior to the addition of the coagulant to estimate the required coagulant dose. Coagulants, such as aluminum sulfate (alum), ferric sulfate, or ferric chloride, are then added to destabilise the particles, followed by fast mixing. The addition of a flocculant (e.g. polyamines, polyDADMACs, polyacrylamides, polytannate) followed by slow mixing helps to aggregate the particles (Figure 2.2). Generally, the surfaces of particles are

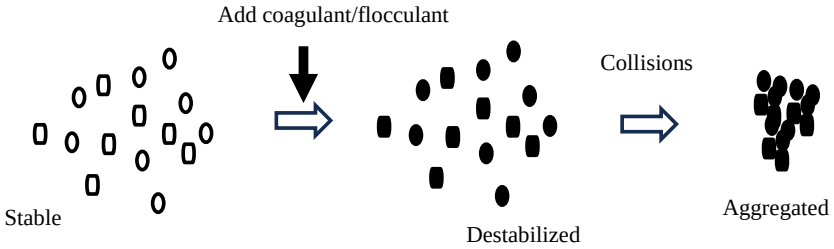

Figure 2.2: Mechanism of destabilization and aggregation of particles.

negatively charged and repel each other, resulting in a stable suspension in water. Particle surfaces contain functional groups such as -OH and -COOH which impart an overall negative charge. These surface charges attract positively charged ions in the solution, such as H^+ ions in water molecules (H_2O). Therefore, negatively charged oxygen creates a negatively charged surface around the molecules. When a coagulant is added to water, positive charges such as Al^{3+} or Fe^{3+} are attached to the negative charge, resulting in an overall neutral charge, reducing the stability of the particles in solution (Bratby, 2016). Hence, the particles are destabilised, and hydrophobic interactions lead to the aggregation of these molecules, which leads to the sedimentation of the particles.

Conventional coagulation/sedimentation and direct filtration are the two techniques used in water treatment processes (Figure 2.3). These two techniques are selected according to the raw water quality of the source, where the raw water should have consistently low colour (e.g. less than 40 TCU) and low turbidity (e.g. less than 10 NTU) for direct filtration (Ministry of Health NZ, 2021). During this process, suspended particles such as metals, iron, manganese, colour, taste, odours, and microorganisms (to a certain degree) are removed (Greaves, 2022; Ministry of Health NZ, 2021).

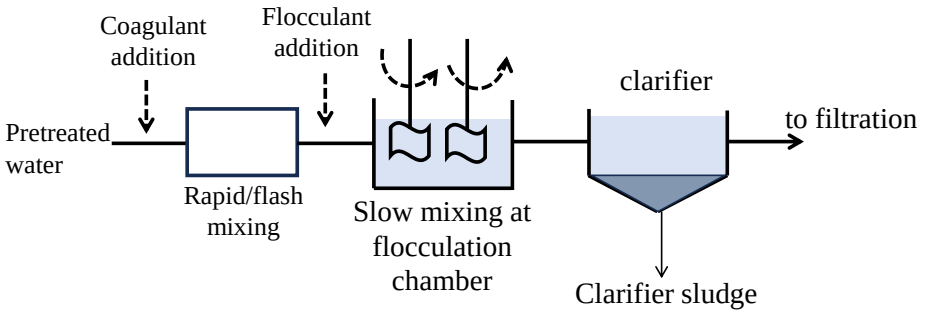

(a)

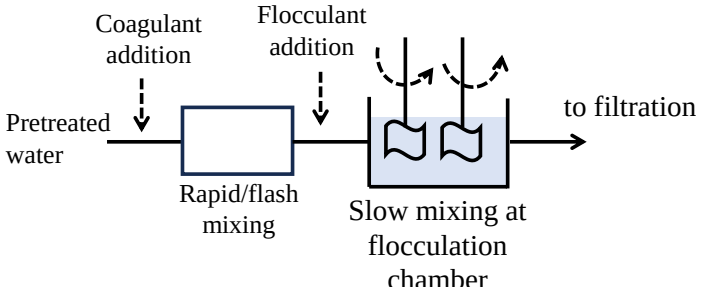

(b)

Figure 2.3: Two procedures involve in coagulation, flocculation and sedimentation (a) Conventional coagulation and sedimentation method, (b) direct filtration method.

Source water characteristics, such as turbidity, colour, odour, alkalinity, surface charge, and pH values, may change due to rainfall, stormy weather, and flow changes,

causing operational issues for water treatment plants, such as changes in water treatment effectiveness, for example, at the coagulation and flocculation steps. These variations are adapted to pretreatment or during the coagulation and flocculation processes with the necessary chemical doses. Applying the coagulant solution at a concentration of approximately 0.5% is recommended, and it should be kept below 1% (Wagner and Pinheiro, 2001). Adjustment of coagulants requires attention; if not, under-dosing and overdosing can contribute to issues in the coagulation process. Under-dosing causes poor destabilisation of particles which leads to poor removal of turbidity and microorganisms. However, overdosing can be a waste of resources, and this can form very small floc particles that can be difficult to settle or filter (Saritha *et al.*, 2017). In addition, Baghvand *et al.* (2010) tested the reduction in turbidity with increased coagulant doses in different water influent turbidities. Their results show that when the influent water turbidity increases above 200 NTU, the residual turbidity is between 20 and 80 NTU even after applying alum and ferric chloride. This proves that particle spiking in inflow does not support reducing turbidity, even with increased coagulant doses.

The mixing conditions and apparatus maximised the coagulant effectiveness. Rapid, high-energy mixing (such as mechanical mixers, in-line blenders, and jet sparge mixing) is required to ensure that it is thoroughly mixed in a very short time interval; otherwise, it may lead to an underdeveloped floc. The goal of flocculation and coagulation operations is to produce particles large enough to be removed and separated by other clarifying processes or subsequent sedimentation. In flocculation, smaller particles are mixed at a slow rate for 10–30 min, allowing them to agglomerate into larger particles that can be settled or filtered. Mixing must be slow enough to allow contact between particles for floc formation without turbulence and shear that damage the floc.

Another parameter influencing floc formation is water temperature. When water enters a lake or reservoir from its main tributary and branch streams, it normally finds its way to water with the same specific gravity, which typically translates to water at the same temperature. However, rainfall and flood water result in high temperatures at the surface and lower temperatures at the bottom, which might lead to the discolouration of the water in the lake or reservoir. Water temperature also influences the rate of particle settlement. This can cause an increase in water turbidity.

The most effective parameters for coagulation and flocculation are pH and alkalinity. In New Zealand, many surface waters have an alkalinity of less than 20 mg/L as $CaCO_3$ (Ministry of Health NZ, 2021). The addition of 1 mg/L alum consumed 0.5 mg/L of alkalinity. Neutralisation of alkalinity in water stops floc formation which is controlled by the dose of alum used for the process. However, increasing alkalinity decreases the pH in water, which is mostly adjusted by dosing soda ash, caustic soda, or hydrated lime.

Clarifier types

Most large-scale water treatment plants use clarifiers (or sedimentation tanks) after coagulation and flocculation processes to settle floc particles. There are different types of clarifiers, such as conventional clarifiers, dissolved air flotation (DAF), lamella settlers, buoyant media clarifiers, and pulsed blanket clarifiers. In clarifier design, the key parameter is the surface loading rate, which is the flow (m^3/h) that occurs over the horizontal area (m^2) of the settling zone of the tank. An explanation of each clarifier design is provided below, according to the guidelines for drinking-water quality management in New Zealand Ministry of Health NZ (2021).

Conventional clarifiers are classified based on the following factors: shape (circular, rectangular, or hopper/wedge-bottomed), flow direction (horizontal, radial, or up-flow), and presence or absence of a sludge blanket. Upflow clarifiers can handle high turbidities in raw water, requiring 3–6 min of flocculation time, but they are sensitive to variations in flow. Conventional clarifiers typically have surface loading rates of 2 m/h. With the application of polyelectrolytes, this can reach 5 m/h.

Lamella settlers, often referred to as plate or tube settlers (Figure 2.4a), use slanted plates or tubes to enhance the effective surface area for settling, thereby improving the settling efficiency. The footprint of a lamella settler is significantly smaller for a given throughput than that of a traditional clarifier. The usual rates of surface loading are 5–15 m/h. Compared to traditional clarifiers, lamella settlers are less susceptible to changes in flow.

Buoyant media clarifiers (Figure 2.4b) combine flocculation and clarification into a single process which is also called adsorption clarification. The coagulated water travels through a medium of buoyant adsorption material (usually plastic) maintained in place by a screen. Consequently, flocs can cling to the medium and be drawn out of the water through contact flocculation. Solids continue to accumulate until the media becomes clogged. The media must then be expanded, and the solids must be removed, requiring backwashing, which works well with raw water sources that are low in colour and turbidity and frequently calls for a higher dose of polyelectrolyte. High turbidity levels cause extensive backwashing and quickly clog the media. Standard surface loading rates of 19–25 m/h which are five-fold higher than those of conventional clarifiers, can be used.

DAF is a technology used to remove algae cells in medium-turbidity water with a surface loading rate of 10–12 m/h (Figure 2.4c). The procedure involves pumping tiny air bubbles close to the flotation tank's intake, which adhere to flocs (sometimes made of aluminum) created in a different flocculation tank and cause them to float to the top. Typically, flotation takes 15–20 minutes. Next, the clarified water is moved to a separate tank, where approximately 5–10 percent of the flow is recycled, pressurised, and saturated with air. Through a series of nozzles, the recycled water re-enters the

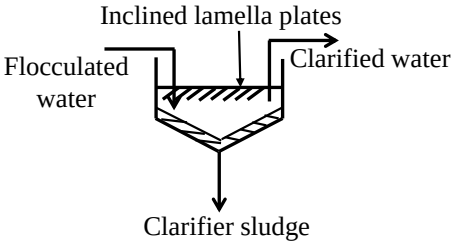

(a) Lamella Settlers

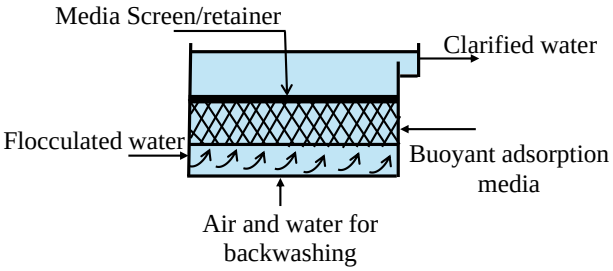

(b) BuoyantMediaClarifier

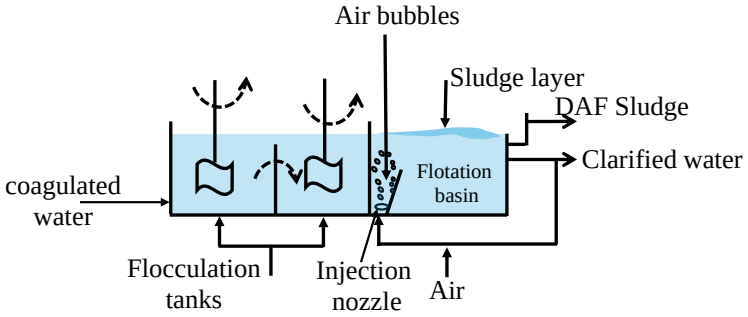

(c) DAF

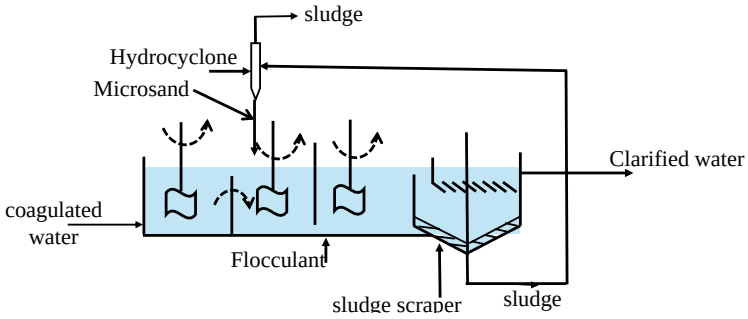

(d) Actiflo

Figure 2.4: Different types of clarifiers used in water treatment plants

flotation tank, with the drop in pressure causing tiny air bubbles to form. The floated flocs gathered at the water surface to form a sludge layer. Either mechanical skimming, which creates thicker sludge, or hydraulic flooding of the flotation tank causes the sludge layer to pour over the collection weir during periodic de-sludging. A modification of the standard DAF process, in-filter DAF (sometimes called DAFF) combines filtration and clarification in a single stage by converting the DAF tank's base into a fast granular media filter.

Pulsed blanket clarifiers use a vacuum system to generate pulsations to maintain the sludge blanket in suspension and aid flocculation. Actiflo uses a micro-sand ballasted clarification process, as shown in Figure 2.4d. There are three chambers, where the first is used for coagulation addition and mixing, the second chamber is used to add polyelectrolytes and micro-sand, and flocculation occurs in the final chamber. Flocculated water is pass through a lamella settler. Settled sludge is passed via a hydrocyclone which separates the micro-sand and sludge. Micro-sand is recycled and used in the system, whereas sludge is disposed of separately.

Performance Issues of Clarifiers

The system is designed to operate within a particular hydraulic load and turbidity range. In clarifiers, high turbidity influences poor performance, resulting in lower particulate removal which is then passed on to the filters. Ministry of Health NZ (2021) indicated that an effluent with turbidity of no more than two NTU should be produced by a properly functioning clarifier. While high-rate clarification systems are less vulnerable to such fluctuations, conventional clarifiers are sensitive to them.

Water temperature influences particle settlement, with higher settlement occurring at higher temperatures compared to lower temperatures. This indicates that particle settlement was higher in summer than in winter. For example, owing to the temperature differential between the incoming water and the water in the tank, a short-circuiting current can occur in a hopper-bottom up-flow clarifier type, which results in a billowing of the floc blanket that leads to the floc being carried over to the filters.

2.2.3 Filtration

After coagulation, flocculation, and clarification, low-turbidity water is passed through a filtration process that uses adsorption to further reduce particulates and pathogens. It is expected to remove 99% (2 $\log_{10}$) of *Cryptosporidium* when only filtration is used. Rapid sand, slow sand, diatomaceous earth (DE), and bag filtration are some of the filter types used in New Zealand (Ministry of Health NZ, 2021). Apart from the aforementioned techniques, there are other filter types, such as membrane filtration, which is subcategorised into micro, nano, ultra, and hyper filtration, and is used according to the application (Gregory, 2005).

Diatomaceous earth filtration — A substance that is movable that forms a filter wall on a membrane. Diatomaceous earth (DE) is a thin, powdery material composed of tiny algae called diatoms. It exists in the form of mined, dried, graded, and bagged natural deposits.

Slow sand filtration — This method is the most effective method of water treatment. However, it requires a large amount of land, and is one of the cheapest and simplest methods. Slow sand filters can be subcategorised according to their operation: a surface filter that processes the water biologically ; and a deep sand bed that purifies the water by adsorption and some straining.

Membrane filtration — In the context of water treatment, there are 4 types of membrane filters:

- Micro-filtration (MF)
- Ultrafiltration (UF)
- Nano-filtration (NF)
- Reverse Osmosis (RO)

In drinking water treatment plants, MF and UF are commonly used membrane filters that use a sieving mechanism to remove suspended and colloidal particles. These filters operate under low pressure, normally in the range of 3–50 psi, or -3–12 psi if using a vacuum system (Ministry of Health NZ, 2021). Different materials and manufacturing techniques can be used to create membranes, resulting in diverse pore diameters. The pore range of MF membranes is 0.1 to 0.2 μm; occasionally, MF with pore diameters of 10 μm are available on the market. UF filters capable of removing protozoa with 99.9% (3 log removal), which have a pore size from 0.01 to 0.05 μm. Rather than having a specific pore size, some UF membranes are categorised based on their molecular weight cut-off (MWCO). This membrane type measures the molecular weight and acts as a barrier to compounds or molecules according to the specified MWCO.

Regarding the level of contamination removal, NF and RO membrane processes are superior to MF/UF membrane processes. For instance, NF systems can eliminate particles as fine as 0.001–0.002 microns. Although almost all bacteria and viruses can be eliminated by NF and RO, these methods are used less frequently in drinking water applications. This is primarily because they require much higher pressures, such as 800–1,000 psi (or 5,500–6,900 kPa or kN/m2) for NF and even higher pressures for RO, which can require up to 10,000 kPa in desalination plants.

Bag filtration — Bag filters consist of a single-use bag that is placed into a housing or reception vessel for filtered water. Both pressurised and open (gravity) versions

are available. In terms of functionality, they function similarly to cartridge filters, providing a single-barrier filter. However, the flow direction is from the inside of the bag to the outside, in contrast to most cartridges. Bag filters have a low particle loading capacity. To extend the filter life and eliminate the majority of particle matter, these systems typically require pretreatment, unless the raw water is extremely clean. The water entering the filter should, as a general rule, have a turbidity of less than three NTU. However, even with the finest mesh size available on the market, bag filters cannot eliminate dissolved contaminants or colloidal colours.

Operating problems of filters

Operating problems with filters may result from backwashing filters, regulating the flow through the filter, or chemical treatment performed prior to the filter (Minnesota Rural Water Association, 2012). Backwashing is used to maintain the filter operation, as colloids and suspended materials cover the pores of the filter membrane, reducing the operational flow. There can be several issues that come with improper backwashing of filters, one such issue is the formation of mud balls. The flocs that the filter was meant to remove solidified into mud balls, which were created by the filter medium. These mud balls can sink to the bottom of the filter and occupy an important filter volume as they become heavier. Consequently, the unplugged portions of the filter will experience an increase in flow. Mud-ball formation may also lead to further issues, including media separation from the filter walls and filter cracking. The filter should be flat and smooth, with no cracks or mud balls on the surface, following a properly functioning filter backwash.

Another issue is filter bed shrinkage. There is virtually minimal compaction when the media grains are physically pressed against each other in a clean filter. A soft layer that surrounds the filter media in a dirty filter leads to filter compaction. Consequently, the filter bed cracks and the filter media separates from the filter walls. It is evident that the filter will short-circuit when damaged. The flow will look for a crack and pass right through it, making the effluent extremely turbid.

The backwash valve opens too soon, forcing the supporting gravel to the top of the filter and causing gravel separation, which is another problem associated with improper backwashing. The unequal distribution of backwash water could also be the result of an obstructed filter under the drain. This results in boiling because of the higher filter velocity. After entering the filter through the under-drain system, the filter media began to wash out. If there is evidence of displacement, the filter media must be removed and replaced, ensuring that each grade of media is positioned correctly.

Air binding of the filter is uncommon as long as the filter is frequently cleaned. Air binding occurs when the pressure of the filter decreases during operation. Short

filter runs and resistance are the results of the dissolved air in the water rising to the surface and getting stuck in the filter. A filter with fewer than five feet of head above an unexpanded filter bed typically experiences a negative head. The water being extremely saturated with air and cold might also result in air binding. As the water warms, the air bursts. The operator cannot exert control over this circumstance. In the event that it does, more regular backwashing of the filter is required to address the filter's air binding.

Loss of media occurred with every filter. Every time the filter is backwashed, some media are lost, particularly if a filter surface wash is employed. If a significant quantity of media is lost, the washing procedure must be examined and adjusted. During the backwash cycle, the bed should not be enlarged by more than 20 percent. Turning off the surface wash approximately two minutes before the backwash is about to end can be helpful. Should this fail to resolve the issue, it could be necessary to elevate the filter troughs in order to stop the excessive loss of media.There shouldn't be any boils at the surface and the bed should appear to move laterally during the backwash. The filter should be cleaned uniformly. An under-drain issue may occur if certain regions are not clean.

The flocculation and coagulation phases of the water treatment process must be continuously monitored. To prevent the filter from becoming saturated with suspended material, the amount of coagulant injected must be frequently adjusted. This overflow could lead to the filter hitting its maximum head loss before it should.

The turbidity of an effluent may fluctuate when a filter is subjected to abrupt changes in flow rate, and the impact is larger for dirtier filter material. To generate the necessary water, the filter flow must be adjusted in tandem with variations in the plant flow. To lessen the impact on the filter, if an increase is required, it should ideally be made gradually over a ten-minute period. The effect on the filter effluent can also be reduced by adding filter aids. One filter cell is momentarily rendered inoperable during backwashing, necessitating the remaining filter cells to absorb the extra flow. This sudden change in flow may result in turbidity breakout. Having a backup filter ready to accommodate this extra flow will help prevent this issue. Additionally, this will stop surges to the filters if the plant includes backwash storage basins. The start-up at the beginning of the day produces a surge to the filter(s) because many plants are not operated constantly. Before resuming operation, the filters should be backwashed or left in waste mode until the effluent satisfies the regulations.

2.2.4 Disinfection

The final stage of the treatment process is disinfection which can be performed using chemicals such as chlorination, ozonation, and/or ultraviolet (UV) irradiation to inactivate pathogens remaining in water, making it safer to consume. Chlorination is the

cheapest disinfection method that inactivates bacteria,viruses, and cyanotoxins. Different disinfectants, such as chlorine, hypochlorous acid, chlorine dioxide, and chloramine, are used for chlorination. This disinfectant method works for most bacteria, some viruses, and *Giardia*. However, chlorine cannot be used to inactivate *Cryptosporidium* (Nokes, 2008).

Ozone is a strong oxidising agent used in water treatment which inactivates all types of pathogens, including *Cryptosporidium*. However, due to the strong reactivity of ozone, it cannot be used as a disinfectant residual after treatment, and it must be produced on-site. Therefore, dry air, oxygen, or both in a mixture were sent via two electrodes separated by an electric and discharge gap. When a high voltage is supplied, electrons flow through the discharge gap. Ozone is created when oxygen molecules dissociate, and electrons supply the energy needed for this process. The four major components of an ozone treatment system are as follows:

- gas feed
- ozone generator
- ozone contactor
- ozone off-gas destructor

There are a few important factors related to the efficiency of ozone as a disinfectant. Temperature can negatively impact the overall ozonation process efficiency because it accelerates the rate at which organisms are inactivated by a disinfectant. This is because when the temperature increases, ozone transfer into water becomes less effective.

Compared to monochloramine, chlorine dioxide, and chlorine, ozone can disinfect at shorter contact times and lower concentrations. However, because of its instability and reactivity, ozone cannot leave a residue that can be used for disinfection. Ozone typically serves as the main oxidising and disinfecting agent. Chlorine or monochloramine is added as a secondary disinfectant to create a residual.

Ozone loses stability as the pH and temperature increase. At 15°C and pH 7.6, the residual's lifetime is approximately 40 min, but at higher temperatures, it may be as short as 10–20 min.

The residual ozone should be completely depleted before adding chlorine (or chloramine) if it is to be used as a secondary disinfectant. Chloramine/chloramine dose requirements would increase as a result of the interaction between ozone and these compounds. Chlorates can also be produced as a result of the oxidation of chlorine.

According to MW Le Chevallier (2004), ozone in an aqueous solution may react with microbes either directly with molecular ozone or indirectly with the radical species formed when ozone decomposes. Ozone is known to attack unsaturated bonds, forming aldehydes, ketones, or carbonyl compounds. Additionally, ozone can participate in

electrophilic reactions, particularly with aromatic compounds, and in nucleophilic reactions with many components of the microbial cell. Carbohydrates and fatty acids react only slightly with ozone; however, amino acids, proteins, protein functional groups (e.g. disulphide bonds), and nucleic acids react very quickly with it. Therefore, it is likely that microbes become inactivated through ozone acting on the cytoplasmic membrane (due to the large number of functional proteins), the protein structure of a viral capsid, or nucleic acids of microorganisms. Free radicals formed by the decomposition of ozone are generally less effective for microbial inactivation than molecular ozone because microbial cells contain a high concentration of bicarbonate ions that quench the free radical reaction, and many microbial cells also contain catalase, peroxidase, or superoxide dismutase to control the free radicals produced by aerobic respiration.

Generators should be inspected daily, and professional specialists are required for maintenance. If the plant lacks skilled maintenance personnel, the equipment manufacturer should handle this task.

UV disinfection is the most widely adopted technology in water treatment plants to inactivate pathogens, and UV light of 254 nm wavelength is used to damage the DNA of microorganisms. Some water treatment processes use a mixture of these methods to control contaminants, such as *Cryptosporidium*. UV disinfection to meet cryptosporidium treatment requirements must demonstrate that at least 95% of the water delivered each month is treated by UV reactors operating within validated limits of turbidity, flow, and UV intensity (USEPA, 2010). Furthermore, materials such as humic acids act as a sheath for bacteria and reduce UV penetration (Templeton *et al.*, 2006). Similarly, flocs that contain organic solids such as carbon, protein, DNA, and humic substances, as well as inorganic solids such as minerals, clay, and solids, also contribute to sheltering oocysts in UV treatment plants.

The removal of different contaminants during different treatment processes in water treatment plants is listed in Table 2.1. The biological pathogens and particles that are mostly eliminated during the stages of particle removal and disinfection are listed in table.

2.3 UV Disinfection in water treatment

In UV disinfection, UV emission is the most important part, as it is directly involved in the inactivation process. On the electromagnetic spectrum, UV emission lies between the X-ray and visible ranges, and the UV wavelengths range from 100 to 400 nm. These wavelengths are divided into four bands: vacuum UV, UV-C, UV-B, and UV-C, where UV-B and UV-C are the most efficient in disinfection (Randtke and Horsley, 2012).These two bands are in the wavelength range of 200 to 300 nm and inactivate the replication of microorganisms by damaging their nucleic acids. Nucleic acids are molecules responsible for defining the metabolic functions and reproduction of all forms of life (USEPA, 2010).

Table 2.1: Contaminant removal by the different processes in water treatment plants (WaterTreatment, 2008).

Treatment process	Primary contaminants
pretreatment	
Chlorine	Iron, manganese
Ozone	Iron, manganese
Potassium permanganate	Iron, manganese
Copper sulphate	Cyanotoxins (by control of cyanobacterial growth)
Aeration	Gases (eg, hydrogen sulphide, carbon dioxide) and volatile trace organic compounds
Particle removal	
Combined processes	
Coagulation/flocculation/rapid sand filtration	Particles, protozoa
Individual filtration processes	
Bag filtration	Particles, protozoa
Cartridge filtration	Particles, protozoa
Diatomaceous earth filtration	Particles, protozoa
Membrane filtration	Particles, bacteria, protozoa
Slow sand filtration	Particles, bacteria, protozoa
Greensand filtration	Iron, manganese
Disinfection	
Chlorine	Bacteria, viruses, cyanotoxins
Ozone	Bacteria, viruses, protozoa, cyanotoxins
UV irradiation	Bacteria, viruses, protozoa
Chlorine/UV	Bacteria, viruses, protozoa, cyanotoxins
Chlorine/ozone	Bacteria, viruses, protozoa, cyanotoxins
Additional processes	
Ion exchange	Iron, manganese, hardness
Activated carbon	Pesticides, industrial solvents, taste and odour compounds, cyanotoxins

The UV absorption coefficient for water can be as low as 10^{-3} to 10^{-4} cm^{-1} in the wavelengths between 200 to 300 nm, as shown in Figure 2.5. These wavelengths represent the usable UV bands for disinfection. Therefore, light source energy is absorbed by the microorganisms, leading to the inactivation of pathogens.

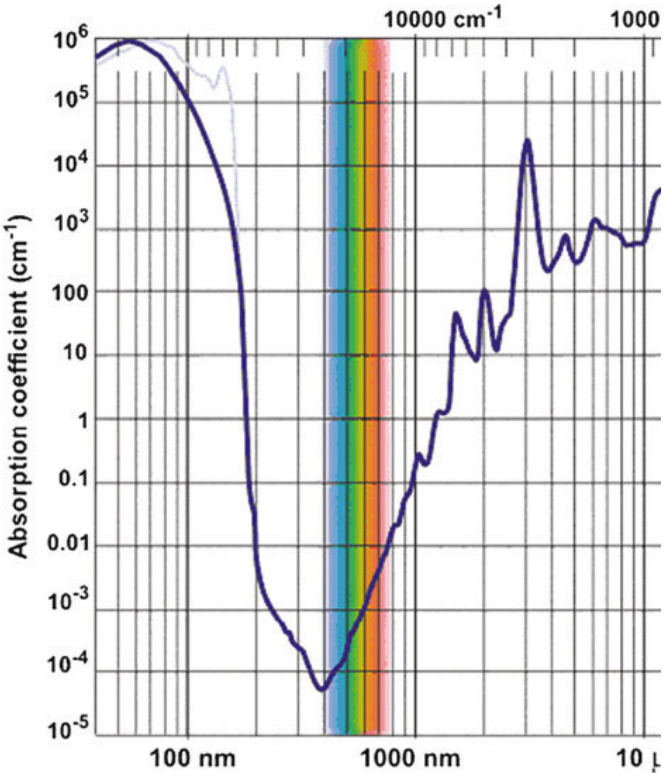

Figure 2.5: Water absorption spectrum [Subhash and Wang (2013)]

2.3.1 UV disinfection system

This section explains the parts of an UV disinfection system, which consists of a UV reactor, UVT (UV transmittance) analyser, and a control panel, as shown in Figure 2.6. The UV reactor contains a UV lamp, UV sensor, temperature sensor, and cleaning processes where disinfection occurs. The UVT analyser tests the UV transmission of the water influent, and this measurement is correlated with the efficiency of UV disinfection. The DNA of most pathogens is affected by UV light at a wavelength of 254nm (Randtke and Horsley, 2012). UV lamps are designed to provide the intensities within the 200–400 nm bandwidth. The most commonly used UV lamps are low-pressure lamps, low-pressure high-output (LPHO) lamps, and medium-pressure lamps with mercury vapour. Low-pressure lamps emit monochromatic light at a wavelength of 253.7 nm, and medium-pressure lamps produce light in the range of 200–400 nm Shah *et al.* (2021). Apart from mercury vapour-based UV lamps, the recent development of metal halide lamps, xenon lamps, eximer lamps, UV lasers, and UV LEDs has been tested for UV treatment and wastewater treatment (Randtke and Horsley, 2012).

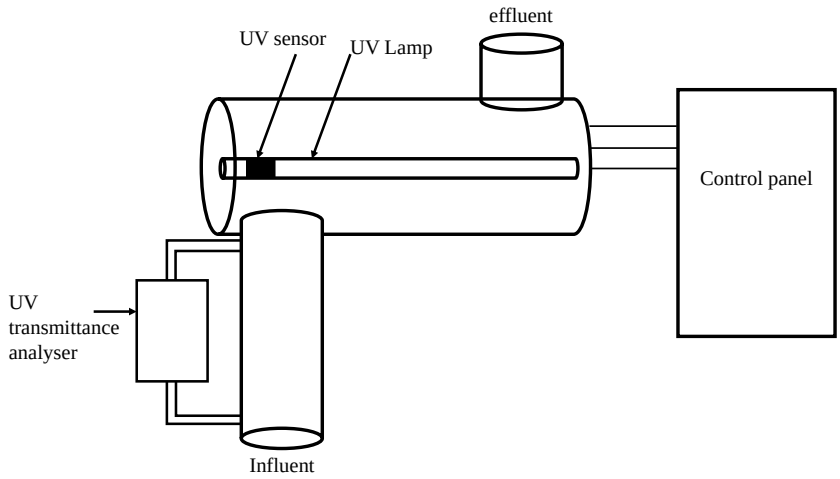

Figure 2.6: Schematic of UV disinfection system

The UV sensors in the reactor measured the UV intensity at a point. This measurement indicates changes in the lamp power settings, lamp aging, and lamp sleeve fouling. This sensor measurement can also be used as a reference for the UVT analyser. The UV sensor consists of a photodetector with a high spectral response between 250–280 nm and an amplifier to increase the signal gain. Some UV sensors have an optical filter added to measure the peak response at the germicidal wavelength.

It is compulsory to add a UVT analyser to water treatment plants, as it acts as a control and monitoring unit that measures the absorption of UV irradiance in water samples. According to the standards in water treatment, this unit was required to be tested weekly for its performance, and the measurements were compared with a bench-top spectrophotometre reading (USEPA, 2010).

A water temperature sensor was used to test the water temperature, which is required to maintain the water temperature, especially for medium-pressure UV lamps that are cooled using water.

2.3.2 Microorganism inactivation using UV

The UV dose(or influence) is a measure of UV intensity (energy) delivered per unit area over a specific time, which is measured in mJ/cm^3. The microbial response is a measure of the sensitivity of microorganisms to UV light and is unique to each microorganism. The UV dose-response was determined by irradiating water samples containing the microorganism with various UV doses using a collimated beam apparatus and measuring the concentration of infectious microorganisms before and after exposure. The microbial

response is calculated using Equation 2.1,

$$\text{Log Inactivation} = \log\left(\frac{N_0}{N}\right) \tag{2.1}$$

where N_0 − concentration of infectious microorganisms before exposure to UV light and N − Concentration of infectious microorganisms after exposure to UV light. This is known as log removal during UV treatment. A 3 log removal (i.e. 99.9% removal) is required to inactivate *Cryptosporidium* in treated water. To achieve this, the oocyst must be exposed to the equivalent of 12 mJ/cm^2 of UV light, as shown in Table 2.3 (USEPA, 2010).

Table 2.2: Log removal requirement to inactivate *Cryptosporidium* according to the concentration

Average *Cryptosporidium* **concentration (oocysts/L)**	**Additional** *Cryptosporidium* **inactivation requirement**
≤ 0.01	2 log
> 0.01	3 log

Table 2.3: UV dose requirement to inactivate three different microorganism

	Additional Log inactivation							
Microorganism	**0.5**	**1.0**	**1.5**	**2.0**	**2.5**	**3.0**	**3.5**	**4.0**
Cryptosporidium	1.6	2.5	3.9	5.8	8.5	12		
Giardia	1.5	2.1	3	5.2	7.7	11		
Viruses	39	58	79	100	121	143	163	186

2.4 Challenging situations in water treatment

Substantial occurrences of waterborne pathogen outbreaks have been documented globally, and recent protozoan outbreaks were reviewed by Efstratiou *et al.* (2017) and Ma *et al.* (2022). Most of these outbreaks are found in developed countries, owing to the availability of surveillance and record-keeping systems in these countries (Islam *et al.*, 2020). Daly *et al.* (2010) and Hrudey and Hrudey (2019) report health outbreaks in Canada, USA and New Zealand associated with drinking water and the causes are mainly due to an insufficient disinfection or inadequate treatments. Table 2.4 shows the outbreaks that occurred in these countries from 2013 to 2023. Most outbreaks are due to untreated water, untreated recreational water, swimming pools, environmental contamination, and damaged sewage systems. However, it is interesting to observe that there are few occasions where outbreaks are caused due to poor maintenance of treatment plants (De Silva *et al.*, 2016; Gharpure *et al.*, 2019).

High rainfall, calving season, floods, and droughts can cause contaminant concentrations to spike, leading to heavy loading in treatment plants (Chhetri *et al.*, 2019). In addition, the initial start-up after filter backwash might lead to an increase in the number of particles passing through the disinfection part of the water treatment process. These sudden spiking events and high flows through the treatment plants can reduce the overall UV inactivation of pathogens in UV reactors.

Most urban cities have access to properly managed water treatment plants, and treated water is accessible to the majority of consumers. However, in rural areas, small-scale treatment plants or wells are used for potable water, and no frequent water testing or particle counts are performed to detect any contaminants. Furthermore, there are social and financial problems associated with providing quality water to people in rural areas (Harris and McFarlane, 2018).

An unfiltered public water system requires at least 3 log inactivation of *Giardia* and 4 log inactivation of viruses to maintain the disinfection criteria (USEPA, 2010). Rural small-scale treatment plants are exempt from using filtration and use only UV disinfection to inactivate microorganisms, which might lead to disease outbreaks during high-flow events. Moreover, Soleimanpour Makuei *et al.* (2022) tested the impact of UV disinfection on unfiltered water and found that the electrostatic surface charge attraction between particles and microorganisms increased UV resistance, reducing UV disinfection effectiveness.

Furthermore, poor monitoring and maintenance lead to process or equipment failures, which is also a challenging situation in treatment plants (Jenkins, 2006). The equipment and chemical costs in a sudden failure can lead to possible failures in disinfection, which may cause an outbreak.

Overall, these challenging conditions and processing systems may lead to the development of a new water system or an update of regulations.

Table 2.4: Countries experienced outbreaks between 2013 and 2023.

Year	Location	Pathogen	Estimated cases	Cause	Reference
2013	USA	*Giardia spp*	38	Environmental contamination or consumption of inadequately treated water	(Rosenthal *et al.*, 2017)
2013	Germany	*C. hominis IbA9G2*	167	River Saale overflowed the floodplain, parts of the city centre and damaged sewage system	(Gertler *et al.*, 2015)
2013	Poland	*Cyclospora, cayetanensis*	3 outbreaks	Travellers drink contaminated water in Indonesia Drinking water	(European Centre for Disease Prevention and Control, 2019)
2013	USA	*C. parvum IIaA15G2R1*	2780	City water treatment facility chlorinated but not filtered water.	(De Silva *et al.*, 2016)
2013	New Zealand	*Cryptosporidium spp. Giardia and Crypto*	21 outbreaks, 66 cases, implicated in 1 outbreak (2 cases)	77.4% untreated water, 40.3% inadequately treated water supply (percentages relate to a total number of 56 waterborne outbreaks)	(Institute of Environmental Science and Research,New Zealand, 2013)
2013	Ireland	*Cryptosporidium spp.*	3 community outbreaks (29 outbreaks),2 swimming poolout-breaks (5cases)	Contamination of drinking and swimming pool water, respectively	(Health Protection Surveillance Centre, 2014)
2013	UK	*Cryptosporidium spp.*	6 outbreaks	Swimming or similar pools	(Public Health England(PHE), 2015)

Continued on next page...

Table 2.4 – *Continuied from previou page*

Year	Location	Pathogen	Estimated cases	Cause	Reference
2014	Ireland	*Cryptosporidium spp.*	5	Swimming pool	(Health Protection Surveillance Centre, 2015)
2014	UK	*Cryptosporidium spp.*	24	Contaminated water supply to holiday cottage on a farm	(Chalmers *et al.*, 2019)
2014	USA	*Cryptosporidium spp.*	100	Contaminated water from a river in a farm setting	(Benedict *et al.*, 2017)
2014	New Zealand	*Cryptosporidium spp.*	10 outbreaks, 26 cases	92.9% untreated water, 21.4% inadequately treated water supply	(Institute of Environmental Science and Research,New Zealand, 2014)
2015 - 2017	USA	*Cryptosporidium spp.*	63 outbreaks	53 related to treated recreational water, 9 related to untreated recreational water, and 1 related to drinking water	(Gharpure *et al.*, 2019)
2016	New Zealand	*Cryptosporidium spp.*	3 outbreaks	Waterborne Unknown	(Institute of Environmental Science and Research,New Zealand, 2018)
2016	New Zealand	*campylobacter*	42 hospitalisations, 4 deaths	untreated, groundwater derived drinking water supply	(Gilpin *et al.*, 2020)
2016	Jorden	*Cryptosporidium spp.*	160	Unknown, but consumption of contaminated water was not excluded	(Hijjawi *et al.*, 2017)

Continued on next page...

Table 2.4 – *Continuied from previou page*

Year	Location	Pathogen	Estimated cases	Cause	Reference
2017	New Zealand	*Cryptosporidium spp.*	2 outbreaks, 6 cases	Waterborne Unknown	(Institute of Environmental Science and Research,New Zealand, 2019)
2018	Ireland	*Cryptosporidium spp.*	3 outbreaks, 9 cases	associated with hotel swimming pool; 3 associated with private house waterborne unknown	(Health Protection Surveillance Centre, 2019)
2018	Brazil	*Toxoplasma gondii*	1162	Treated water	(Minuzzi *et al.*, 2021)
2023	New Zealand	*Cryptosporidium spp.*	45 cases	unknown at the time of writing	(Baker *et al.*, 2023)

2.5 Particle influence on the inactivation of microorganisms

In the process of flocculation, particles in water can protect pathogens by containing or shielding them, and some materials either absorb or scatter (reflect) UV radiation, which reduces the amount of UV radiation required to inactivate microorganisms. Literature shows that the particles influenced the inactivation of microorganisms and their ability to aggregate in different forms and shapes owing to changes in water properties such as pH, turbidity, and particle size (Cantwell and Hofmann, 2008; Templeton *et al.*, 2006; Kollu and Örmeci, 2012; Emerick *et al.*, 2000). The efficiency of UV disinfection is reduced with organic particle sizes less than 2 µm, according to the study carried out by Templeton *et al.* (2006). Research by Cantwell and Hofmann (2008) states that inorganic particles, such as kaolin, do not protect pathogens from UV light; however, the UV absorption of organic particles, such as humic acid and sludge, protects pathogens from exposure to low-pressure UV light. In addition, it also reports an organic particle as small as 11 µm capable of shielding coliform bacteria. Furthermore, Kollu and Örmeci (2012) mentioned that the aggregated *Escherichia coli (E. coli)* and particle sizes larger than 25 µm reduce the inactivation of *E. coli*. The particle size may also vary with the type of microorganism protected by the particles. A model was developed by Emerick *et al.* (2000) to estimate the required UV exposure to inactivate coliform bacteria in particles in a wastewater secondary effluent. This model has been tested only for coliform bacteria, and UV dose and particle size can be modelled accurately only if the inactivation rate and total number of particles in the sample are known. A recent study demonstrated that particle association with microorganisms increases with turbidity, more negative surface charge in water, and the type of floc material in the sample (Makuei and Peleato, 2023). Most of these studies used MS2 and T4 bacteriophages to demonstrate the UV inactivation of microorganisms, which have a size of 23 × 28 nm for MS2 type and T4 having 115 × 85 nm capsid or 92 × 24 nm tail or 145 nm motile fibres (Raza *et al.*, 2022). *Cryptosporodium* oocysts are 4–6 μm in size citepgerace2019cryptosize, and their hard core might require a higher UV dose for inactivation.

Many different parameters are involved in estimating the UV dose required to inactivate different pathogens. Hence, studying UV and light penetration via flocs might help determine whether the methods used for disinfection are appropriate.

2.5.1 Particle influence in untreated water

It is evident that outbreaks mostly occur due to a lack of treatment of water from small plants, ground (well)water, and spring water. Therefore, it is worthwhile to explore the correlation between higher numbers of particles and pathogens. Experiments carried out

by Soleimanpour Makuei *et al.* (2022) examined the influence of turbidity,absorbance, and zeta potential on the UV dose in the UV disinfection of unfiltered water. They claimed that there is a risk of using UV disinfection only on unfiltered water.

2.6 Detection techniques for pathogen

Pathogen detection is mainly carried out in laboratories using specialised instruments and technicians, which require money and time for test results. Detection of bacteria, viruses, and protozoa uses clinical testing methods such as culture-based methods, molecular techniques, and immunoassays to identify pathogens in a sample (Girones *et al.*, 2010; Guliy *et al.*, 2023). Furthermore, environmental testing is performed using microscopic analysis, mass spectrometry, next-generation sequencing (NGS), and flow cytometry testing in laboratories (Alimova *et al.*, 2005). Nevertheless, the development of sensor probes improves the speed of on-site results, which is very helpful for taking necessary precautions when needed (Vikesland and Wigginton, 2010a). Table 2.5 summarises the different techniques used to identify pathogens in water and environmental samples, including the detection range of the measurement.

Table 2.5: Pathogen detection techniques used to test in water and environmental samples

Technique	Type of sample	Pathogen	Detection range	Reference
Bacterial culture	Hot water samples	*L.pneumophila*	2.5 × 103 CFUml^{-1}	(Gill, 2017; Bargellini *et al.*, 2011)
	Wash water	*E.coli*	8 × 108 CFUml^{-1}	(Tilton *et al.*, 2019)
Metagenomics Biochemical tests	Drinking water	*E.coli*	14≥ 1600 cells/100 ml	(Chauhan *et al.*, 2017)
ELISA	Drinking water	*E.coli O157: H7*	1 × 103 CFUml^{-1}	(Zhang *et al.*, 2016)
IMS	Environmental water	*V. parahaemolytica*	101 CFUml^{-1}	(Lun *et al.*, 2018)
NASBA	Treated tap water	*E.coli*	1viable cell/100 ml	(Heijnen and Medema, 2009a)
LAMP	Fresh and marine water samples	*E.faecalis*	10 CFUml^{-1}	(Heijnen and Medema, 2009b)
PCR	Soil and environmental samples	*E.coli O157: H7*	2.6 × 104 CFUg^{-1}	(Ibekwe and Grieve, 2003)
qPCR	River water	*Cryptosporidium spp.*	1 Oocyst	(Masago *et al.*, 2006)
Mass sensitive biosensors	Water samples	*E.coli*	2 CFUml^{-1}	(Gupta *et al.*, 2019)
	Tap and grey water	*P. aeruginosa*	500–1000 CFUml^{-1}	(Mondal *et al.*, 2019)
Lateral Flow Immunoassay	Tap and lake water	*E.coli O157: H7*	3.8 CFUml^{-1}	(Pandey *et al.*, 2017)
	Water samples	*E.coli 0157: H7*	133 CFUml^{-1}	(Hassan *et al.*, 2019)
μPADs	Drinking water	*E.coli*	50 CFUml^{-1}	(Altintas *et al.*, 2018)
	Field water samples	*E.coli*	10 CFUml^{-1}	(San Park and Yoon, 2014)

2.6.1 Detection techniques of *Cryptosporidium*

Cryptosporidiosis is a common food- and water-borne disease that affects animals and humans worldwide (Rossle and Latif, 2013). Therefore, detection has been a priority for assessing the quality of drinking water. Techniques used to detect *Cryptosporodium* parvum are laboratory-based, and large samples are needed for analysis to obtain accurate results (Smith and Nichols, 2010). There are several laboratory tests used to detect *Cryptosporidium* parvum in New Zealand, according to the Ministry of Health (Ministry of Health, 2018).

- *Cryptosporidium* antigen detection,
  - detection of direct fluorescence using monoclonal antibodies
  - detection of antigens using a rapid antigen test
  - enzyme immunoassay
- detection of *Cryptosporidium* nucleic acid
- visualisation by direct microscopy detection of *Cryptosporidium* cysts.

The selection of the above-mentioned methods is based on the diagnosed symptoms of the patient. Microscopic examinations are mostly performed using faecal samples. Different techniques are used, such as wet mount examinations, staining methods, and electron microscopy. Apart from this, there are immunological methods which come under antigen or antibody detection (Khurana and Chaudhary, 2018). Water and food samples are required to prevent the spread of the disease. Biosensors have been developed using different transducers, such as electrochemical, optical, and mechanical, with various techniques, namely cyclic voltametric, amperometric, impedimetric, surface plasmon resonance (SPR), and cantilever (Luka *et al.*, 2015, 2019).

Focusing on detection methods to identify protozoa in water, some of the mentioned techniques can be adapted. According to (Jain *et al.*, 2019), new technologies have been developed to sense pathogens using surface-enhanced resonance Raman spectroscopy (SERRS), using fluorophores with nanomaterials, and specific nucleic acid sequences (DNA or RNA) known as aptamers are used instead of antibodies. However, these fluorophores with nanomaterials, DNA, or aptamers are named as labels in biological measurements, and it is suitable to use techniques without these labels as it will reduce environmental pollution. (Houssin *et al.*, 2010) has developed impedance spectroscopy using an electrode array to measure the phase and the magnitude of the impedance by varying the frequency in the range 10 Hz to 1 MHz to measure the concentration of *Cryptosporidium* oocysts where it shows that it capable of measuring 10 oocysts per millimetre. Although the samples were prepared in the laboratory, they were not tested with real environmental samples. These samples should be tested with standards to

verify the robustness of these methods. Hence, more analysis needs to be carried out before recommending these techniques.

Different methodologies have been adapted to detect *Cryptosporodium* in water sources. Ultrafiltration and capsule filtration methods (Simmons *et al.*, 2001) can remove oocysts from surface water. (Zhang *et al.*, 2013) developed a protocol that uses coagulation and real-time polymerase chain reaction (real-time PCR) methods to identify the *Cryptosporidium* parvum and *Giardia lamblia*. Traditional methods, such as latex agglutination, immuno-diffusion, impedance microbiology, and immuno-precipitation, are used to detect pathogens. These methods have multiple steps, and are therefore time-consuming. However, biosensors show many improvements compared to traditional methods, such as high stability, high sensitivity, reduced reagent volumes, and reduced detection times (Li *et al.*, 2015). On the other hand, optical sensors provide highly sensitive and selective results, making them more popular owing to their compactness, flexibility, and small probe size.

Furthermore, (Wong *et al.*, 2014) describes a biosensor that senses the drain current of a field-effect device to detect *Cryptosporidium* oocysts which is more suitable for medical testing in small samples. Recent findings prove that sintered membranes which are synthesised membranes, possess the best filtration performance, as confirmed by the use of fluorescent particle tracers as a surrogate for *Cryptosporidium parvum* to test the removal efficiency (Li *et al.*, 2019). Furthermore, a cascaded silicon filter was introduced by (Pires and Dong, 2014) to remove *Cryptosporidium parvum* from environmental water, and the recovery rate was two to three times higher when a pre-filter was used along with the filter. Immuno-magnetic separation is another method used to remove the *Cryptosporidium parvum* and (Kuhn *et al.*, 2002) states that the recovery influence the pH value of the sample, the optimal is and it is more effective when the pH is 7. However, most of these methods are still under investigation.

2.7 Particles properties towards inactivation of microorganism

Among the compounds that form small flocs in water treatment, clay and humic substances play a major role. Hence, in this section, the chemical and physical properties of clay and humic acid are discussed.

2.7.1 Clay

Various types of clay can be found in different water sources that affect the composition and characteristics of the water due to its geographical, geological, and surrounding nature. Some common types of clay materials are kaolinite, illite, montmorillonite, smectite, chlorite, and mixed-layer clays (Khan *et al.*, 2023).

Kaolin

Kaolin is an odourless white to yellowish powder which contains kaolinite and a hydrous aluminosilicate (National Center for Biotechnology Information, 2012). Its molecular formula is $Al_2H_4O_9Si_2$ and the chemical structure is shown in Figure 2.7. In addition, pH level is ranged between 4.5–6.5 and there are three refractive indexes 1.549,1.564 and 1.565. Functional groups in the structure facilitate adsorption onto other materials.

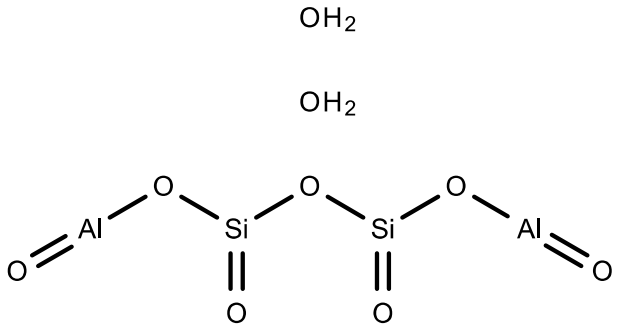

Figure 2.7: Chemical structure of kaolin

Varga (2007) states, kaolinite which is the main constituent of kaolin has a silicon oxygen tetrahedral layer connected to a alumina octahedral layer. These layers are composed of a 1:1 sheet structure, which forms a plate-like structure for kaolinite. The isomorphic substitution of silicon for aluminium in the crystal lattice causes the negative charge in kaolin. A low pH value results in a higher surface charge, whereas a high pH value may decrease the surface charge.

Bentonite

Bentonite is an example of a montmorillonite clay type that is absorbent and forms by the de-vitrification of volcanic ash, which has a similar behaviour to kaolin.

2.7.2 Humic

Humic substances are dark matter found in soil and natural waters which are slightly soluble in water. These substances are complex, naturally occurring organic compounds formed by the decomposition and transformation of plant and animal residues. Furthermore,due to the complex structure of these substances, they are macromolecules consisting of aromatic rings, aliphatic chains, and functional groups such as carboxyl, phenolic, and hydroxyl groups, which results in a high molecular weight. Humic matter has a low pH value, making it weakly acidic, and its ion-exchanging properties make it more binding with organic and inorganic properties. These characteristics have a

positive impact on soil metabolism and microbial activity, influencing nutrient cycling and decomposition processes. Humic acid, fulvic acid, and humin are the three main types of humic substances. Fulvic acids are water soluble, whereas humic acids are partially soluble in water. Humin, an insoluble fraction, is insoluble in water or weak acids.

Humic acid

Figure 2.8 shows the chemical structure of humic acid, which is a macromolecule comprising a humic substance.

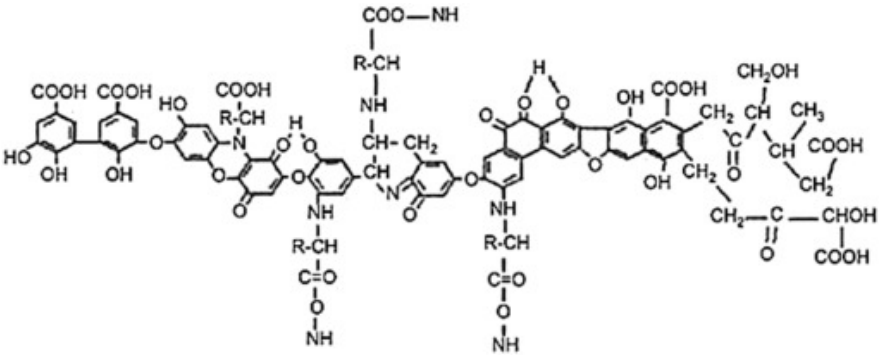

Figure 2.8: Chemical structure of Humic acid

Fulvic acid

A complex mixture of small molecules with low molecular weights in fulvic acid is shown in Figure 2.9. Various functional groups help to chelate metal ions, and their solubility makes them better transport media for the soil.

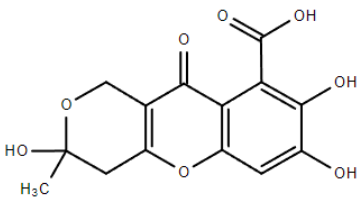

Figure 2.9: Chemical structure of Humic acid

2.8 Summary

Water treatment processes are used to remove contaminants and pathogens that negatively affect human health. However, particulates can escape the clarification and

filtration steps and may shield pathogens from downstream UV treatment. Understanding the materials and pathogens present in particulates would help optimise UV treatment.

Chapter 3

Review of Fluorescence Lifetime Measurements

Fluorescence measurement techniques have been incorporated into the development of sensor technologies for many decades. Spectroscopy analysis is a commonly used technique to determine fluorescence molecules in a sample, where the intensity is measured with respect to the wavelengths. Fluorescence lifetime measurement is another technique used for medical, environmental, and chemical analyses, and a benefit is that the measurement is independent of the concentration of the fluorophore. This chapter provides the basic theory, instrumentation, and technical issues related to fluorescence lifetime measurements.

3.1 Fluorescence

The energy of an incident light photon is absorbed by a molecule, which excites it into a higher energy state, and after some time, it returns to its ground or stable state by emitting low-energy light known as luminescence. There are two types of luminescence: fluorescence and phosphorescence. The Jablonski diagram shown in Figure 3.1 illustrates the two phenomena using energy states.

According to the Jablonski diagram, an absorbed photon of light causes the electrons in a molecule to jump from the ground state (S_0) to a higher energy (S_3) state. Due to the energy lost in internal interactions (e.g. vibrations of molecules), electrons fall to a lower energy S_2 state. Then, the electron releases its energy as light (photon) by dropping from the S_2 state to the S_0 state which is known as fluorescence. The time taken for this process is known as the fluorescence lifetime which is typically between 1 and 10 ns. In some instances, the energy is transferred through an internal-system crossing (S_1), which takes a longer time before releasing energy in the fall back to the S_0 state. This emission is known as phosphorescence, and the time taken for the process

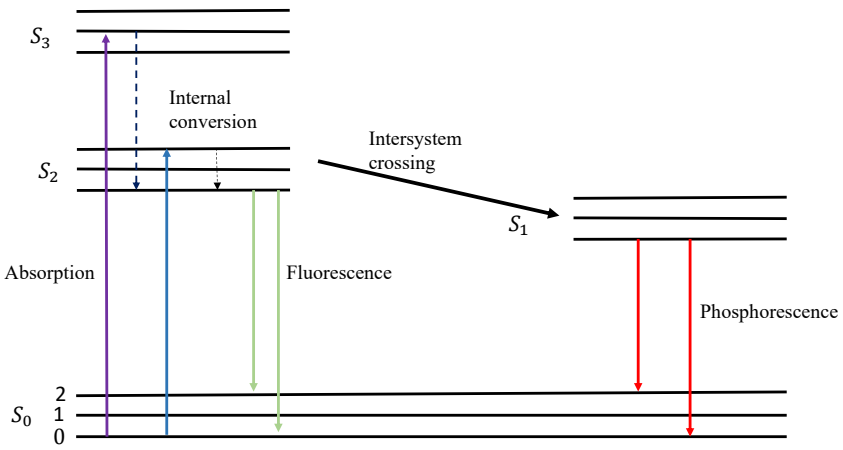

Figure 3.1: Jablonski diagram of fluorescence and phosphorescence

(lifetime) is approximately milliseconds or seconds as it travels through triplet states before emission (Lakowicz, 2006).

The energy difference between absorption and emission is visualised by the two spectra, where the absorption peak maximum has a shorter wavelength than the emission peak maximum. Stokes discovered the Stokes shift which is the difference between the absorption and emission peaks, and is a characteristic of fluorescence (Lakowicz, 2006). In addition, the emission spectra are independent of the excitation spectra.

Fluorescence measurements can be used to measure low or trace levels of substances; hence, they are used for sensitive and selective measurements to identify or quantify certain molecules in a sample (Thompson *et al.*, 1999; Hui *et al.*, 2019). It is a non-destructive technique that provides precise information about the concentration of substances, which is useful in analytical chemistry and biochemistry (Lakowicz, 2006). It is also used in biological applications, environmental monitoring, and material science (Saito Nogueira *et al.*, 2017; Kissinger and Wilson, 2010; Wöll and Flors, 2017).

3.2 Fluorescence measurement

Fluorescence measurements are based on intensity and lifetime. Fluorescence intensity has been used to identify or quantify particles in a sample, and it is influenced by the concentration of the fluorophore, which is discussed in detail in Chapter 2. The fluorescence lifetime technique is commonly used for sensing inorganic ions, pathogens, and proteins, as well as in medical imaging applications (Szmacinski and Lakowicz, 1995; Yahav *et al.*, 2018; Becker, 2012; Bitton *et al.*, 2021).

3.2.1 Fluorescence intensity

Beer's law can be used to predict the concentration of absorbing particles related to the measured optical density. Let the incident light intensity be I_0, light transmitted be I, the length of the solution(or medium) be X, and the absorbing cross-section be A. A square cube is used to analyse the intensity of the absorbing particles, as shown in Figure 3.2.

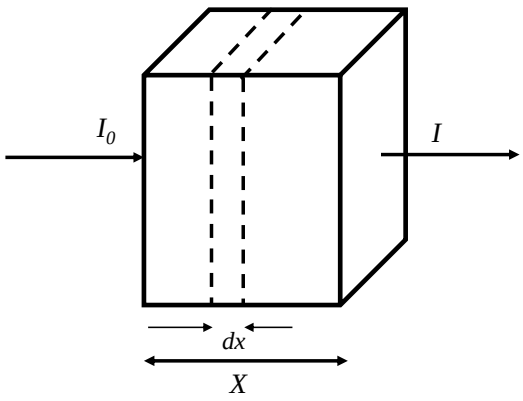

Figure 3.2: Light absorption via a solution

Consider a thin slice dx and A is an effective cross-section for the absorption of the solution that contains n absorbing particles. Light intensity absorbed by the slice is proportional to the intensity of incident light, according to

$$\frac{dI}{dx} = -IAn \tag{3.1}$$

integration with the boundary conditions $I = I_0$ at $x = 0$ and $I = I$ at $x = X$, yields

$$\ln \frac{I_0}{I} = AnX \tag{3.2}$$

Beer-Lambert equation used in an alternative form when it is used in an optical density measurement, which is given as

$$\log \frac{I_0}{I} = \varepsilon cX \tag{3.3}$$

where ε is the molar extinction coefficient and c is the concentration in moles per litre. Equation 3.2 and Equation 3.3 can be used to evaluate unknown number of absorbing agents using

$$n = 2.303\frac{\varepsilon c}{A} \tag{3.4}$$

when the effective cross-section and concentration of the sample are known (Lakowicz, 2006).

3.2.2 Fluorescence lifetime

The fluorescence lifetime is the time that an excited molecule remains in the excited state, and the intensity decay of a fluorophore is shown in Figure 3.3. Let the fluorescence

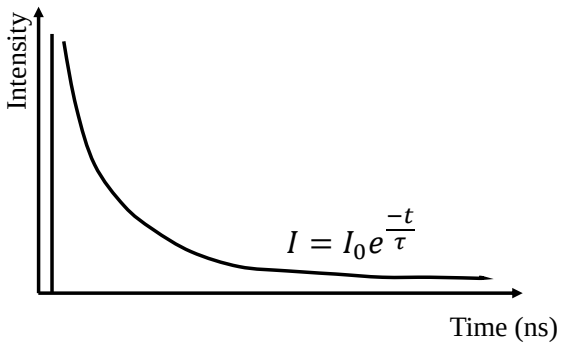

Figure 3.3: Fluorescence lifetime decay

lifetime be τ and the fluorescence intensity be $I(t)$ with I_0 being the intensity at time $t = 0$. The fluorescence intensity decays according to,

$$I(t) = I_0 e^{-t/\tau} \tag{3.5}$$

Methods used to measure fluorescence lifetime can be characterised in the time and frequency domains (Lakowicz, 2006). An excitation source is used to generate pulses to excite the sample, and the fluorescence emission with lower energy is detected by a photon multiplier tube (PMT) or single-photon avalanche detector (SPAD) in the time domain. The received intensity is then analysed with respect to time, and a histogram was plotted to obtain the fluorescence lifetime (Lakowicz, 2006; Wang *et al.*, 2014). In frequency domain analysis, a modulated light source is used with a continuous wave (CW) to generate the excitation signal. The fluorescence emission has the same modulated frequency as the excitation, with a shifted phase. The phase shift between the excitation and emission signals or the modulation index was used to calculate the lifetime of the fluorophore (Kumar *et al.*, 2008).

Time domain fluorescence lifetime

The slope of the plot of $\log(I(t))$ versus t is used to determine the fluorescence lifetime. However, there are two other approaches for measuring fluorescence lifetimes in the time domain. A commonly used method is time-correlated single-photon counting (TCSPC), in which the time between excitation and emission pulses is measured to plot the lifetime decay, which is then used to calculate the fluorescence lifetime. The TCSPC process is described below

The sample is excited with a narrow, high-energy pulse, and simultaneously, a

signal triggers an electronic circuit that starts the time counter. When the fluorescence signal arrives at the detector, the time counter stops. This process repeats continuously, and the fluorescence intensity is plotted against the time delay. The data are used to construct a histogram that depicts the fluorescence decay (Wei *et al.*, 2017). This process is illustrated in Figure 3.4.

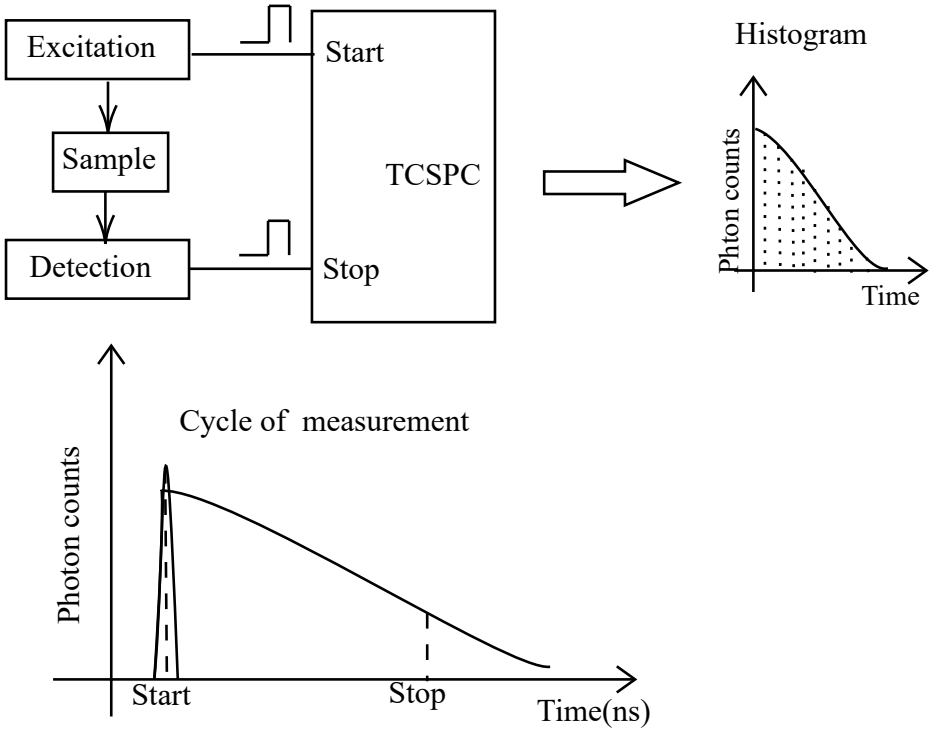

Figure 3.4: Block diagram of time correlated single photon counting technique and graphical representation of measurement of photon detection.

Another method, known as time gating, is used to measure the fluorescence decay curve with several time gates of equal width. Two time gates with equal widths can be used to measure a single fluorescence decay (Wei *et al.*, 2017). Equation 3.6 is used to calculate the fluorescence lifetime with a monoexponential decay.

$$\tau = \frac{\Delta T}{\ln\left(\frac{N_1}{N_2}\right)} \tag{3.6}$$

where ΔT is the time interval between the time gates, N_1 and N_2 are the photon numbers within the two equal time gates, as shown in Figure 3.5a. The error between the measured and theoretical lifetimes can be minimised by selecting a smaller time-gate width between equal time-gates. Below 0.5ns, this technique has low efficiency (Gerritsen *et al.*, 2002).

Alternatively, Figure 3.5b shows the time-gate scanning technique, in which the

photons are detected in narrow time gates synchronised with the excitation pulse. This process is repeated for a sufficient time, and the time-gate is automatically adjusted to picosecond time steps, and the detection is repeated. Finally, the measured data were plotted in a histogram to obtain the fluorescence lifetime of the fluorophore.

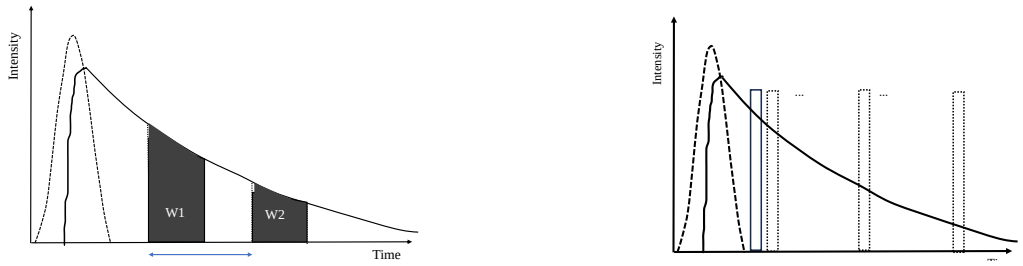

Figure 3.5: The two techniques of time-gated fluorescence detection graphical representation of the two processes. The fluorescence decay curve plotted using (a) two time-gates with equal widths (b) time-gate scanning method.

Frequency domain fluorescence lifetime

The fluorescence lifetime can also be calculated using the measured phase shift and modulation depth from the modulated excitation and fluorescence emission signals. Let the excitation signal be,

$$E_{ex}(t) = a + b\cos(\omega t) \tag{3.7}$$

Then the received emission signal is given by,

$$E_{em}(t) = A + B\cos(\omega t + \phi) \tag{3.8}$$

The lifetime injects a phase shift ϕ into the received signal (Redford and Clegg, 2005). Figure 3.6 elaborates on the process with the help of excitation and emission waveforms, with the two parameters phase shift (ϕ) and modulation depth (m).

The convolution method was used to derive the parameters. Intensity decay of a fluorophore and the modulated signal is given by Equation 3.5 and Equation 3.7 respectively.

The observed fluorescence decay, $f(t)$ is given by the convolution of $T(t)$ and $u(t)$, which is

$$f(t) = \int_0^{\infty} (a + b\cos\omega(t - t^{'})e^{-(t^{'}/\tau)}) \tag{3.9}$$

To solve the equation,

$$f(t) = a\int_0^t e^{-(t^{'}/\tau)} + b\int_0^t e^{-(t^{'}/\tau)}\cos\omega(t - t^{'})$$

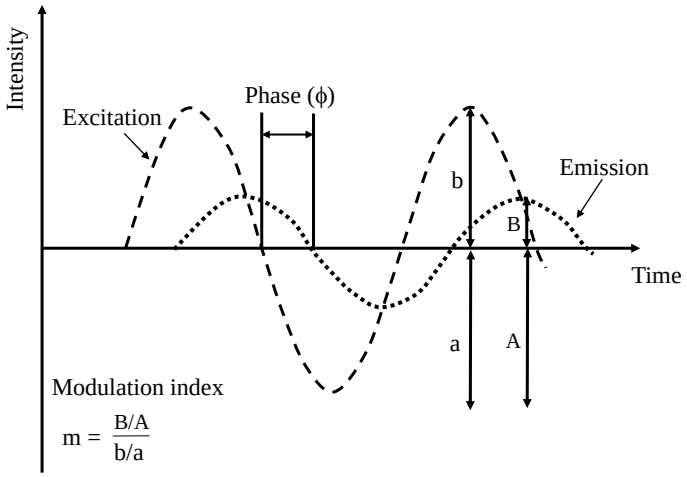

Figure 3.6: Modulated excitation signal and phase shifted fluoressence emission in frequency domain with the intensity measurement needs to obtain the modulation index (or depth).

Integration by parts gives,

$$\int_0^t e^{-(t^{'}/\tau)} \cos\omega(t-t^{'}) = -\frac{e^{-(t^{'}/\tau)} \sin\omega(t-t^{'})}{\omega} - \frac{1}{\omega\tau}\int_0^t e^{-(t^{'}/\tau)} \sin\omega(t-t^{'})dt^{'} \quad (3.10)$$

A second integration by parts gives,

$$\int_0^t e^{(-t^{'}/\tau)} \sin\omega(t-t^{'})dt^{'} = \frac{e^{-(t^{'}/\tau)} \cos\omega(t-t^{'})}{\omega} + \frac{1}{\omega\tau}\int_0^t e^{-(t^{'}/\tau)} \cos\omega(t-t^{'})dt^{'} \quad (3.11)$$

Hence,

$$\int_0^t e^{-(t^{'}/\tau)} \cos\omega(t-t^{'}) = -\frac{e^{-(t^{'}/\tau)} \sin\omega(t-t^{'})}{\omega} - \frac{1}{\omega^2\tau} e^{-(t^{'}/\tau)} \cos\omega(t-t^{'}) - \frac{1}{\omega^2\tau^2}\int_0^t e^{-(t^{'}/\tau)} cos\omega(t-t^{'})dt^{'} \quad (3.12)$$

which can be solved to give,

$$\int_0^t e^{-(t^{'}/\tau)} \cos\omega(t-t^{'})dt^{'} = \frac{\tau}{1+\omega^2\tau^2}\left[\omega\tau \sin\omega t + \cos\omega t\right] \quad (3.13)$$

Substituting back into,

$$f(t) = a\tau + b\frac{\tau}{1+\omega^2\tau^2}[\omega\tau \sin\omega t + \cos\omega t] \quad (3.14)$$

Now,

$$\begin{aligned}\frac{\tau}{\sqrt{1+\omega^2\tau^2}}\left[\frac{\omega\tau\sin\omega t}{\sqrt{1+\omega^2\tau^2}}+\frac{\cos\omega t}{\sqrt{1+\omega^2\tau^2}}\right] &= \frac{\tau}{\sqrt{1+\omega^2\tau^2}}[\cos\phi\cos\omega t+\sin\phi\sin\omega t] \\ &= \frac{\tau}{\sqrt{1+\omega^2\tau^2}}\cos(\omega t-\phi)\end{aligned} \tag{3.15}$$

Provided $\cos\phi = \frac{\omega\tau}{\sqrt{1+\omega^2\tau^2}}$ and $\sin\phi = \frac{1}{\sqrt{1+\omega^2\tau^2}}$ which is true if

$$\tan\phi = \omega\tau \tag{3.16}$$

Hence, we see that the emission is attenuated by the factor $\frac{1}{1+\omega^2\tau^2}$ and the signal is delayed by the phase angle ϕ with reference to the excitation signal.

3.3 Factors influence fluorescence lifetime measurements

There are several factors that potentially impact the lifetime of fluorescence, in particular the fluorophore structure, polarity, and the presence of fluorescence quenchers (Berezin and Achilefu, 2010). Furthermore, the fluorescence lifetime is affected by environmental factors such as pH, temperature, and turbidity (Paviolo *et al.*, 2013; Vishwanath *et al.*, 2002; Pacheco-Linan *et al.*, 2016). Below is a list of sensors which have been developed using fluorescence lifetime techniques to sense water, chlorophyll, oxygen, and bacteria. Chang *et al.* (1997) developed a water-sensitive solid film sensor to measures the water percentage in six solvents using multi frequency approach to measure phases with a precision of 0.2 degrees. Chlorophyll in plants is used to determine plant growth using the time domain technique to measure the fluorescence lifetime (Wenbo *et al.*, 2013). An oxygen sensor was developed as a detector chip using a metal-oxide semiconductor which reads the phase using zero crossing detection and measures the time which is converted using a time to digital converter, and then calculates the delay. The oxygen concentration, which is proportional to the luminescence lifetime of ruthenium-based dyes, was used to test the sensor (Guo *et al.*, 2012). Another oxygen sensor based on fluorescence domain fluorescence lifetime imaging (FD-FLIM) was developed to test in vitro cell studies, as oxygen is a key variable that influences biological activities (Wu *et al.*, 2019). In both sensors, the luminance lifetime decreased with increasing oxygen concentration. A sensor was developed to measure variations in the autofluorescence of collagen and elastin to distinguish between healthy and wounded skin (Li *et al.*, 2015). Pathogen detection is another important area of study, and the FD-FLIM technique with crossing point analysis has been used to differentiate between healthy and infected individuals using the fluorescence lifetime (Yahav *et al.*, 2018).

In the medical sector, cells and tissues analysed using autofluorescence in red blood

cells, blood plasma, neutrophils, and eosinophils have mean lifetimes of 0.1, 1.1, 1.3, and 0.9 ns, respectively Bitton *et al.* (2021). The time domain time correlated single photon counting (TCSPC) technique and time-resolved flow cytometry methods are discussed with crossovers and outlooks of the two techniques. Similarly, fluorescence lifetime imaging has been adapted to diagnose different cancers (Marcu, 2012).

Research has been conducted to identify metal ion concentrations using fluorescence lifetimes. This lifetime can be used to measure concentrations within certain ranges according to the selected fluorophore. For example, Thompson *et al.* (1999) reported that, in a medium of carbonic anhydrase II, the fluorescence intensity and lifetime are changed by the presence of copper, zinc, cadmium, cobalt, and nickel ions which enables one to identify the identification of metals in a solution. Another biosensor was developed using turquoise to measure the fluorescence lifetime in the presence of different calcium concentrations (van der Linden *et al.*, 2021). The same method has been used to develop sensors that measure pH and dissolved organic carbon (DOC); pH sensors that are operable in the range of pH 6 to 10 (Szmacinski and Lakowicz, 1996; Draxler and Lippitsch, 1995) and a DOC sensor to measure DOC in rivers and coastal areas (Clark *et al.*, 2002). These developments indicate that fluorescence lifetime may be a useful technique for detecting water parameters such as DOC. On the other hand, fluorescence lifetime eliminates the errors caused by the measurements of intensity in transmission and absorption, as the lifetime is unaffected by signal intensity. However, it is important to note that the signal-to-noise ratio (SNR) of the lifetime measurement degrades as the signal intensity weakens; therefore, the measured value has greater uncertainty.

3.4 General problems associated with fluorescence lifetime

Issues related to fluorescence lifetime measurements include delays in instruments, fast decays of fluorophores, contamination by excitation signals, low intensities of fluorophores, and multiple lifetimes in samples (Lakowicz *et al.*, 2000; Reinhart *et al.*, 1991; Roding *et al.*, 2014; Wöll and Flors, 2017; Vitta *et al.*, 2012). These problems can be divided into two categories: instrumentation-related problems and sample-related problems.

3.4.1 Delays due to the instrument parts

Electronic delays are introduced in a system, mainly due to the electronic components, transmission guides, frequency-dependent components, and path lengths. These delays give rise to phase measurements. Current fluorescence instruments use a blank sample

and a second detector in the system to avoid phase measurements owing to background effects. In (Reinhart *et al.*, 1991), AC, DC, and phase measurements were taken from the composite signal and the background to remove the background signal. Two signals are given below,

composite signal: $(AC)_C, (DC)_C, \phi_C$

background signal: $(AC)_B, (DC)_B, \phi_B$

Then the X,Y coordinates of the signal are considered,

X coordinates of composite signal$(C_x) = (AC)_C \times \cos\phi_C$

Y coordinates of composite signal$(C_y) = (AC)_C \times \sin\phi_C$

X coordinates of composite signal$(B_x) = (AC)_B \times \cos\phi_B$

Y coordinates of composite signal$(B_y) = (AC)_B \times \sin\phi_B$

where $(AC)_C$ is the composite signal and $(AC)_B$ is the background signal. These X and Y coordinates were used to recover the fluorescence signal.

Hence, the fluorescence signal $(AC)_F$ is

$$(AC)_F = \sqrt{(C_x - B_x)^2 - (C_y - B_y)^2} \tag{3.17}$$

and the fluorescence phase angle (ϕ_s) is given as,

$$\phi_s = \tan^{-1}\left[\frac{C_y - B_y}{C_x - B_x}\right] \tag{3.18}$$

According to the authors, the instrument requires three sample holders to test an unknown sample using this method; however, the use of polarised excitation reduces the number of sample holders to two.

Another method is discussed as a suppression of the background in Lakowicz *et al.* (2000). Researchers have used a time-gated detector to avoid background contamination with fluorescence; the background signal with a shorter emission time compared to the lifetime of the fluorophore will not be measured during the gated time. The theoretical explanation for this method is presented below. In a single sample, two lifetimes can be represented as the background and sample emissions.

$$I(t) = \alpha_B e^{\frac{-t}{\tau_B}} + \alpha_S e^{\frac{-t}{\tau_S}} \tag{3.19}$$

where α_i are the amplitudes related to the two lifetimes, τ_B and τ_S, due to background and sample fluorescence, respectively. Hence, gated detection is used to measure the fluorescence of the sample without interference from the background signal.

3.4.2 Measuring fast decays

Most fluorescence lifetimes of fluorophores are below 10 ns, with fast decays that require high time resolution in measurement systems (Roding *et al.*, 2014; Wöll and Flors,

2017). These problems can be addressed with the advancement of detector technologies and high-performance computers (Franch *et al.*, 2017; Lawrence *et al.*, 2008; Scarcella *et al.*, 2013).

3.4.3 Excitation contamination

Signal contamination by excitation affects the measurement accuracy. Spectral filters (De Jong and Lucy, 2005) or monochromators (Lakowicz, 2006) are used to avoid contamination of the excitation signal. Fluorescence probes use spectral filters instead of monochromators, as the latter are more expensive, and spectral filters are used according to the application. Bandpass spectral filters are more convenient to use because they can evade contamination from excitation light. However, when the spectral bandwidth of the fluorophore is broad, long-pass filters are needed, which might lead to signal contamination, as it directly contributes to the phase measurement. This issue was addressed by Vitta *et al.* (2012), who demonstrated an analytical method for the frequency response function. However, this technique is accurate when the fluorescence-to-background ratio is low, which is not helpful in a highly scattered medium. The interference of scattering directly contributes to the phase. This issue was reported by Szmacinski and Lakowicz (1996), who used a known fluorophore in the scattered media to measure the scattering effect. Another source of excitation contamination occurs when the application uses low quantum yield fluorophores that require exposure to high excitation power.

3.4.4 Multiple lifetimes in a sample

The analysis of a sample with multiple lifetimes is challenging. This can be solved using different techniques; for example, an experiment used to test the decay curve fitting to a multi-exponential model is described in Lakowicz (2006). When a sample consists of a mixture of fluorophores, the multi-frequency approach is one of the methods used to measure the lifetime. The sample is excited either 351 nm argon ion laser or 325 nm He-Cd laser with multiple excitation frequencies from 1 to 140 MHz, and the data are analysed based on least square estimation (Gratton *et al.*, 1984). In general, multi emissions can be expressed as a multi exponential model, which is given by

$$I(\lambda, t) = \sum_{i}^{n} \alpha_i(\lambda) e^{(-t/\tau_i)} \tag{3.20}$$

where I is the impulse response function of wavelength and time, τ is the lifetime of i^{th} component. $\alpha_i(\lambda)$ is the pre-exponential factor of the same component at wavelength λ.

When multiple lifetimes are present, the following equations are used to obtain the

phase and modulation factors:

$$N_\omega(\lambda).J(\lambda) = \sum \frac{\alpha_i(\lambda)\omega\tau_i^2}{1+\omega^2\tau^2} \tag{3.21}$$

$$D_\omega(\lambda).J(\lambda) = \sum \frac{\alpha_i(\lambda)\tau_i}{1+\omega^2\tau^2} \tag{3.22}$$

and

$$J(\lambda) = \sum \alpha_i(\lambda)\tau_i \tag{3.23}$$

where ω is the angular frequency. Then N_ω and D_ω are used to calculate phases and modulation factors, which are given by

$$\phi_c = \tan^{-1}\left[\frac{N_\omega(\lambda)}{D_\omega(\lambda)}\right] \tag{3.24}$$

and

$$m_c = \frac{1}{[N_\omega(\lambda)^2 + D_\omega(\lambda)^2]^{1/2}} \tag{3.25}$$

The goodness of fit can be estimated using the measured phase (ϕ_ω), modulation factor (m_ω), calculated phase ($\phi_{c\omega}$), and modulation factor ($m_{c\omega}$).

$$\chi_R^2 = \frac{1}{v}\sum_\omega \left[\frac{\phi_\omega - \phi_{c\omega}}{\delta\phi}\right]^2 + \frac{1}{v}\sum_\omega \left[\frac{m_\omega - m_{c\omega}}{\delta m}\right]^2 \tag{3.26}$$

where v is the number of degrees of freedom. The lifetime of the fluorophore is required to calculate the phase and modulation information using least square estimation.

Gratton *et al.* (1984) followed the multi-exponential decays approach and they were able to resolve three lifetimes of mixture when the lifetimes are with two to ten folds apart. Separate emission bandpass filters were used to obtain the data required for lifetime calculations.

Another technique has been reported to measure multiple lifetimes using a polar representation (Redford and Clegg, 2005). In this technique, the time-varying part of the modulation signal is considered, and trigonometric identities are used to obtain the phase measurement. The sine and cosine parameters were then used to draw the polar plot, as described by (Redford and Clegg, 2005). The plot is based on single frequency measurements, and the formula to calculate the optimum frequency depends on the lifetime of the fluorophore. However, Redford and Clegg claimed that this method could be used to distinguish multiple lifetimes in the sample. Fluorescence lifetime can be calculated using Equation 3.27 and Equation 3.28

$$\omega\tau = tan\phi \tag{3.27}$$

and

$$\omega\tau = \sqrt{\frac{1}{m^2} - 1} \tag{3.28}$$

These two equations can be rewritten using coordinates as

$$\frac{y}{x} = \sqrt{\frac{1}{x^2 + y^2} - 1} \tag{3.29}$$

Hence, solving Equation 3.29

$$x^2 + y^2 = x \tag{3.30}$$

Hence, a semicircle with a centre of (0.5, 0) and a radius of 0.5 is represented by Equation 3.29. In addition, the same technique was used to measure multiple lifetimes by Štefl *et al.* (2011).

3.4.5 Environment influence

The lifetime measurements of different fluorophores are influenced by the medium, pH, and temperature of the sample (Boens *et al.*, 2007). These parameters can be problematic in situations such as microscopy or imaging; however, they can be helpful in identifying variations in the environment or sample to develop different sensors and probes.

3.4.6 Limitation in frequency

In the frequency-domain analysis, a modulated frequency is used as the excitation signal. An increase in frequency increases the phase angle between excitation and emission, which helps to obtain a better SNR. However, according to Equation 3.27 at high frequencies, the angle variation decreases as $\tan\phi$ limits the usable range of the phase angles. It is known that the emission intensity decreases with increasing frequency (Lakowicz, 2006). Therefore, it limits the usable bandwidth operable in fluorometry. In addition, the separation of fluorophores or materials that fluoresce at the same wavelengths requires different techniques which can be an area of interest.

3.5 Instrumenting fluorescence measurements

Fluorescence fluorometers consist of optical and electronic components, similar to the instrumentation used in fluorescence spectroscopy and microscopy. All these systems require a light source, monochromators or spectral filters, detector/s, and a processing unit to serve the purpose. Two configurations are shown in Figure 3.7 and the selection of the light source,optics, and detectors in the instrument is application-oriented.

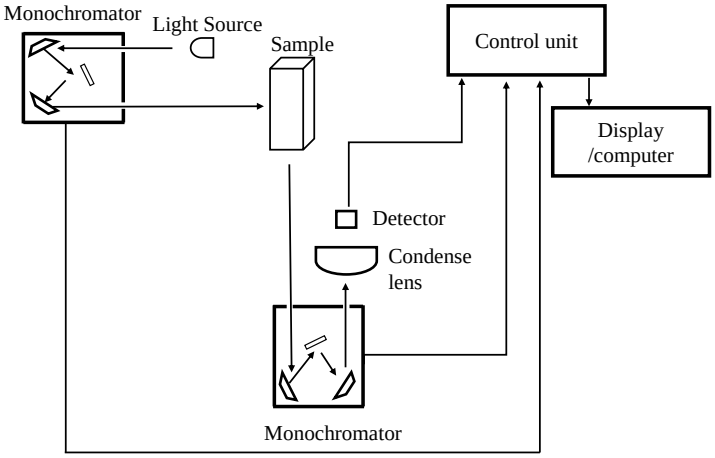

(a)

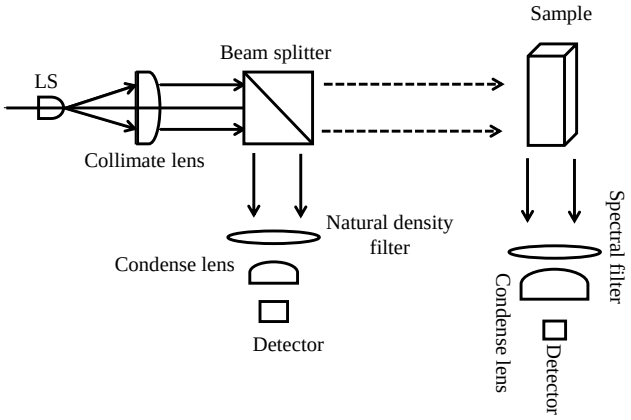

(b)

Figure 3.7: Block diagram of the fluorescence fluorometry and spectroscopy

3.5.1 Different light source

Table 3.1 provides a description of the different light sources with their operating wavelengths (Lakowicz, 2006). Xexon and mercury lamps provide high intensities in

Table 3.1: Comparison of light sources used in fluorescence measurements

Source	Operating spectrum (nm)	Description
Arc and incandescent xenon (Xe) lamps	200 – 700	Generate high light intensity, consume more power and generate lot of heat
Pulsed Xe lamps	200 – 700	Controlled intensity, consume less power and generate less heat
High pressure mercury (Hg) lamp	200 – 1000	Higher intensities than Xe
Xe-Hg arc lamps	200 – 400	Higher intensities in UV range
Quartz Tungsten halogen (QTH) lamp	400 – 1200	Output is high in IR region
Light emitting diodes (LED)	200 – 1200	Long lifetime and less power consumption, can modulate up to 100 MHz
Laser diodes	405 – 1500	Emits monochromatic radiation, can modulate up to GHz

the UV and visible regions, and these lamps provide a broad spectrum that is used in spectroscopy to obtain different wavelengths according to the requirements of the user. However, these lamps consume a lot of power. On the other hand, LED and Laser diodes consume less energy, but require separate sources with a single wavelength. Currently, these diodes are available with a wide range of excitation wavelengths and can be modulated at MHz or GHz frequencies (Landgraf, 2004; Boens *et al.*, 2007). Moreover, significant improvements have been made in LED technology (Kuo *et al.*, 2004; Obeidat *et al.*, 2008; Bui and Hauser, 2015), as described below. Kuo *et al.* (2004) found a high power UV/blue LEDs that operate at 488 nm and 405 nm, which is an alternative light source to be use in chip based flow cytometry and capillary electrophoresis instead of argon lasers. Another high-intensity LEDs was used to develop a multisource portable spectrofluorometer for EEM analysis (Obeidat *et al.*, 2008). These developments have focused more on fluorescence sensing using intensity analysis. However, there is a possibility of using these LEDs in time-resolved fluorometry

where the intensity is used for the time measurement with additional optics collimate the beams. Furthermore, LEDs can operate in the MHz range, which limits their usability in fluorometry instrumentation for nanosecond and picosecond lifetime measurements. On the other hand, laser diodes can operate up to the GHz range which can be used to measure even picosecond measurements with high intensity of monochromatic light (Fukasawa, 2015). High-speed focused light beams provide opportunities for quality imaging (Becker, 2012). Therefore, laser diodes create pathways to advanced technology with a high budget.

3.5.2 Optical components

A system that measures fluorescence requires optical hardware to attenuate and focus the light beam using lenses, mirrors, and filters. It is then necessary to use interference, spectral, or absorption filters to collect fluorescence that provides the information of interest. Hence, optical components play a unique role in these systems (Dandin *et al.*, 2007).

Monochromators

Excitation and fluorescence emission require filtration to avoid contamination. In spectroscopy, a monochromator is a widely used component to split the incident light into the required wavelength, which is done using prisms or a diffraction grating. Generally, gratings are mostly used in spectrometers for better dispersion, higher efficiency, and low stray light levels (Lakowicz, 2006). Planar gratings are produced manually, and concave gratings are produced by holographic and photoresist methods (Palmer and Loewen, 2005). Most commercially available spectrometers use a xenon lamp as a light source because a lamp with a broad spectrum, along with an adjustable monochromator, can be used in laboratory testing to excite samples with different wavelengths. Owing to the high cost of monochromators, optical filters are used in time-resolved fluorescence applications as well as in portable instruments (Kissinger and Wilson, 2010; Li *et al.*, 2015; Wenbo *et al.*, 2013).

Spectral filter selection

The spectral filters are constructed with a cut-off or band-pass wavelength, where a specific band of wavelengths can be selected with the application. Hence, different filters are required according to the fluorophores used in the application. For example, if the emission wavelength of the fluorophore is known, the maximum sensitivity can be obtained using spectral filters. Several types of spectral filters, such as acousto-optic tunable filters (AOTFs), liquid crystal tunable filters (LCTFs), and thin-film tunable filters (TFTF), are commonly used in spectral imaging (Favreau *et al.*, 2014).

Lenses

Lenses are mainly used to converge or collimate light beams in spectrometers and fluorometers. Hence, convex lenses are used in microscopy and spectroscopy applications. Convex lenses are subcategorised into biconvex, planoconvex, double convex, cylindrical, spherocylinder, aspheric, and fresnel. A detailed explanation of the lenses is provided in Chapter 4.

3.5.3 Detector selection

Detectors play an important role in fluorometry, and a photo multiplier tube (PMT) is commonly used in fluorescence applications because of its large active area (Iwata *et al.*, 2000; Lakowicz, 2006). In a PMT, the current is proportional to the light intensity, which can be measured as individual photons. Figure 3.8 shows the internal structure of a PMT, which consists of a photoemissive cathode, dynodes, and anode in a vacuum. The use of a higher negative potential in the cathode and dynodes ejects more photoelectrons, leading to a higher amplification which is advantageous for low-level light detection. The

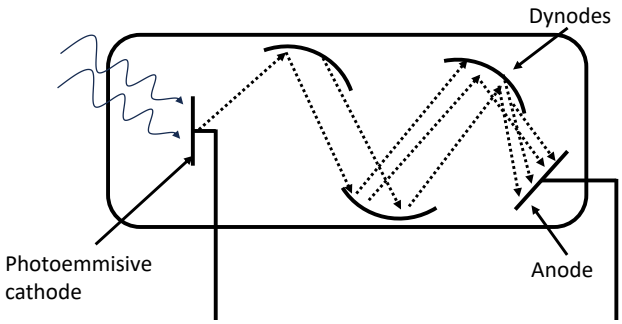

Figure 3.8: Internal structure of a photomultiplier tube

spectral response of the PMTs depends on the incident wavelength, and PMTs operating in different spectral bands were selected based on the appropriate chemical composition of the photocathode and transparent material used for the tube. Furthermore, the usable bandwidth of the PMTs can be adjusted by changing the material composition of the cathode. This variation in composition was used to develop PMTs with a bandwidth ranging from 100 to 1500 MHz (Kaufmann, 2004).

With the advancement of semiconductors, solid-state detectors have been introduced for low-light applications, such as fluorescence spectroscopy and fluorometry. An avalanche photon detector (APD) is a solid-state detector developed using a PN and a PIN diode, which helps absorb and multiply photons (Elmer, 2006). The basic internal structure and conduction diagram of an APD are shown in Figure 3.9. APDs have two operating modes. The linear mode is suited for high sensitivity and fast response times, whereas the Geiger mode is used to detect single photons, obtain high gains, and

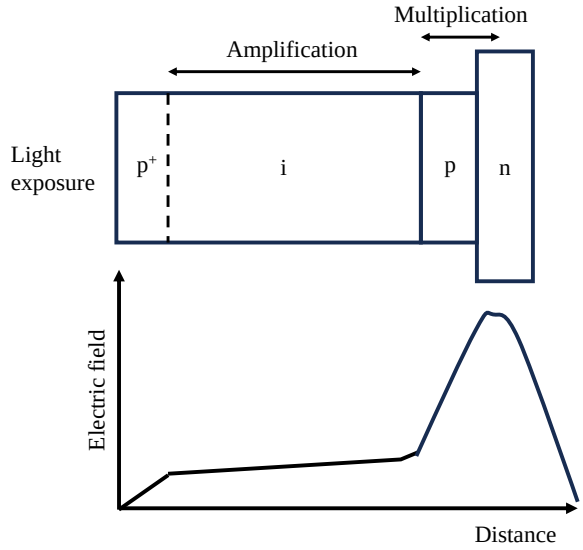

Figure 3.9: Internal structure of an avalanched photon detector and the electric field variation inside the detector showing the amplification and multiplication.

accomplish short resolving times in picoseconds. A single-photon avalanche detector (SPAD) is similar to an APD that operates in the Geiger mode. An array of SPADs was used for fluorescence lifetime measurements and imaging (Franch *et al.*, 2017; Pancheri *et al.*, 2013).

3.5.4 Control unit

The electronic/software developments inside the control units depend on the applications, where time-domain operation requires high-speed electronics as the measurement is dependent on the time measurements of excitation and emission signals (Franch *et al.*, 2017; Saito Nogueira *et al.*, 2017). Furthermore, pulse fluorometry uses a constant function discriminator, time-to-amplitude counter (TAC), window discriminator, programmable gain amplifier, and analogue-to-digital converters (ADC) or a computer (Lakowicz, 2006). Recent developments in time-resolved systems use a field-programmable gate array (FPGA) to generate the input signals to the light source and detector which is integrated with time-gating photon-counting circuitry, enabling the maintenance of the minimum distance between devices (Rae *et al.*, 2010). On the other hand, frequency-domain measurements require less complicated electronics than time-domain measurements because they measure the phase difference between the excitation and emission signals (Lakowicz, 2006; Medina-Rodríguez *et al.*, 2013). The phase measurements were performed using a digital oscilloscope, and the data were analysed using a computer.

3.6 Applications of fluorescence fluorometry

Fluorescence lifetime measurement techniques in the time and frequency domains are tabulated in Table 3.2. Recent developments have used lasers and LED as light sources, and PMT is the commonly used detector; however, there are studies that test SPAD and avalanche photodiodes (APD) as alternatives to PMT. The avalanched photon detector is manufactured using semiconductor technology and has better performance in the red and infrared wavelengths (Lawrence *et al.*, 2008) compared to PMTs. Charged coupled detectors (CCD) and single-photon avalanche diode (SPAD) arrays have been used in fluorescence microscopy and imaging. Furthermore, SPAD technology has been improved for different applications, such as depth ranging, fluorescence lifetime imaging (FLIM), fluorescence correlation spectroscopy (FCS), and DNA sequencing. This detector can be fabricated in a complementary metal-oxide semiconductor (CMOS) with better characteristics of high photon detection efficiency, sensitivity, and low dark counting rate. Using this technology, Villa *et al.* (2012) developed a SPAD detector capable of measuring photon timing and counting for use in different applications. In addition, Scarcella *et al.* (2013) presented a design of an SPAD array with 32 channels that operate in the 300 – 900 nm range for time-resolved measurements, which is an upgraded version of the 1024 SPAD CMOS imager (Villa *et al.*, 2014).

Table 3.2: Comparison of time and frequency domain fluorometers

Investigation on	Methodology	Reference
Time Domain	Time Domain TCSPC technique was used to measure the lifetime using a laser diode, and the fluorescence was measured using SPAD.	Franch *et al.* (2017)
	Time-gated technique used to estimate the lifetime using 405 nm LED and detection was done using APD.	Wang *et al.* (2014)
	An algorithm was developed to measure fluorescence in droplet sorting with microfluidics using TCSPC technique.	Lieske *et al.* (2017)
	TCSPC use lasers 378 or 445 nm, bifurcated fibre optic probe, spectrometer or a hybrid PMT. The fluorescence and backscattered via using the same probe.	Saito Nogueira *et al.* (2017)
Frequency Domain	Phase modulation use with UV LED of 370 nm with a PMT for the detection of fluorescence.	Iwata *et al.* (2000)
	Fourier-transform phase modulation used with UV LED and PMT to improve the multi lifetime measurements.	Iwata (2003); Iwata *et al.* (2005)
	Blue LED and silicon photodiode with 1GHz bandwidth have used to develop a low cost portable fluorometers	Kissinger and Wilson (2010)

3.7 Fluorophore

Fluorophores play a vital role in fluorescence applications, such as probes, antigens, and imaging, in the fields of medicine, environment, and chemistry. Fluorophores are categorised as internal or natural fluorophores, such as aromatic amino acids, flavins, chlorophyll, and reduced nicotinamide adenine dinucleotide (NADH) (Lakowicz, 2006), and external fluorophores, such as coumarin 6, fluorescein, rhodamine, and quantum dots (QD) (Lakowicz, 2006; Wang and Hu, 2014; Vikesland and Wigginton, 2010b). Figure 3.10 shows the chemical structures of the intrinsic (a,b) and extrinsic (c,d) fluorophores.

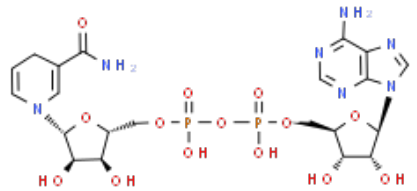

(a) NADH

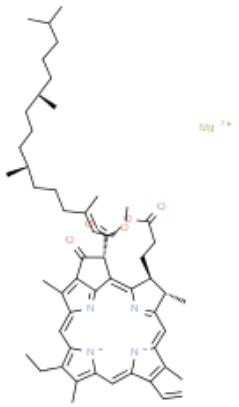

(b) Chlorophyll

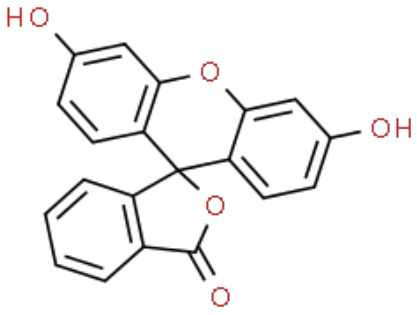

(c) Fluorescein

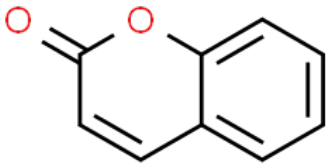

(d) Coumarin

Figure 3.10: Chemical structure of intrinsic and extrinsic fluorophores

Extrinsic fluorophores are mostly used in the absence of intrinsic fluorophores, as they can change the spectral properties of the sample, and are mostly used in fluorescence resonance energy transfer (FRET) applications, such as imaging and sensors (Jares-Erijman and Jovin, 2003; Pickup *et al.*, 2005). There are several factors that can be sensitive to the fluorescence measurement corresponding to the fluorophore structure as

internal factors as well as external factors, for example, temperature, polarity, and the presence of fluorescence quenchers (Berezin and Achilefu, 2010). These external factors contribute to the development of sensors and probes.

Recent developments in fluorescent probes have enabled the detection of different pathogens in environmental and medical studies, (Key *et al.*, 2009; Singh *et al.*, 2016) where fluorophore characteristics were changed with modifications in the chemical structure of the coumarin fluorophore to produce efficient emissions and a fluorescein-tagged aptamer combined with molybdenum (IV) disulfide nanosheets (MoS_2-Ns) as a binder that reduces fluorescein in the presence of the pathogen's DNA. Furthermore, fluorescent microparticles made of polymethyl methacrylate were substituted as *Cryptosporidium parvum* comparing the pathogen size and the gravity which is on average 5 μm and 1.19 g/cm^3 to test the efficiency of a metallic membrane in drinking water treatment (Li *et al.*, 2019).

An experiment carried out by Pang *et al.* (2009) used modified microspheres to study pathogen transport in groundwater. These particles were constructed using 20 nm carboxylated microspheres covalently coated with casein, a phosphoprotein. This modification targets the acquisition of pathogen surrogates with similar size, density, shape, and surface charge, as the surface charge influences the behaviour of a pathogen in a medium. These modifications helped simulate the environment required to observe the particle behaviour, which helped understand the parameters affecting UV disinfection. These microspheres only indicate their presence in water.

During the past decade, the use of carbon quantum dots (CQD) in fluorescence applications has increased owing to their colourful luminance, photostability, and low toxicity (Mao *et al.*, 2010; Zhang and Yu, 2016). CQD are mostly used to sense different ions such as Cu^{2+}, Hg^{2+}, Fe^{2+} and so on. Moreover, CQDs can identify molecules such as NO_2 and H_2S in aqueous media and living cells (Yu *et al.*, 2013).

3.8 Summary

Instrumentation plays a vital role in the detection of chemicals, pathogens, and ions in different atmospheres. There is evidence supporting the variation in fluorescence lifetimes in the presence of ion concentration,environments, and attachment to pathogen DNA or RNA. Hence, the behaviour of the fluorophore in the presence of water flocs might provide information on the material, size, and other parameters that guide the required UV exposure in the UV reactor in a water treatment plant. Therefore, the next chapter focuses on the development of a frequency-domain fluorometer to test the floc samples in treated water.

Chapter 4

Prototype Development of Fluorescence Lifetime Measurement

Floc particles present in treated water after the clarification and filtration steps in water treatment can shield microorganisms from UV light during disinfection using UV reactors. This can prevent the inactivation of pathogens, such as protozoans. The aim of this work is to develop a device to determine composition of the floc and light penetration into the floc. While fluorescence spectroscopy provides detailed information on the spectral absorption and transmission of fluorophores present in materials, as well as organic and inorganic material composition based on intensity measurements, it requires expensive components that can adjust the excitation wavelength and measure emissions over a range of wavelengths. Fluorescence lifetime measurements based on time and frequency domain techniques are also capable of measuring the physical and chemical properties of fluorophores in different materials and environments, but have much simpler demands on equipment, such as a light source with a single wavelength and a detector that can measure emissions within a selected range. Hence, a frequency-domain technique was developed which consisted of a light source, collimation lens, filters, and detectors. This chapter focuses on the design and development of a prototype for measuring fluorescence lifetime.

4.1 Hardware development

Frequency-domain fluorometers require a fluorophore, light source to excite the fluorophore present in the sample, lens to focus and collimate the excitation light beam, spectral filters to filter the emission light from the fluorophore, and a suitable detector that is sensitive enough to detect the fluorescence emission. In this section, each com-

ponent is discussed in terms of theory, requirements, choices, availability, and cost. Figure 4.1 shows the improvements in the development in four steps. Light sources play a major role as they are the energy sources that supply the energy required to excite the fluorophore. In step 1, a sample is excited using a light source, this configuration is appropriate for intensity measurements.

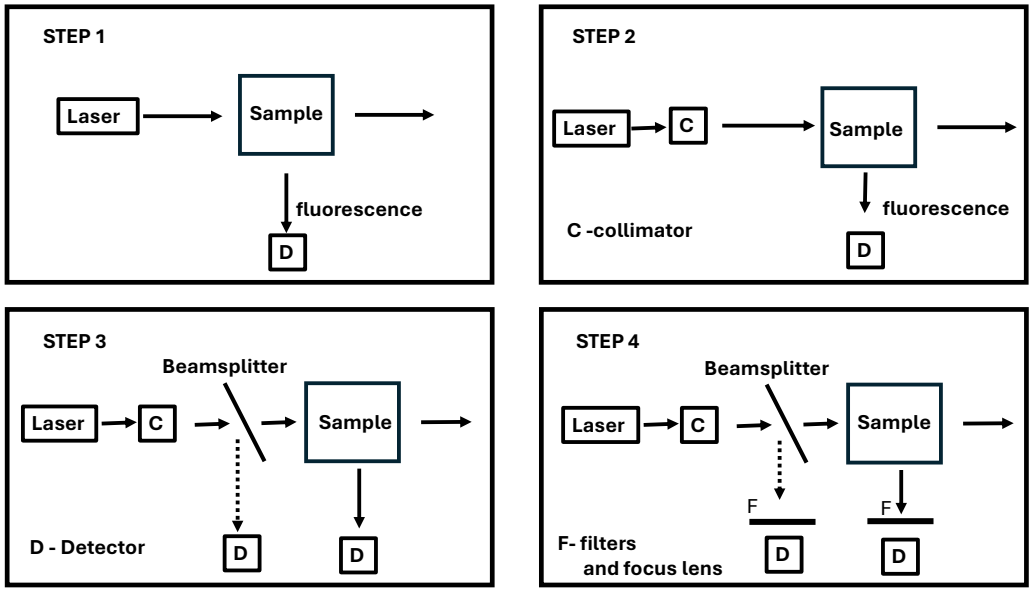

Figure 4.1: Design steps for the development of fluorescence lifetime measurements.

However, a collimated light beam has many advantages for intensity measurements, as it excites the sample with a uniform distribution of energy, which is advantageous for improving signal quality and maintaining the beam area/radius constant over the distance. Hence, a collimated unit is required in the system, as shown in Step 2.

Step 1 and 2 systems are most compatible with intensity and phase measurement system. When performing phase measurements, phase differences can arise due to impedance variations in the cables, which change with signal frequency. Additionally, in free space, the phase shifts increase with distance, as discussed in Chapter 3. These added phase components can be eliminated using a reference measurement. Therefore, a beamsplitter is required to divide the light beam, allowing a reference signal to be captured by a second detector, as illustrated in Step 3.

Detectors used to measure the reference and fluorescence emissions have a smaller active area than the beam area; therefore, it is necessary to capture the majority of the signal using a focus lens, such as a convex or condense lens. According to the specifications of the maximum measurable power in the detector, the beam strength may need to be lowered using neutral density filters, and to filter the fluorescence, band-pass or long-pass filters must be used according to the emission wavelength. Hence, Step 4 illustrates the main design of the fluorescence lifetime measurement system.

4.1.1 Fluorophore selection

The selection of the excitation light source, filters, and detectors is driven by the properties of the fluorophore used in the system (Bui and Hauser, 2015; Boens *et al.*, 2007; Kuo *et al.*, 2004; Obeidat *et al.*, 2008; Landgraf, 2004).

Initially, graphene quantum dots were selected from the range of fluorophores available (discussed in Chapter 3). GQD are nanoparticles that can penetrate or attach to the surface of materials. A 50 ml of 1 mg/ml aqua green graphene quantum dots from Sigma-Aldrich was purchased. The purchased GQD had a 17% quantum yield, excitation and emission wavelengths of 485 nm and 530±10 nm, respectively, were non-toxic, and had a particle size lower than 5 nm.

A fluorescence spectrophotometer (F7000) was used to observe the emission spectra of four GQD samples prepared at concentrations of 0.2–0.8 mg/mL (Figure 4.2). The GQD emission spectrum ranged between 500 and 600 nm, and the narrow spike at approximately 350 nm was the excitation wavelength. As the GQD concentration increased, the excitation peak decreased, indicating the absorption of light energy due to the increased number of GQD particles in the sample. The emission intensity of the sample containing 0.8 mg/ml GQD was reduced compared to that of the other samples, as shown in Figure 4.2, presumably due to the greatly reduced availability of excitation light and reduced transmission of the emission light through the sample due to the increased concentration of GQD.

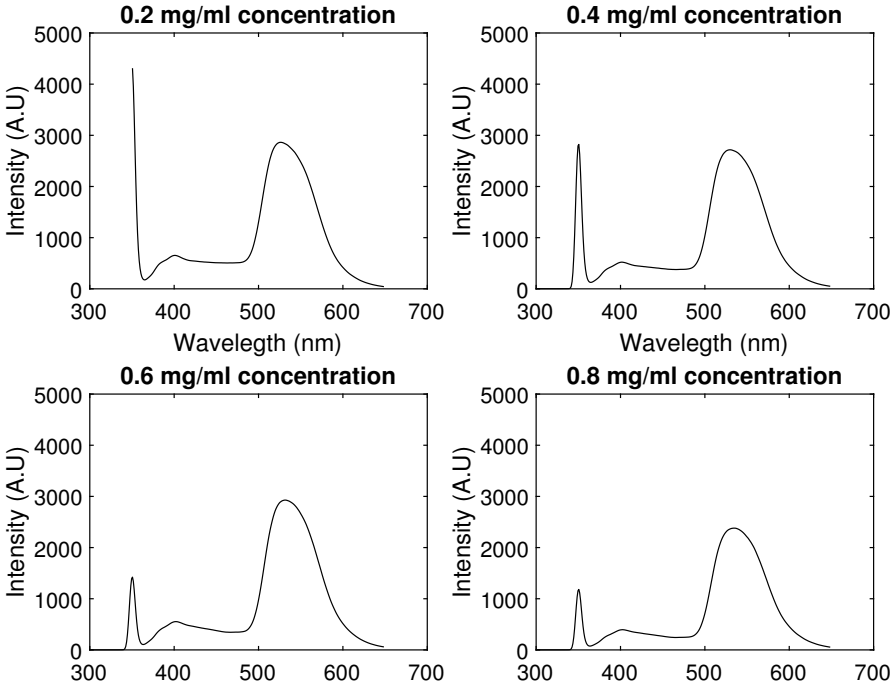

Figure 4.2: Emission spectra of GQDs at different concentrations under 350 nm excitation.

Figure 4.3 illustrates the fluorescence emission of GQD when excited with light at 250, 350, 450, and 485 nm excitation wavelengths. The emission of GQD was the highest at the 250 nm excitation wavelength, which implies the possibility of using this in the UV spectrum and at 254 nm which is the inactivation UV wavelength for pathogens according to Randtke and Horsley (2012). Excitation at 485 nm resulted in higher emissions than excitation at 405 and 350 nm. This means that GQD can be excited using visible wavelengths in the laboratory, which is safer and cheaper than purchasing a light source that can deliver light in the UV range. The only currently available UV laser light source at the time of this research was a 375 nm laser.

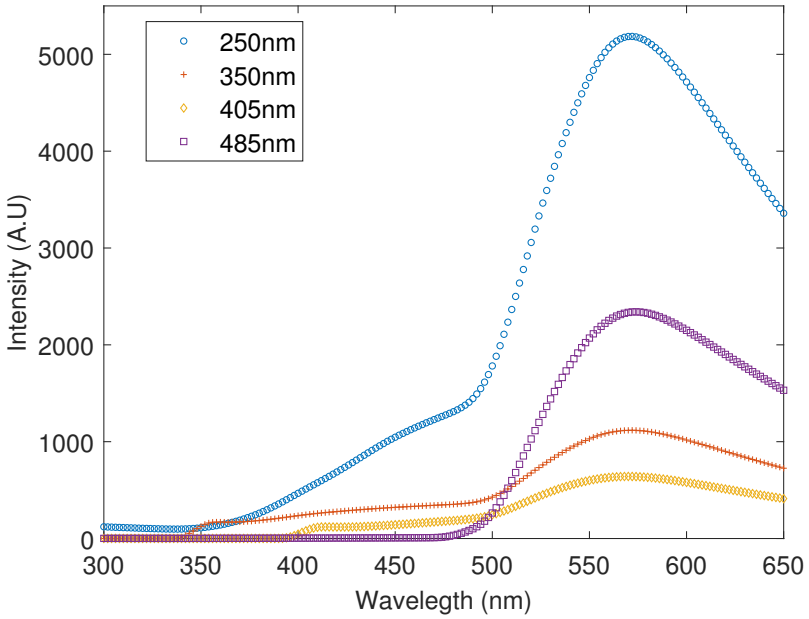

Figure 4.3: Fluorescence emission of GQD, with respect to different excitation wavelengths

During the Covid outbreak, GQD became unavailable; therefore, fluorescein was used instead of GQD as it had similar excitation and emission wavelengths. A fluorescence spectrophotometer (F7000) was used to measure the excitation emission matrix (EEM) to understand the behaviour of fluorescein (Figure 4.4). Fluorescein fluoresces at excitation wavelengths between 250 nm to 330 nm and 450 to 520 nm peaking at the 510 nm emission wavelength, when excited at 260 nm and 490 nm, meaning that fluorescein was a suitable substitute for GQD and could be used in the UV or visible range of excitation wavelengths. Another advantage of using fluorescein is that it has a quantum yield of 95% compared to GQD which have a quantum yield of 17%. That is, for the same number of photons hitting fluorescein, it will emit five times more photons than the GQD. Fluorescein costs $7 per gram through Merck whereas GQD costs $8 per mg, so fluorescein is three orders of magnitude cheaper which is ideal if it is to be used on a large scale. Furthermore, fluorescein has a documented fluorescence lifetime

of 4 ns, whereas the aquagreen fluorescence lifetime of GQDs has not been measured or documented, while the blue fluorescence lifetime of GQDs is 6.7 ns (Roding *et al.*, 2014).

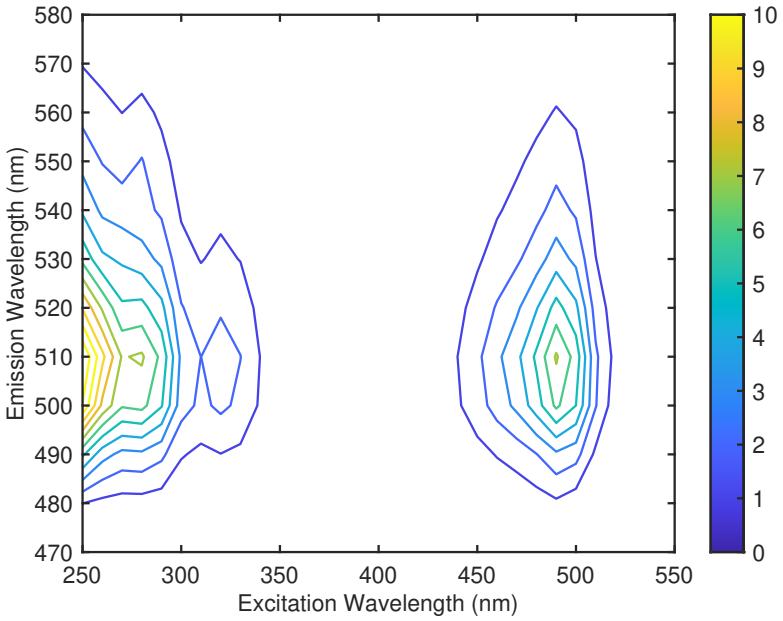

Figure 4.4: Fluorescence emission data for fluorescein at 0.5 mg/L in distilled water.

4.1.2 Light source selection

The light source is an important part of fluorometry, as it is the energy source that excites the fluorophores in the sample. As discussed in Chapters 2 and 3, LEDs and laser sources are solid-state devices that are becoming more popular among fluorometry applications because they require less power to operate than other sources. Furthermore, to operate the system using a frequency-domain technique, it is important to modulate the signal which requires LED and laser sources.

LEDs

A light-emitting diode (LED) is a forward-biased p-n junction made of a direct-bandgap semiconductor material that generates light through injection electroluminescence. Due to their compact size, high brightness, excellent efficiency, high dependability, durability, and toughness, they have become essential in many applications. Visible light-emitting diodes (LEDs) are widely utilised in various applications, such as architectural illumination, traffic signals, mobile phones, laptops, television receivers, games, information displays, flashlights, signage, automobile lighting, and liquid crystal display backlighting.

For consumer electronics like optical mice, keyboards, headphones, microphones, and microphones, infrared LEDs are frequently used as remote controllers (Landgraf, 2004)

Applications of ultraviolet LEDs include decontaminating people and equipment, sterilising surgical instruments, purifying water, and facilitating clandestine non-line-of-sight communications. Chemical and biological substances can also be detected using UV LED, as many of them exhibit fluorescence at specific wavelengths when exposed to ultraviolet light. Hence, UV LEDs are of special consideration for the application of this study.

However, LEDs are incoherent light sources used in fluorometry. Lenses are necessary to collimate the light beam. Another disadvantage is that LEDs can only be modulated up to kHz to MHz frequencies which limits their usefulness for frequency domain fluorimetry, where the fluorescence lifetimes of GQD blue and fluorescein are in the 4-6 nanosecond range. For example, an experiment conducted by Wang *et al.* (2014) used a 405 nm LED that operated at fixed frequencies from 4 Hz to 4 kHz, limiting measurements up to 4 kHz, whereas for GQD and fluorescein, measurements would ideally need to be taken in the MHz modulation frequency range (Chapter 3). Fluorescence lifetime measurements are typically represented in the tangent domain, where angular resolution is meaningful, whereas higher modulation frequencies do not offer an advantage in measuring phase angles.

Laser Diodes

Laser diodes are devices that transform electrical current into a coherent (unidirectional) beam in the 350 to 2000 nm range at power outputs from 0.2 mW to 2 W. Lasers can be single-mode or multi-mode lasers, and multi-mode lasers are mostly used for high-power applications where they need to operate above 100 mW (Sun, 2012).

There are individual laser diodes (more commonly used for lab-based applications) and diode-pumped solid-state (DPSS) lasers (e.g. used in laser pointers). Some use helium neon gas chambers and are typically used for IR applications from 600 nm wavelengths or greater. Lasers can generate light pulses in the nanosecond, picosecond, and femtosecond ranges or as continuous beams. Lasers come in different packages, such as TO-cans, butterfly, laser pigtails, and chips on submounts. They can also be fibre-coupled, for example, for fibre optics. The cost of lasers ranges from $100 to $3500, depending on the mode and application. Thorlabs and Edmund Optics are the main suppliers of laser components.

The selection of the laser depends on the required wavelength, power, available mount, and laser control driver. Based on the fluorescence properties of the selected fluorophore, a laser that could deliver a beam at a wavelength of 450 nm was selected. The laser mount available for this research was an LDM56/M laser mount which can mount 5.6 mm diameter TO-can lasers and can operate up to 500 mA. It is equipped

with a thermoelectric cooler and controller to control the diode temperature. It also has an integrated bias-T adapter to take an RF signal from a function generator to modulate the laser current up to 600 MHz. The laser mount has two inputs to control the current and temperature, which are controlled using LDC205C and TED200C drivers, respectively. The function generator available for the research was a Tektronix AFG3102 which can modulate the signal up to 100 MHz. Available laser diodes in the range of 450 to 500 nm wavelength are either low power single-mode in the 20 to 60 mW range and 3.8 mm package diameter which is not compatible with the available laser mount. Therefore, an L450P1600MM 450 nm multi-mode laser diode was selected as the light source. It has a 20 nm excitation bandwidth and is operable up to 1600 mW.

4.1.3 Selection of optics for the design

The L450P1600MM laser emits a beam through an aperture of 1.6 mm, with a 23 °divergence, and the light intensity has a flat-top distribution over an area perpendicular to the beam with a rectangular shape (as compared to a single-mode laser which has a Gaussian distribution, also known as a standard or TM_{00} beam, over an area with a circular shape). The fluorophore will be dispersed in a liquid in a 10 x 10 x 40 mm quartz cuvette. The cuvette must be within 100 mm of the laser at maximum; however, a beam splitter is placed between the cuvette and the laser. Therefore, to ensure that most of the beam is focused on the cuvette and provides sufficient space for the beam splitter, a collimator lens is required.

Laser packages with collimated outputs are available for red and infrared wavelengths. However, their low-power emissions make them unsuitable for the required wavelength. An alternative is to use an optical lens to collimate the light beam. The most commonly used lenses for this purpose are convex, plano-convex, and aspheric lenses. Among these, the plano-convex lens is the most frequently used as a collimator. The focal length of collimator lens was calculated according to the Equation 4.1,

$$\tan(\theta/2) = \frac{h/2}{f}. \tag{4.1}$$

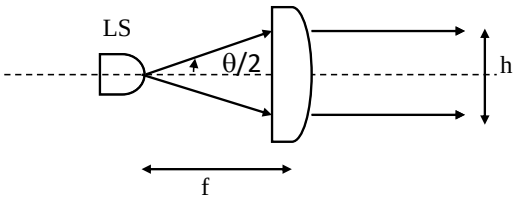

Figure 4.5: Collimating a laser using plano-convex lens

where θ, f and h are the beam divergence, focal length, and height of the beam for the plano-convex lens, respectively, as shown in Figure 4.5. The beam divergence of the

selected laser diode was 23°. The laser beam needed to be 10 mm in height when it reached the cuvette; therefore, the focal length of the lens should be 24.57 mm. Thus, a Thorlabs LA1252-A-N-BK7 plano-convex lens (diameter: 25 mm; focal length: 25.4 mm; anti-reflective coating for 350–700 nm wavelength range) was selected.

Beamsplitter

For frequency-domain lifetime fluorimetry, the reference signal of the excitation light must be monitored; therefore, a beam splitter must be installed between the collimator lens and cuvette containing the fluorophore. There are different types of beamsplitters such as plate, cube, pellicle, crystal, polarising and dichroic beamsplitters.

A plate beamsplitter is the best option for limited-space and lightweight applications. Typically, it is positioned at a 45^0 angle to the incident beam, which reflects a portion of the incident beam from the thin layer, and the remainder of the beam passes through. However, the transmission beam is refracted because of the plate width, which creates a reflection on the back surface, known as ghosting. This can be avoided by applying an anti-reflective coating, a 30 arcmin wedge, or a combination of the two to the back surface (Thorlabs, 1999-2024).

A cube beamsplitter was manufactured using two right-angle prisms joined at the hypotenuses, with a thin film coating at the interface where the beam was split. This type requires more space which is a disadvantage for some space-constrained applications. Additionally, the wall thickness increases the optical path length and group delay dispersion owing to refraction inside the cube, compared with other types of beamsplitters.

A pellicle beamsplitter is manufactured using a nitrocellulose membrane, which is a few microns thick, and mounted under tension in a metal housing. The thin layer of the membrane prevents ghosting; however, these beamsplitters are only suitable for low-power applications below 20 mW.

For this research, a 1 cm cube 10:90 non-polarised beam beamsplitter for 400-700 nm wavelengths (Thorlabs) was used which was already available in the laboratory. Figure 4.6 shows the basic block of the cube beamsplitter used in this design.

The beamsplitter was tested by operating the laser at 200 mA, which generated a 100 mW incident beam, measured using a thermal power sensor (S302C) with a digital optical power and energy meter (PM100D). The transmission and reflection beam powers were 49 mW and 0.78 mW, respectively. Visual observation of the incident beam by placing a white screen with a 1 cm × 1 cm grid between the beamsplitter and the laser showed that the height of the incident laser beam was 2 cm; therefore, approximately half of the incident beam was cut by the beamsplitter housing. In addition, 0.5 mW of light was detected on the opposite side of the reflection beam. This was later discovered to be due to the incorrect orientation of the beamsplitter, where the incident beam

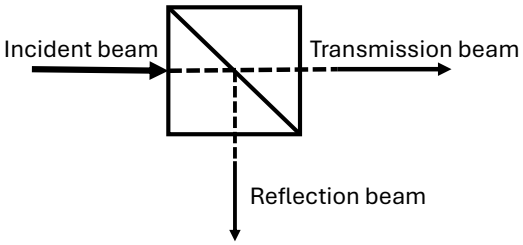

Figure 4.6: Light beam transmission and reflection in a cube beamsplitter

entered the opposite side of the beamsplitter. Normally, one corner of the beamsplitter is marked on the top or bottom to indicate where the incident light should enter; however, in this case, there were additional markings, presumably by another student. However, this would not affect the results of the frequency domain phase measurements.

Filters

Because the laser diode can produce light between 100–1600 mW, and the reflected light from the beam splitter was 0.78 mW for a 100 mW beam, and the detectors are rated to 1 mW maximum optical power, to ensure that the beam intensity was less than 1 mW, it was necessary to instal a 0.5 OD neutral density filter between the detector and the reflected light for a 100 mW beam and a 1 OD filter for a 400 mW beam. A 2 OD filter was used when measuring light transmission through the sample for a 100 mW beam and 2 and 1.5 OD filters in series for a 400 mW beam. All filters were available in the laboratory. Required ODs were calculated using

$$OD = -\log\left(\frac{\mathrm{P_{out}}}{\mathrm{P_{in}}}\right)$$

where OD is the optical density, and $\mathrm{P_{out}}$ and $\mathrm{P_{in}}$ are the power output and input through the ND filter, respectively.

A 500 nm long-pass filter (FELH0500) was used to filter out the excitation light (450 nm) from the fluorescence light (520 nm peak for fluorescein and between 500 and 600 nm for GQD (Figure 4.3)). Because the fluorescence light intensity was low (approximately 0.057 μW), OD filters were not required between the sample and fluorescence detector.

4.1.4 Detector selection

Detectors were required to capture the reference signal from the beam splitter and the fluorescence emission from the sample. Because the fluorescence light intensity was low, as stated in the previous section, an APD detector was used which has a photon

detection efficiency of 80% compared to PMT which is lower than 40% ((Lawrence *et al.*, 2008)). Initially, an APD130A detector was selected with a bandwidth of 50 MHz to detect the fluorescence lifetime on the order of nanoseconds. Later, it was necessary to add another detector to measure the reference signal from the beam splitter to eliminate phase changes due to cable impedances between the function generator and the laser mount, detectors, and the oscilloscope (which became apparent when cables were swapped between 1 m and 2 m in length). If this was not accounted for, the observed fluorescence lifetime was on the order of 6 ns when fluoroscein should have a fluorescence lifetime of 4 ns. The second detector was a UV-Enhanced Silicon APD (APD430A2) with 400 MHz bandwidth and 200–1000 nm detection wavelength range, providing the ability to work with higher laser modulation frequencies and UV light in the future. Both the APD130A and APD430A2 have a responsivity of 6–7 A/W at 520 nm and 40 A/W at 500 nm. The APD130A has an active diameter of 1 mm, whereas the APD430A2 has an active diameter of 0.2 mm. Therefore, an aspheric condenser lens (Thorlabs) with a focal length of 25 mm is used to focus the light onto the detectors.

4.1.5 Equipment setup

Figure 4.7a shows the component arrangement. The equipment was mounted on a 12 inch by 24-inch, 12.7 mm thick, solid aluminium breadboard using $\frac{1}{2}$ inch diameter post holders with 12 mm diameter pedestal posts, $\frac{1}{2}$ inch post mounts, and 25 mm travel crossed-roller bearing XY translation stages. The position of the equipment was adjusted for maximum light detection by the APDs. 50 Ω coaxial cables and subminiature version A (SMA) connectors were used to connect the components and instruments. The experimental setup (Figure 4.7b) was contained in an opaque black box to prevent exposure to ambient light, and the entire setup was placed in a Class 3 laser facility.

4.2 Prototype measurements

The function generator (Tektronix AFG3102) was set to a 50 MHz frequency and 3 V peak-to-peak sinusoidal waveform to generate the excitation signal for the laser. A digital storage oscilloscope (Keysight DSO604A) with a 6 GHz bandwidth and 10 GS/s sampling rate (f_s) was used to capture the detector signals.

Primarily tests used configuration of Figure 4.7 and, raw data captured via the two detectors, reference and fluorescence signals detected by APD430A2 and APD130A detectors, respectively, are shown in Figure 4.8. Figure 4.8 (a) shows the signal captured using a narrow active area with an active diameter of 0.2 mm^2 and 10 mV amplitude, while Figure 4.8 (b) shows the signal captured using an active diameter of 1 mm^2 and

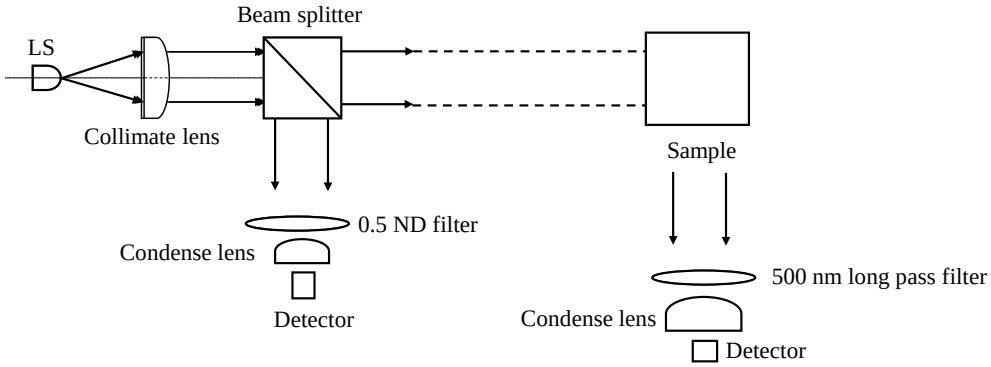

(a)

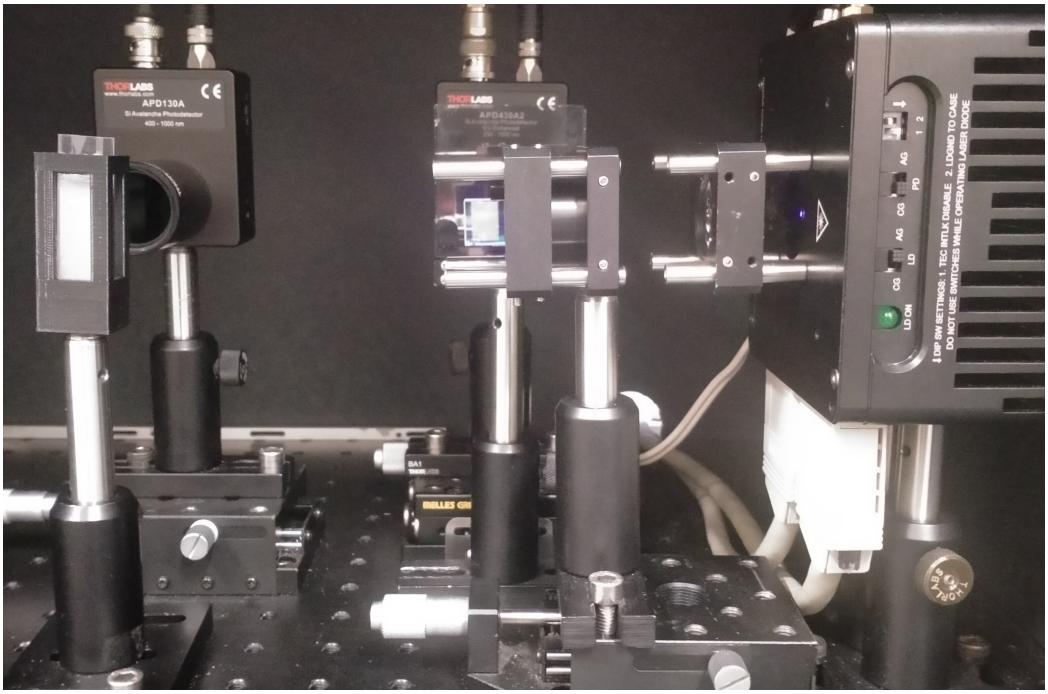

(b)

Figure 4.7: (a) Schematic diagram (b) Experimental setup to measure the lifetime of fluorophores

20 mV amplitude for GQD fluorescence. Figure 4.9 shows the approximate 20 mV amplitude for both detector captures of fluorescein. With reference to APD430A2 (which acts as the reference), the phase shift due to the fluorescence lifetime can be observed in Figure 4.8 and 4.9.

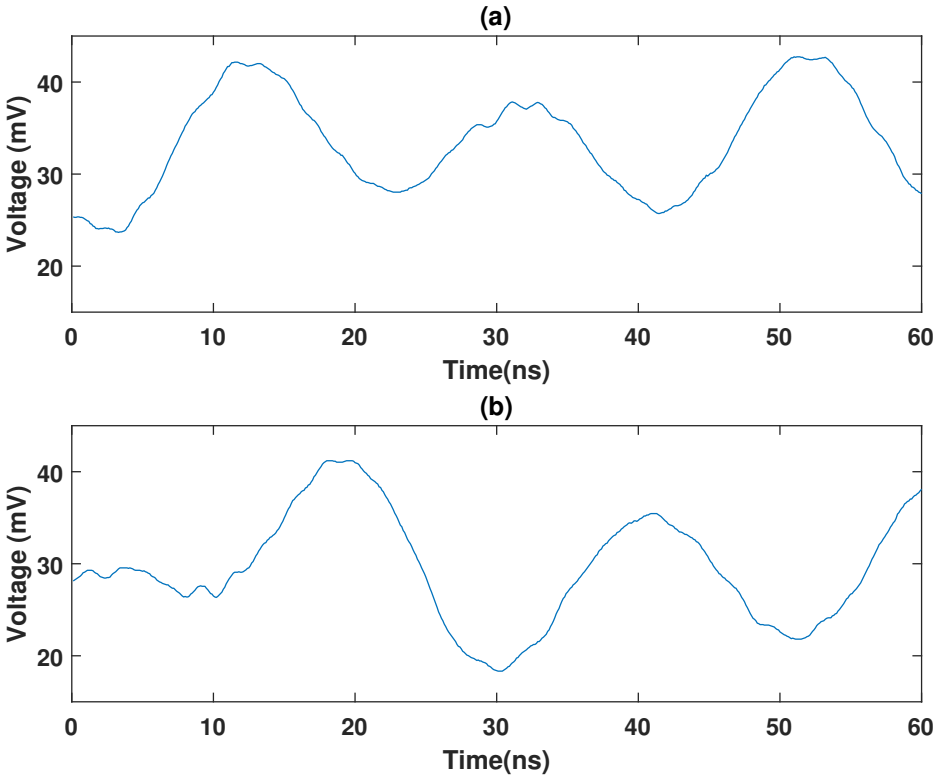

Figure 4.8: GQD fluorescence emission detected signals captured using (a) reference from APD430A2 (b) fluorescence from APD130A at 1000 acquisition points, modulation frequency of 50 MHz and 10 GSa/s

The time-domain data signal from both detectors was converted to frequency-domain data in MATLAB using the Fast Fourier Transform (FFT), which is based on the sampling rate (f_s) (Equation 4.2), sampling interval (Δt), and number of samples (N) collected during acquisition from the oscilloscope. The frequency spacing (Δf) (Equation 4.3) of the sample was determined, and the signal was decomposed into components or bins of different frequency ranges, each determined by the frequency spacing. For example, if the number of samples is 1000, then using Equation 4.3, the frequency spacing of a sample (Δf) is 10 MHz. Hence, 50 MHz signal will be in the 5^{th} bin. Decomposed signals which appear in the other bins are noise generated from the function generators, cables, detectors, and other equipment.

$$f_s = 1/\Delta t \tag{4.2}$$

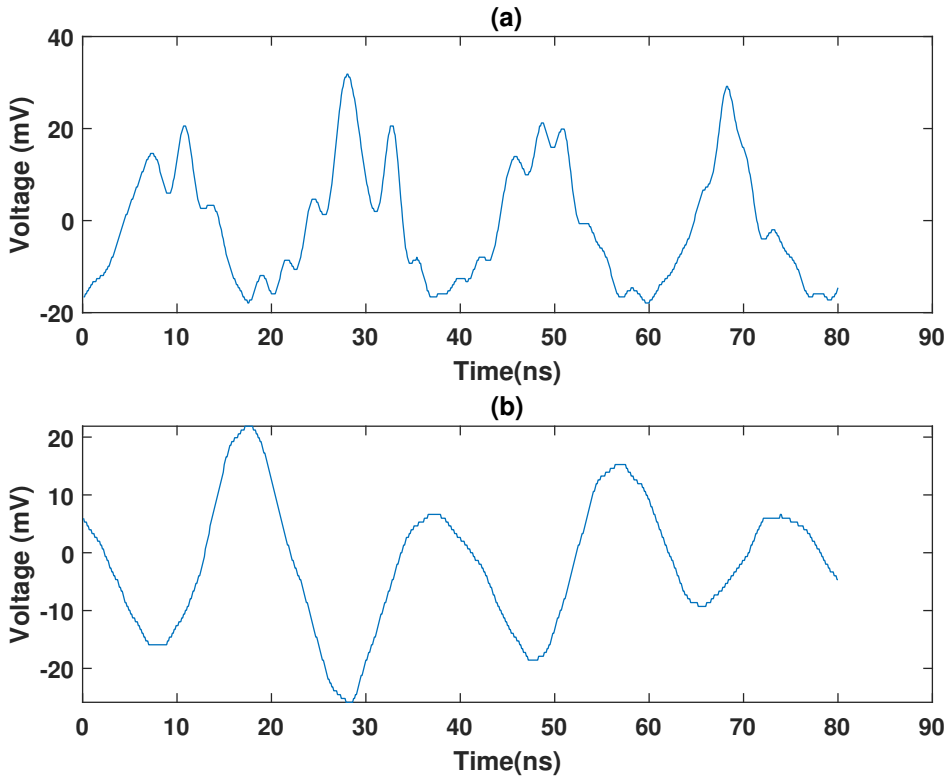

Figure 4.9: Fluorescein fluorescence emission detected signals captured using (a) reference from APD430A2 (b) fluorescence from APD130A at 10,000 acquisition points, modulation frequency of 50 MHz and 10 GSa/s

$$\Delta f = f_s/N \tag{4.3}$$

An example of the FFT signal generated from the analysis of the reference excitation light and fluorescence light for GQD collected at 10 GSa/s over 0.1 μs is shown in Figure 4.10, where the 50 MHz modulation excitation signal is noticeable, while the fluorescence signal is detectable among the other noise components in the other frequency bins.

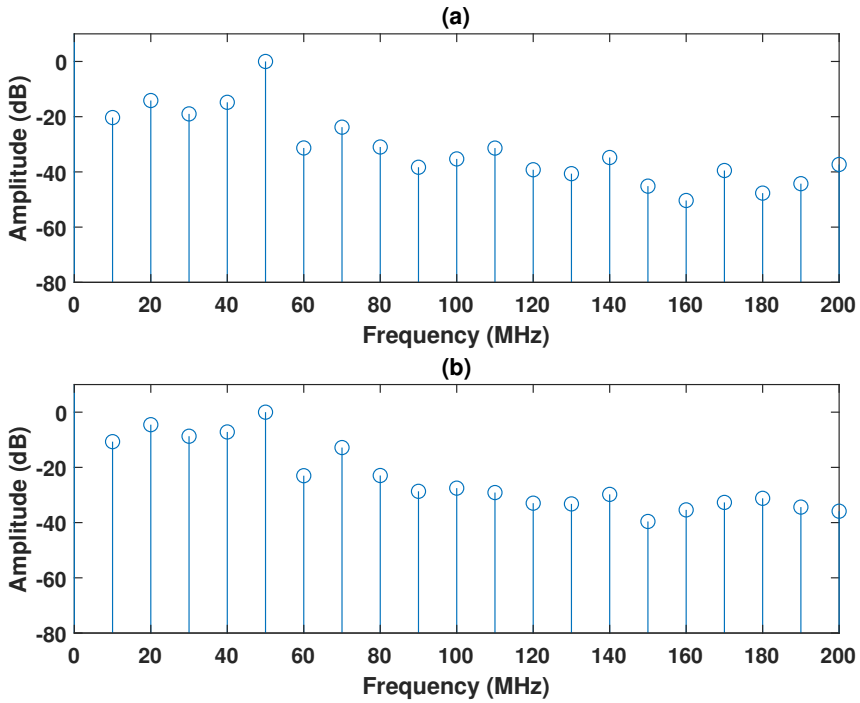

Figure 4.10: FFT signal generated from FFT analysis of (a) reference excitation light modulated at 50 MHz from APD430A2 (b) GQD fluorescence light from APD130A at 1000 acquisition points and 10 GSa/s

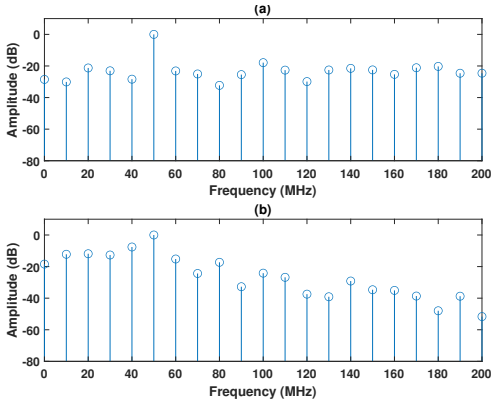

(a) 1000 acquisitions

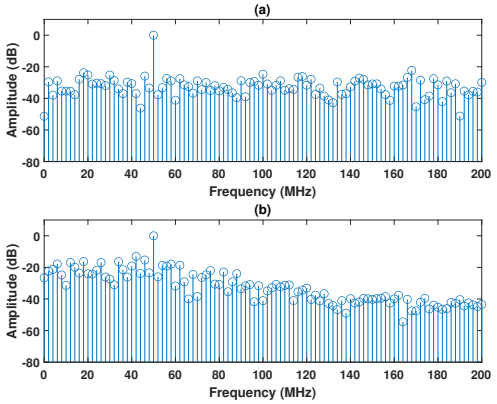

(b) 5000 acquisitions

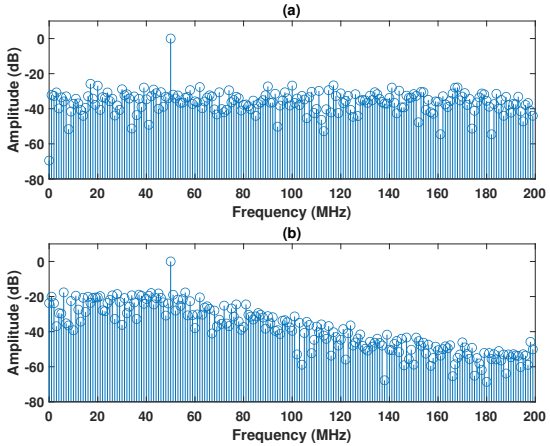

(c) 10000 acquisitions

Figure 4.11: FFT signal generated from FFT analysis of (a) reference excitation light modulated at 50 MHz from APD430A2 (b) fluorescein fluorescence light from APD130A for 1000, 5000, and 10000 acquisition samples.

Figure 4.11 shows the results of the FFT analysis of the 50 MHz modulation excitation signal and fluorescein fluorescence signal collected using acquisition points of 1000, 5000, and 10000. In all cases, the signal was observable at 50 MHz. As the number of acquisition points increased, the clarity of the 50 MHz signal increased. In the 10000 acquisition samples, both 50 MHz signals can be clearly seen, and in the case of the excitation signal, there is a 30 dB difference between the signal and noise, and in the case of the fluorescence signal, there is a 20 dB difference. In contrast, at 1000 acquisition points, there is a 20 dB difference for the excitation signal and a close to 10 dB difference for the fluorescence signal.

Therefore, the number of acquisition points acquired for a sample influences its signal accuracy. Hence, the number of cycles collected within the extracted acquisition points is tabulated in Table 4.1, with the relation of the modulation frequency, period of the signal, and cycles collected within the extraction of 1000,5000,10000 acquisition points.

Table 4.1: Cycles at different acquisition points and modulation frequencies.

Modulation frequency (MHz)	Period (ns)	Cycles per collection		
		Sample acquisition points		
		1000	5000	10000
10	100	1	5	10
20	50	2	10	20
30	33	3	15	30
40	25	4	20	40
50	20	5	25	50
60	17	6	30	60

Therefore, the number of cycles per acquisition increases with the number of acquisition points and modulation frequency. A higher sampling rate or larger sample acquisition would better distinguish the excitation and fluorescence signals from the noise, but the digital storage oscilloscope (Keysight DSO604A) used was limited to 20 GSa/s, so the sample acquisition could be increased, but this would depend on whether or not photobleaching of the fluorophore was occurring (i.e. a reduction in fluorescence over time with repeated exposure to light). Therefore, the sample acquisition time was kept short to reduce the exposure of the fluorophore to light. Therefore, sample collection at 5000 acquisition points was used as a compromise.

After these steps, the MATLAB angle function was used to extract the phase angle of the signals from the appropriate frequency bin (for example 50 MHz bin if 50 MHz was modulation frequency) from the FFT analysis. The difference in the phase angle between the reference signal (θ_{ref}) and the fluorescence signal (θ_{sample}) was measured for each acquisition sample. The mean difference in the phase angle was then obtained. To check for the change in phase angle due to light scattering, the cuvette was packed

with sucrose crystals, and water was added to form a supersaturated solution with largely undissolved sucrose, resulting in a densely packed medium with multiple internal scattering interfaces. In such a system, the incident modulated light can experience multipath propagation, where photons travel through slightly different optical paths before detection. Each path contributes a small phase difference proportional to the optical path length difference, which can be estimated using the relation:

$$\alpha_{multipath} = \frac{\Delta L}{\lambda} \times 2\pi. \tag{4.4}$$

where ΔL is the path length and λ is the wavelength of the excitation signal.

This means that even slight variations in particle spacing or refractive index within the packed sucrose structure can introduce minor phase shifts. For a path length of approximately 10 mm, the calculated phase shift changes only slightly with modulation frequency—from about 0.002 rad at 10 MHz to 0.013 rad at 60 MHz—corresponding to less than one degree over the entire frequency range. This shows that the influence of multipath propagation on the measured phase is very small. These small, frequency-dependent variations remain stable for a fixed optical geometry and are therefore effectively included in the modulation baseline calibration. The experiment was repeated using a solution containing undissolved sucrose to determine the difference in the phase angle owing to the light scattering of the excitation light.

Scatter solution was prepared using sucrose to measure the transmission of light without fluorescence as a reference solution and the phase measurement was calculated using Equation 4.5, which is given in

$$\theta_{diff}^{scatter} = \frac{\sum_{j=1}^{n}(\theta_{sample} - \theta_{ref})}{n}. \tag{4.5}$$

where θ_{sample} is the phase measured from the detector that collects fluorescence and θ_{ref}) is the phase measurement detected at the reference (reflection) beam from the beamsplitter. n is the number of samples collected, each having a selected number of acquisitions per sample.

Then the sample change with the GQD to measure phase due to the fluorescence emission, which is given by,

$$\theta_{diff}^{fl} = \frac{\sum_{j=1}^{n}(\theta_{sample} - \theta_{ref})}{n}. \tag{4.6}$$

Difference of θ_{diff}^{fl} and $\theta_{diff}^{scatter}$ was used to calculate the difference of phase that directly contributes to fluorescence lifetime calculation, that is using Equation 4.7,

$$\tau_{fl} = \frac{\tan\left(\theta_{diff}^{fl} - \theta_{diff}^{scatter}\right)}{2\pi f}. \tag{4.7}$$

Tables 4.2 and 4.5 present the calculated phase angle measurements of the two detectors when excited with sucrose, GQD, and fluorescein samples.

Table 4.2: Phase measurements using sucrose and 0.2 mg/mL GQD samples, exposed at 50 MHz. Data were acquired over 20 acquisitions, each with 1000 points at a 10 GSa/s sampling rate. [SD: standard deviation]

Exposed sample	Repeat 1		Repeat 2		Repeat 3		Repeat4	
	Phase (rad)	SD (rad)	Phase(rad)	SD(rad)	Phase (rad)	SD (rad)	Phase (rad)	SD (rad)
Sucrose	0.4445	0.0525	0.4644	0.0981	0.4737	0.0887	0.478	0.0976
Reference	2.4907	0.0947	2.5018	0.0698	2.4717	0.0919	2.445	0.0732
phase(scatter)	-2.0462	0.108279	-2.0374	0.120398	-1.998	0.127724	-1.967	0.122
0.2 mg/ml GQD	-2.4775	2.3798	-2.7211	2.426	-2.7763	2.692	-2.7169	2.2248
Reference	2.4878	0.0935	2.4496	0.1088	2.4602	0.0832	2.4948	0.0754
phase(flu)	-4.9653	2.381636	-5.1707	2.428438	-5.2365	2.693285	-5.2117	2.226077

Table 4.3: Phase measurements using sucrose and 0.5 mg/L fluorescein samples, exposed at 50 MHz. Data were acquired over 20 acquisitions, each with 1000 points at a 10 GSa/s sampling rate. [SD: standard deviation]

Exposed sample	Repeat 1		Repeat 2		Repeat 3	
	Phase (rad)	SD (rad)	Phase(rad)	SD(rad)	Phase (rad)	SD (rad)
Sucrose	-4.3488	0.0345	-4.3588	0.0417	-4.3363	0.0453
Reference	-2.7322	0.0435	-2.7355	0.0460	-2.7245	0.0511
phase(scatter)	1.6166	0.0555	1.6232	0.0620	1.6118	0.0683
0.5 mg/L fluorescein	-5.2034	0.1688	-5.2006	0.1403	-5.2762	0.1641
Reference	-2.7347	0.0488	-2.7306	0.0491	-2.7499	0.0496
phase(flu)	2.4687	0.1757	2.4700	0.1486	2.5263	0.1714

Table 4.4: Phase measurements calculated using sucrose and 0.5 mg/L fluorescein samples, exposed at a 50 MHz modulation frequency. Data were acquired over 20 acquisitions, each containing 5000 points at a 10 GSa/s sampling rate. [SD: standard deviation.]

Exposed sample	Repeat 1		Repeat 2		Repeat 3	
	Phase (rad)	SD (rad)	Phase(rad)	SD(rad)	Phase (rad)	SD (rad)
Sucrose	-4.3499	0.0187	-4.3527	0.0202	-4.3439	0.0198
Reference	-2.7238	0.0196	-2.7346	0.0274	-2.7241	0.0265
phase(scatter)	1.6260	0.0271	1.6180	0.0340	1.6199	0.0294
0.5 mg/L fluorescein	-5.2017	0.0948	-5.1765	0.0739	-5.2762	0.1641
Referencen)	-2.7321	0.0288	-2.7297	0.0230	-2.7499	0.0496
phase(flu)	2.4695	0.0991	2.4467	0.0774	2.5263	0.1714

Table 4.5: Phase measurements calculated using sucrose and 0.5 mg/L fluorescein samples, exposed at a 50 MHz modulation frequency. Data were acquired over 20 acquisitions, each containing 10000 points at a 10 GSa/s sampling rate. [SD: standard deviation.]

Exposed sample	Repeat 1		Repeat 2		Repeat 3	
	Phase (rad)	SD (rad)	Phase (rad)	SD (rad)	Phase (rad)	SD (rad)
Sucrose	-4.3539	0.0145	-4.3535	0.0157	-4.3509	0.0161
Reference	-2.7205	0.0122	-2.7334	0.0191	-2.7217	0.0167
phase(scatter)	1.6334	0.0190	1.6201	0.0247	1.6292	0.0232
0.5 mg/L fluorescein	-5.2049	0.0586	-5.1981	0.0603	-5.2034	0.0532
Reference	-2.7284	0.0201	-2.7314	0.0196	-2.7330	0.0213
phase(flu)	2.4765	0.0619	2.4667	0.0635	2.4704	0.0573

Initial experiments were conducted using the GQD with 1000 acquisition points. From Table 4.2 repeat measurements of the reference detector signal have a percentage uncertainty below 7%; however, the GQD signal has a very high percentage uncertainty of approximately 96%. This can be attributed to the low signal-to-noise ratio, as shown in Figure 4.10 and the low acquisition point used. On the other hand, the fluorescence signal (fluorescein) captured using 1000 acquisition points in Table 4.3, shows a percentage uncertainty of the reference sample below 4.5%, while that of the sample with 0.5 mg/L fluorescein is approximately 6 to 8%. Furthermore, the fluorescence quantum yield of 95% might have an influence on capturing a better signal compared to the 17% quantum yield in GQD.

With increased acquisition points, 5000 and 10000 (Tables 4.4 and 4.5), the percentage uncertainty of the reference sample decreased to 2% for 5000 acquisition points and less than 1% for 10000 acquisition points. The percentage uncertainty of the fluorescein sample was higher than that of the reference sample. The percentage uncertainties were reduced with an increase in the number of acquisition points. This proves that the acquisition points of a signal and the number of cycles captured during that period influence the uncertainty of the measurement which is related to the error of the signal.

A sample of 0.5 mg/L fluorescein was exposed, and the fluorescence emission of the 50 MHz signal was extracted with 10000 acquisition points. The extracted data were analysed by changing the acquisition points to calculate the fluorescence lifetime, and the results are shown in Table 4.6.

Table 4.6: Fluorescence lifetime calculated with exposed excitation light modulated with 50 MHz frequency to a 0.5 mg/L fluorescein sample, extracted acquisition sample with 1000, 5000, 10000 acquisition points at a sample rate of 10 GSa/s.

Acquisition points	Calculated fluorescence lifetime (ns)									
10000	3.86									
5000	4.21					3.55				
1000	3.64	3.84	4.64	5.02	3.83	4.95	6.81	1.77	4.9	2.32

The calculated fluorescence lifetime (a 0.5 mg/L concentration of fluorescein) for 1000 acquisition samples was 3.64 ns. The 10 samples of 1000 acquisitions showed different fluorescence lifetimes which were not compatible with the fluorescence lifetime of fluorescein. This may be due to the lack of sufficient cycles of the signal within the 1000 segment and the reduction in frequency resolution. However, the fluorescence lifetime(fluorescein) calculated for 5000 and 10000 acquisition samples were 4.21 ns and 3.86 ns, respectively. The calculated values agreed with the Roding *et al.* (2014) calculation of the fluorescein fluorescence lifetime, given as 4.14±0.3 ns.

The fluorescence intensity measurement behaviour with the number of acquisition points extracted per sample might provide a recommendation on the number of ac-

quisition points needed to obtain an accurate and precise measurement. Table 4.7 summarises the fluorescence intensity measured using a 50 MHz modulating frequency and the influence of the number of acquisition points extracted.

Table 4.7: Fluorescence emission (intensity) calculated with exposed excitation light modulated with 50 MHz frequency to a 0.5 mg/L fluorescein sample, extracted acquisition sample with 1000, 5000, 10000 acquisition points at a sample rate of 10 GSa/s.

Acquisition points	Calculated fluorescence intensity (mV)									
10000	43.0									
5000	43.1					43.0				
1000	44.0	43.4	45.1	43.0	39.8	40.2	39.9	44.8	47.6	42.3

On average, a 43 mV signal was measured using both 5000 and 10000 acquisition points; therefore, using 5000 acquisition points does not influence the measurement accuracy.

4.2.1 Instrument communication

The developed prototype used a Tektronix AFG3102 function generator to feed the modulation signal to the system, whereas a Keysight DSO604A storage oscilloscope was used to capture the signal from the APD detectors, and the data were extracted to a computer. This process can be automated with the ability to communicate via instruments using communication techniques. Different communication techniques are used by the measurement instruments to connect to a PC. Serial, parallel, and Universal Serial Bus (USB) ports are commonly available ports in instruments that support communication via RS-232, General Purpose Interface Bus (GPIB), and Virtual Instrument Standard Architecture (VISA) interfaces, which enable the initialisation of communication between devices.

This study used a Keysight DSO604A storage oscilloscope that used the VISA platform and a Tektronix AFG3102 function generator that used GPIB to communicate with the PC. To write and read from an instrument, the Standard Instructions for Programmable Instruments (SCPI) commands were used to automate the data extraction process.

Data extraction algorithm

The prototype of the fluorescence lifetime measuring system has an input modulated signal that is fed through the Tektronix AFG3102 function generator, which communicates with a computer via MATLAB. The 3 V peak to peak signal and operating frequency between 10–60 MHz were sent at a time which is acknowledged by the function generator before proceed to the next step. The laser signal then operated accordingly to produce

an excitation signal which was fed to the developed system. Finally, two detector signals were measured using a Keysight DSO604A oscilloscope, and the data were read back to the computer, where they could be stored for data processing. This process is illustrated in Figure 4.12. According to the VISA and GPIB protocols, the oscilloscope and function generator were initialised to create an object to initiate communication between the instruments. The frequency generator is fed with the required voltage and frequency and then read back to receive the acknowledgement to clarify the settings of the function generator. The folder is then set to extract the data from the oscilloscope, which digitises the measuring channels, and the channel data are saved in a ". txt" file for both channels.

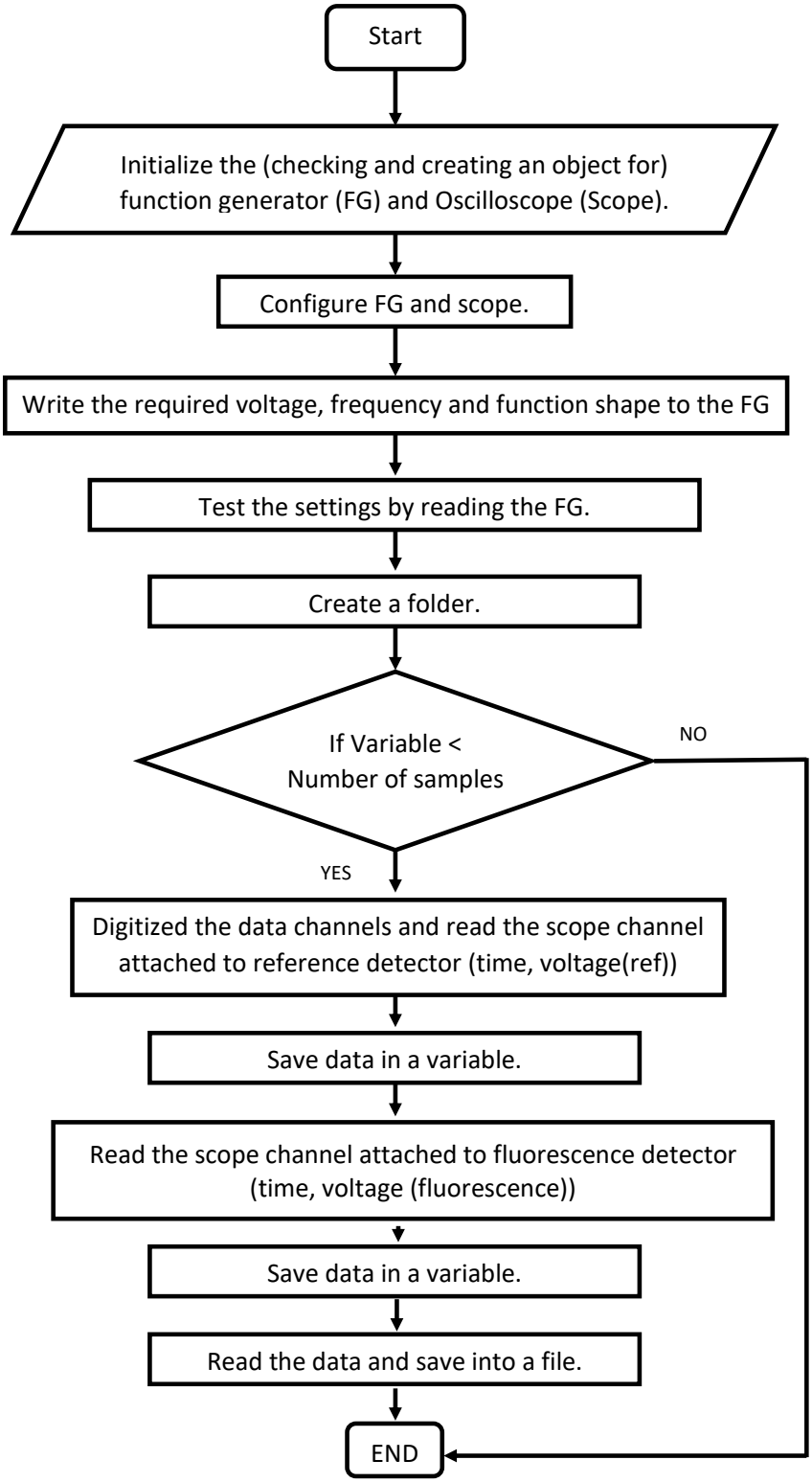

Figure 4.12: An algorithm to set up communication with a function generator and oscilloscope to extract data.

4.3 Fluorophore measurements

4.3.1 Initial analysis using GQD

Initial measurements were performed to test the repeatability of a similar concentration and the variation in the fluorescence lifetime of GQD when the concentration was increased. Hence, 12 GQD samples of 0.2 mg/ml concentration were tested by exciting an optical modulated signal with 3 $V_{(p-p)}$, 50 MHz modulating frequency. The data extracted from the oscilloscope were processed, and the fluorescence lifetime of the GQD is presented in Figure 4.13.

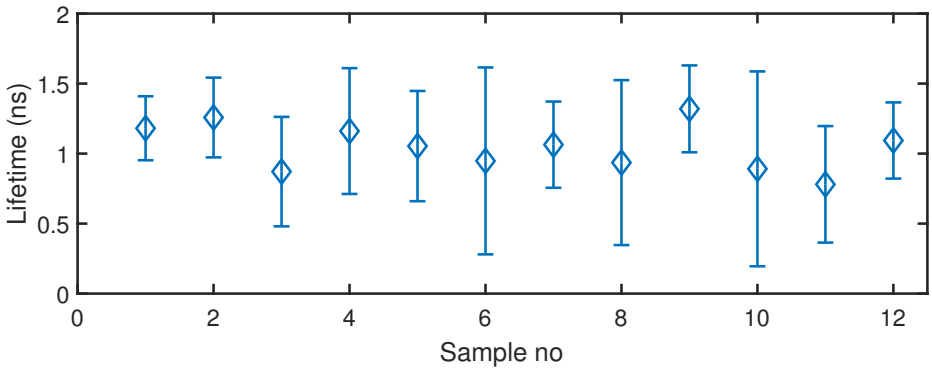

Figure 4.13: Fluorescence lifetime obtained from 12 different GQD samples at 0.2 mg/ml concentration, each expose of excitation collect 7 acquisition samples by collecting 1000 acquisition points for each sample and the sample rate of 10 GSa/s. Error bars indicate uncertainty.

The mean fluorescence lifetime of GQD solutions is 1.05 $\pm$ 0.42 ns. The GQD fluorescence lifetimes of the samples were consistent, and the uncertainty was approximately 0.5 ns in some instances. This can be attributed to the low signal-to-noise ratio with the less fluorescence emission of GQD and insufficient acquisition points captured during the early stages of the research.

The fluorescence lifetime was tested with different concentrations of GQD, and Figure 4.14 illustrates the fluorescence lifetime obtained with 0.1 to 0.9 mg/ml concentration of GQD.

The fluorescence lifetime measurement shows a consistent over the GQD concentrations and on average fluorescence lifetime was calculated as 0.75 $\pm$ 0.5 ns. The results obtained at 0.2 mg/ml concentration of GQD agreed with the measurements shown in Figure 4.13. This proves that the fluorescence lifetime does not vary with the concentration of the fluorophore. The compared results of the averaged fluorescence lifetimes in Figure 4.13 and Figure 4.14 are compatible.

Intensity analysis

The fluorescence intensity provides an idea of the amount of fluorescence emission provided by the fluorophore, and the ratio of the magnitudes of excitation and fluores-

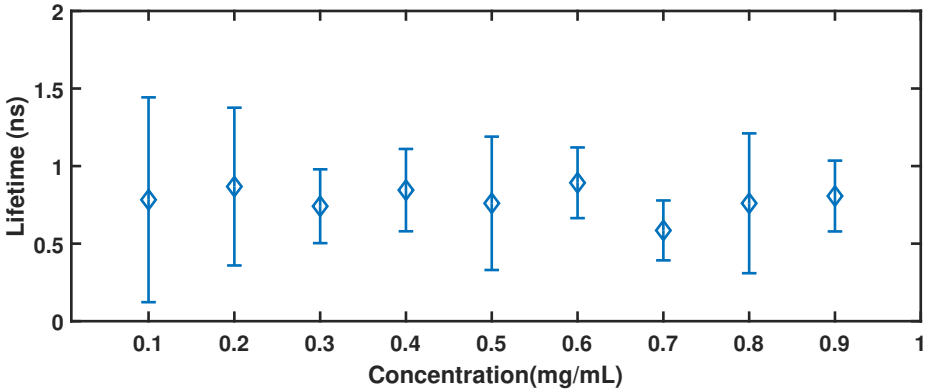

Figure 4.14: Different concentration of GQD tested and calculated for the fluorescence lifetime, each expose of excitation collect 4 acquisition samples by collecting 1000 acquisition points for each sample and the sample rate of 10 GSa/s. Error bars indicate uncertainty.

cence signals was used to calculate the percentage fluorescence intensity (I_f) according to Equation 4.8.

$$I_f = \frac{V_{fl}}{V_{ref}} \times 100\% \tag{4.8}$$

where V_{fl} is the voltage measured by the fluorescence detector and V_{ref} is the excitation signal voltage. The intensity measurements were plotted with different concentrations of GQD, as shown in Figure 4.15.

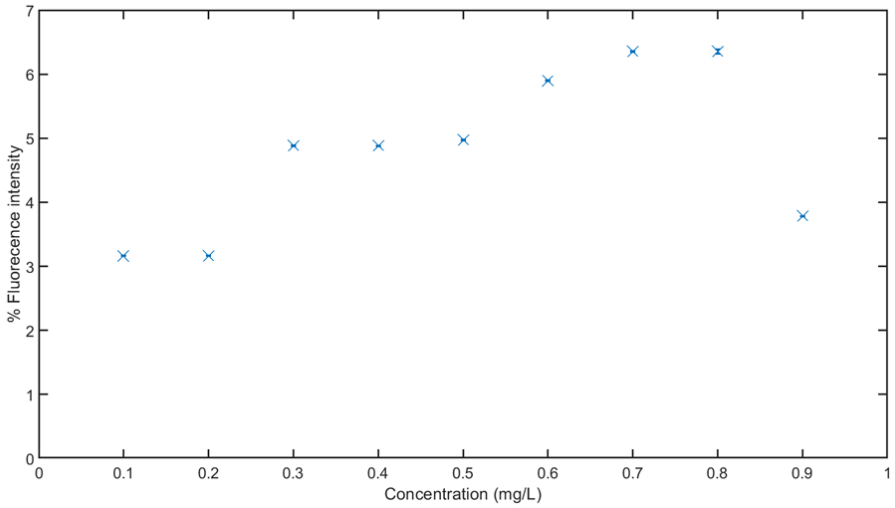

Figure 4.15: Different concentration of GQD tested for intensity analysis

Fluorescence intensity increased until 0.8 mg/ml, then started to decrease with the increased concentration of GQD. Therefore, it is important to test the fluorophore concentration that provides adequate emission to detect the fluorescence signal.

4.3.2 Fluorescein lifetime measurement

As the fluorophore changed from GQD to fluorescein, a 1 mg/ml fluorescein sample was excited with 10–60 MHz modulation frequencies to obtain the fluorescence lifetime. Twenty acquisition samples were extracted by processing each sample with 5000 acquisition points at a sampling rate of 10 GSa/s for each frequency from the oscilloscope. The data were then processed, and the lifetime was calculated using a MATLAB program. An experiment was carried out with the same apparatus using APD130A as the fluorescence detector and APD430A2 as the reference beam detector, and the calculated fluorescence lifetimes are presented in Figure 4.16a. The fluorescence lifetime was calculated using Equation 3.16 considering the signal modulation frequency at the time. The fluorescence lifetime decrease in Figure 4.16a with increasing frequency was identified as a bandwidth limitation of the detector which was 50 MHz. Hence, the positions of the two detectors were interchanged, and the results are shown in Figure 4.16b. Regardless of the position

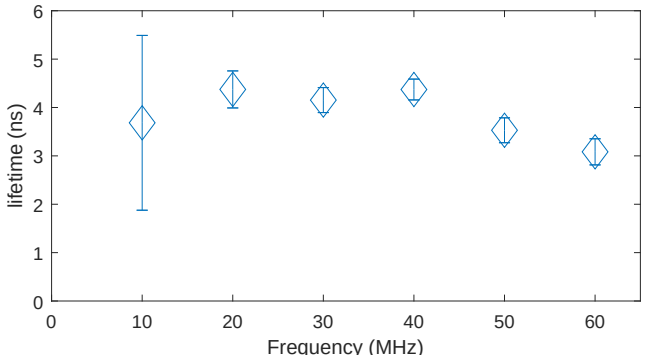

(a) APD130A

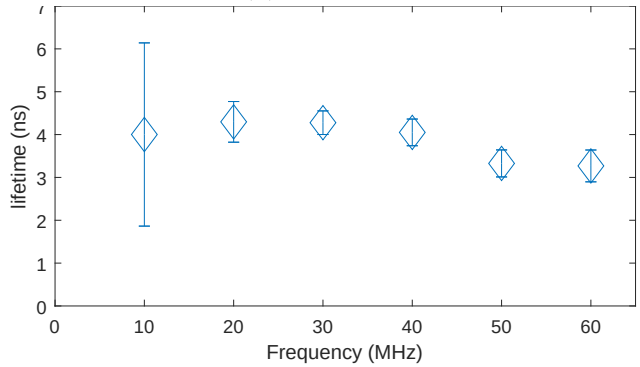

(b) APD430A2

Figure 4.16: Fluorescence lifetime obtained for 10–60 MHz modulation frequencies by processing 20 samples after processing each sample with 5000 acquisition points at a sampling rate of 10 GSa/s. Fluorescence detector used (a) APD130A (b) APD430A2.

of the detector, the calculated fluorescence lifetimes were within the uncertainties. At 10 MHz modulation frequency, the uncertainty is ± 2 ns, which is high compared to the other operated frequencies. A similar decrease in the fluorescence lifetime was observed

which was considered a bandwidth limitation of the detector.

4.4 Contamination of excitation signal

The quantum yield of GQD influences the fluorescence signal measurement, and the fluorescence detection in the scattered (90^0) orientation was between 3 and 6% for different GQD concentrations (Figure 4.15). Therefore, a fluorescence emission detector was placed in front of the sample perpendicular to the transmission beam, and the new configuration is shown in Figure 4.17.

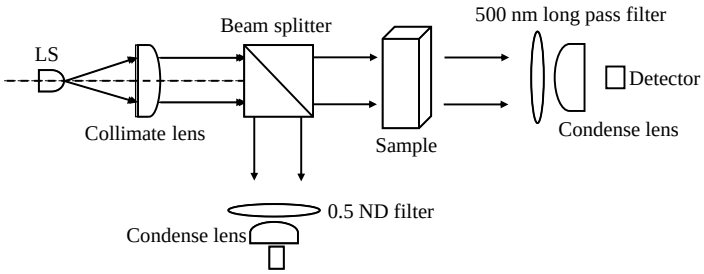

(a)

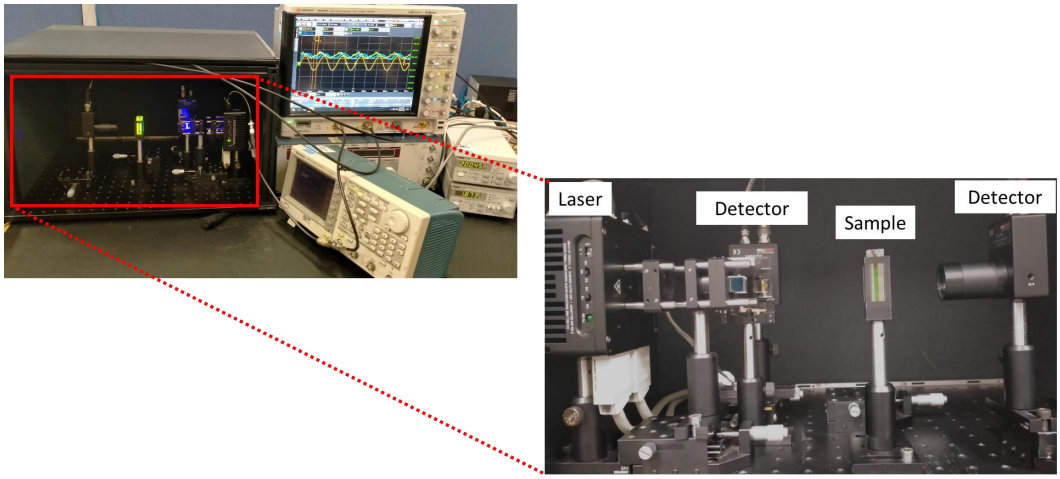

(b)

Figure 4.17: Fluorescence detection using the transmission beam (a) Block diagram (b) Experiment set up that measure the fluorescence.

Optical density (OD) filters are required to be used with the detectors, when the detectors (as the expose power is limited to 1 mW for both detectors) are exposed to the excitation beam to collect fluorescence emission along with the 500 nm long pass filter

(FELH0500) to collect. However, the characteristics of 500 nm long pass filter showed that the optical density of the filter between 450–500 nm is 5.5–5 which indicates any signal power transmit via the 500 nm long pass filter is below 0.5 μW. This corresponds to 0.0001% signal contamination in the fluorescence measurement, compared to the 49 mW excitation light. Hence, a 500 nm long-pass filter (FELH0500) was used with the detector in the transmission path to obtain fluorescence emission from the sample.

However, owing to the limited supply of GQD, these experiments were carried out using fluorescein as an alternative fluorophore with similar fluorescence emission peaks at 520 nm. The data were extracted, and Table 4.8 shows the processed data for six frequencies from 10–60 MHz. A decrease in lifetime with an increased modulation frequency was observed which was similar to the measurements of the scatter configuration (bandwidth limitation of the detector at 50 MHz identified here). The fluorescence lifetime calculated for modulated frequencies between 20 to 40 MHz provided the fluorescein measurement within the uncertainty of the fluorescence lifetime measurements given in Roding *et al.* (2014) (4.14 $\pm$ 0.3 ns).

Table 4.8: Fluorescence lifetimes of 1 mg/ml fluorescein solution measured exciting at 10–60 MHz modulation frequencies, 20 samples after processing each sample with 5000 acquisition points at a sampling rate of 10 GSa/s.

Frequency (MHz)	Lifetime (ns)
10	4.75±0.33
20	4.24±0.25
30	3.81±0.23
40	3.62±0.23
50	3.47±0.22
60	3.40±0.24

The measurements were repeated for three consecutive days for a sample from the 1 mg/ml fluorescein solution. The results are shown in Table 4.9. The lifetime calculated for three days increased, while day1 measurements were considerably higher than those on days 1,2 and 3.

The fluorescein concentration of 1 mg/ml might be a high concentration, and the pH value of the sample was 8.2. The pH of a fluorophore sample is sensitive to the fluorescence lifetime (Kuwana and Sevick-Muraca, 2003). Further analysis is needed to determine the influence of pH on the fluorescence lifetime. Furthermore, placing the fluorescence detector in the transmission path, contamination of the excitation light can influence the measurement, which was considered negligible according to the calculation (below 0.5 μW contamination for an excitation power of 49 mW). The use of condenser lenses to focus fluorescence light to the active area of the detector, might contribute in detecting the excitation light in 450–460 nm in range.

To test whether the contamination dependent on the fluorescence lifetime (Fig-

Table 4.9: Fluorescence lifetimes of 1 mg/ml fluorescein solution measured exciting different modulation frequencies in three days, sample collected with 20 samples after processing each sample with 5000 acquisition points at a sampling rate of 10 GSa/s.

Frequency (MHz)	Lifetime (ns)		
	Day 1	Day 2	Day 3
10	5.31±0.37	4.69±0.33	5.39±0.43
20	4.81±0.33	4.48±0.38	4.34±0.33
30	4.52±0.43	4.24±0.33	4.15±0.34
40	4.32±0.35	4.15±0.28	3.71±0.31
50	4.27±0.33	3.74±0.27	3.88±0.33
60	4.18±0.35	3.65±0.38	3.86±0.33

ure 4.18), a mathematical derivation was given,

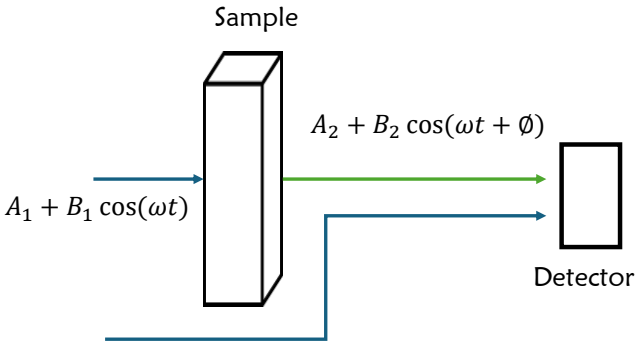

Figure 4.18: Sample contamination of excitation signal

Excitation signal,

$$A_1 + B_1\cos(\omega t)$$

where A_1 and B_1 are the amplitudes of the DC and AC components of the excitation signal, respectively.

Fluorescence signal,

$$A_2 + B_2\cos(\omega t + \Phi)$$

where A_2 and B_2 are the amplitudes of the DC and AC components of the fluorescence signal, respectively.

Signal measured from the detector,

$$A_3 + B_3\cos(\omega t + \Phi) = A_1 + B_1\cos(\omega t) + A_2 + B_2\cos(\omega t + \phi) \tag{4.9}$$

Using trigonometric identities,

$$\tan(\Phi) = \frac{\sin(\phi)}{\frac{B1}{B2} + \cos(\phi)} \tag{4.10}$$

Substituting phase of the Equation 3.16 into ϕ in the Equation 4.10,

$$\tan \Phi_i = \frac{\sin\left(\tan^{-1}(\omega_i \tau)\right)}{C + \cos\left(\tan^{-1}(\omega_i \tau)\right)} \tag{4.11}$$

where ω_i is the measured fluorescence emission phase at each modulation frequency ω_i and $C = B_1/B_2$ is contamination ratio.

As there were measurement of phases using multi frequencies (10–60 MHz), a non-linear fit is performed with the MATLAB nlinfit function to (4.11) to retrieve τ and C.

Excitation contamination was modelled using a multi-frequency approach and simulated to observe the behaviour, and the measured results were compatible with the simulation, as shown in Figure 4.19.

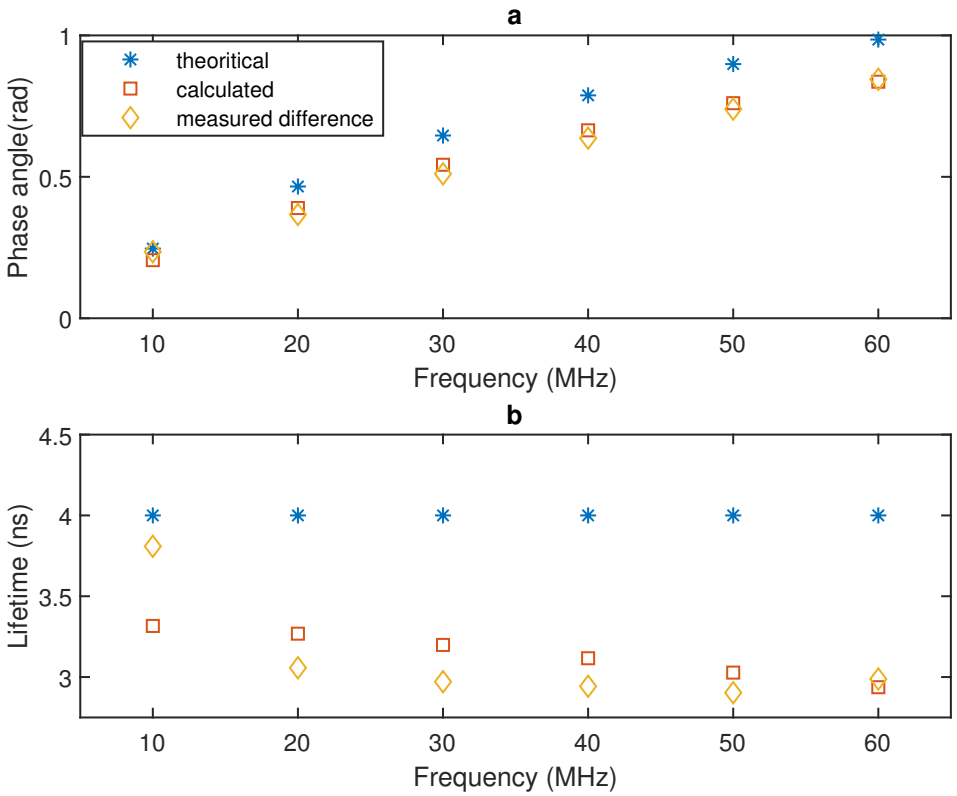

Figure 4.19: Combined signal of excitation and emission influence to (a) phase angle and (b) lifetime of fluorescein

Theoretical phases are calculated considering the fluorescence lifetime of fluorescein to be 4 ns and using Equation 3.16 in Chapter 3 for each modulating frequency, which

are the phases without contamination. These phases are calculated using Equation 4.11 with a 0.1 contamination ratio to obtain the calculated phases. The measured phases were then obtained from the developed prototype system. In the case of excitation contamination, the phases measured via the prototype should be below the theoretical phase without contamination, and the lifetime should always be below the expected fluorescence lifetime. However, the calculated fluorescence lifetimes in Tables 4.8 and 4.9 show lifetimes that are greater than the expected value of 4.1 ± 0.3 ns (Roding *et al.*, 2014).

Some instances the fluorophore can have longer fluorescence lifetime due to lower temperature environment (Paviolo *et al.*, 2013), where the fluorescence lifetime of Rhodamine B is 1.9 ns at 20 ^0C and 1.5 ns at 30 ^0C. Furthermore, intersystem crossing increases the fluorescence lifetime in oxygenated environments (Lakowicz, 2006). Accordingly, environmental conditions might influence the increased phases in days where the environment is colder, or phase variation might be influenced by the pH value of the solution. The fluorophore sample was stored at room temperature which might have contributed to the factors stated. However, further analysis is required to draw a conclusion.

Multi frequency analysis supports the acquisition of more accurate measurements of the fluorescence lifetime, even with contamination. Therefore, this contamination model of multi-frequency measurements analysed using a non-linear regression can be used to estimate the fluorescence lifetime and contamination ratio, which can be used to analyse the properties of floc particles. Figure 4.20 illustrates the measured and estimated data, and the calculated fluorescence lifetime was 3.82 ns which is a considerable value as the fluorescein lifetime is 4.14 ± 0.3 ns according to literature (Roding *et al.*, 2014).

4.5 Summary

A prototype was developed to measure the fluorescence lifetime. This was tested for two fluorophores, GQD and fluorescein, which have a peak fluorescence emission at 520 nm. A beamsplitter was used to obtain the reference excitation signal to eliminate the phase changes introduced to the system through cables and connections. Data acquisition is important, and the SNR can be increased by increasing the number of acquisition points and acquisitions extracted by the system; however, this can increase the time required to take measurements, which can result in photobleaching of the fluorophore.

Scattered orientation is the best position for the fluorescence detector, and the system operates efficiently using high quantum yield fluorophores such as fluorescein. In the case of low quantum yield fluorophores, such as GQD, optical techniques can be adapted to improve the SNR and increase the fluorescence signal. The transmission orientation for collecting fluorescence can be tested using a dichroic filter that passes specific wavelengths while reflecting other wavelengths. This technique is used in

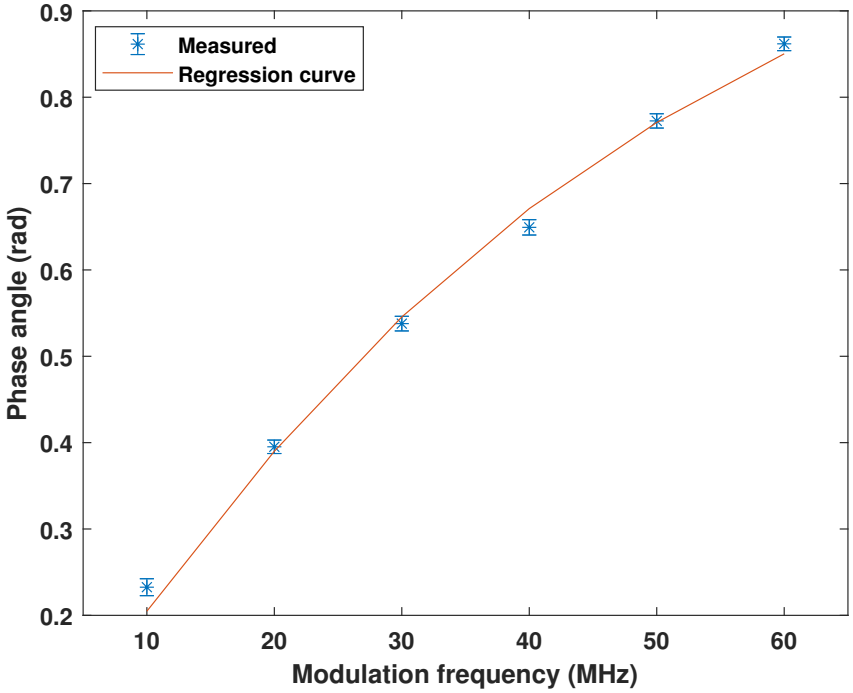

Figure 4.20: Measured phase angle from the multi frequency and the estimated phase angles from non-linear regression

fluorescence microscopy (Esposito, 2012; Wu *et al.*, 2019; Favreau *et al.*, 2014).

A single frequency can be used to calculate the fluorescence lifetime. This is problematic if the fluorescence signal is contaminated with the excitation signal or if other fluorophores with different fluorescence lifetimes are present. Fluorescence lifetime measurements using multi-frequency measurements can be used to separate the fluorescence signals. This is tested in the next chapter.

Chapter 5

Floc and Fluorescence

In water treatment plants, floc particles can be made of materials such as clay, silt, or organic matter. Jar tester is the instrument used to prepare the floc in laboratory. Properties such as turbidity, surface charge, pH, and particle size were measured to understand the floc characteristics. This chapter focuses on providing the experimental methodology developed to test the impact of fluorescence on flocs. The results are discussed to demonstrate the proof of concept of floc behaviour in the presence of light using fluorescence spectroscopy analysis.

5.1 Binding properties of fluorescein

5.1.1 Methodology

Material and methods

Humic acid, kaolin, aluminium sulphate, sodium hydroxide, monobasic potassium phosphate, disodium phosphate, sodium bicarbonate, and fluorescein were supplied by Sigma Aldrich.

A 1 g/L fluorescein solution was prepared with distilled water in a 100 mL volumetric flask. Sodium bicarbonate (50 mg) was added to improve the solubility of fluorescein, and the volumetric flask was mixed until the fluorescein was dissolved before topping up to the final volume with distilled water. The resulting solution was stored in a brown shott bottle at room temperature. 2 L stock solutions of humic acid and kaolin were prepared at 0.5 and 1 g/L concentrations, respectively. A 1 L, 1 g/L aluminium sulphate ($Al_2(SO_4)_3$) solution and a 5 L 0.02 M phosphate buffer solution (pH 7) was also prepared by adding 5.8 g KH_2PO_4 (anhydrous) and 8.2 g $NaHPO_4$ (anhydrous) and adjusting to pH 7 using 1 M NaOH solution. The stock solutions of humic acid and kaolin were then diluted to 20, 40, 60, 80, and 100 mg/L concentrations, 2.5 L of each, unbuffered using distilled water, and buffered using phosphate buffer. The zeta potential

of each unbuffered humic acid and kaolin solution at each concentration was measured by adding 10 mL of the solution to a Mutek Particle Charge Detector (PCD 03) and measuring the zeta potential in mV. The zeta potential was then reduced to zero by gradually adding 50 μl aliquots of aluminium sulphate solution and noting the total volume of alum solution used. The PCD was cleaned between samples. The volume of alum used to reduce the zeta potential to zero for 10 mL was scaled up to 400 mL for each humic acid and kaolin concentration to conduct flocculation experiments using a Boltac jar tester (coagulation and flocculation simulator), as shown in Figure 5.1.

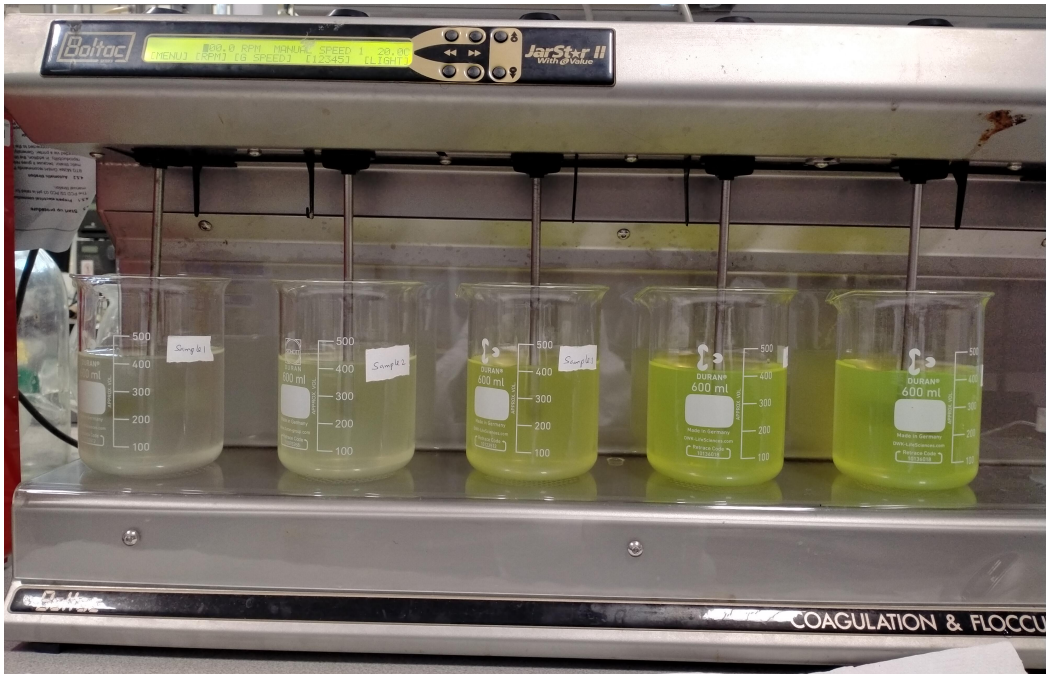

Figure 5.1: Boltac jar tester used as a Coagulation and flocculation simulator

For each flocculation experiment, 400 ml of each humic acid and kaolin solution at each concentration was added to the jar tester, followed by the addition of 0.2 mL of the 1 g/L fluorescein solution and the required volume of alum solution. The mixtures were rapidly mixed at 100 rpm for 2 min, then slowly mixed at 30 rpm for 5 min, and allowed to settle for 5 min. The resulting solution was tested for pH using an Eutech pH150 Meter, turbidity using a 2100P Hach, floc particle size was analysed using a Malvern master particle sizer 3000, and floc morphology using an Olympus BX53 light microscope. 10 ml of each solution was also collected from the 200 ml mark for excitation emission matrix (EEM) fluorescence measurements using a fluorescence spectrophotometer (F7000) 3D scan. The fluorescence was measured by exciting the samples in the 250–580 nm excitation band in 10 nm increments and measuring the emission in the 470–580 nm band, also in 10 nm increments.

In the second set of experiments, 400 ml solutions of 60 mg/L humic acid and 60 mg/L kaolin were mixed with different volumes of 1 g/L fluorescein solution, so

each solution had final fluorescein concentrations of 0.00, 0.12, 0.24, 0.48, 0.72, and 0.96 mg/L. The flocculation experiments were carried out as described in the previous section, and the same tests were conducted on the resulting solutions. In addition, 40 ml of each flocculated solution was collected in 50 mL falcon tubes and centrifuged at 9000 rpm and at a temperature of 4 ^{0}C for 20 min. The supernatant was separated and the pellet was refrigerated at 4 ^{0}C. The supernatant from these samples was tested for fluorescence at an excitation wavelength of 490 nm. This was converted back to fluorescein concentration in the supernatant by comparing the fluorescence against a calibration curve prepared using fluorescein diluted to 0.125, 0.25, 0.5, 0.75, and 1 mg/L in distilled water. The fluorescein concentration in the flocs was calculated by subtracting the final fluorescein concentration in the supernatant from the initial fluorescein concentration, multiplying by the volume of the initial solution, and dividing by the mass of humic acid or kaolin present in the initial solution. An adsorption isotherm was then prepared by plotting the fluorescein concentration in the floc against the final fluorescein concentration in the solution.

5.2 Results and discussion

5.2.1 Zeta potential measurements

The initial zeta potentials of the humic and kaolin solutions at different starting concentrations in distilled water are shown in Figure 5.2 (a). The zeta potential of humic acid solutions was typically around −800 mV, while that of kaolin solutions was around −550 mV. The volume of alum solution required to reduce the zeta potential to zero was largely proportional to the humic acid concentration, while for kaolin, it was proportional up to 80 mg/L kaolin concentration, increasing between the 80 to 100 mg/L kaolin concentration range (Figure 5.2(b)). Al^{3+} dose ranged between 0.14–0.2 g per g humic acid and 0.07–0.14 g per g kaolin. The zeta potential behaviour can be attributed to the different chemical structures of kaolin and humic acid, as described below.

Humic acid is a large organic structure formed from the decomposition of biomass in soil, peat, coal, and sediments, consisting of quinone, phenols, catechol, and sugar moieties, with the phenolic and carboxylic groups readily forming complexes with cations such as magnesium, calcium, ferrous, and ferric ions (de Melo *et al.*, 2016). The Cation Exchange Capacity (CEC) of humic acid was calculated to be between 16 and 23 meq/kg humic acid, which is greater than that of kaolin, as demonstrated by the larger zeta potential of humic acid.

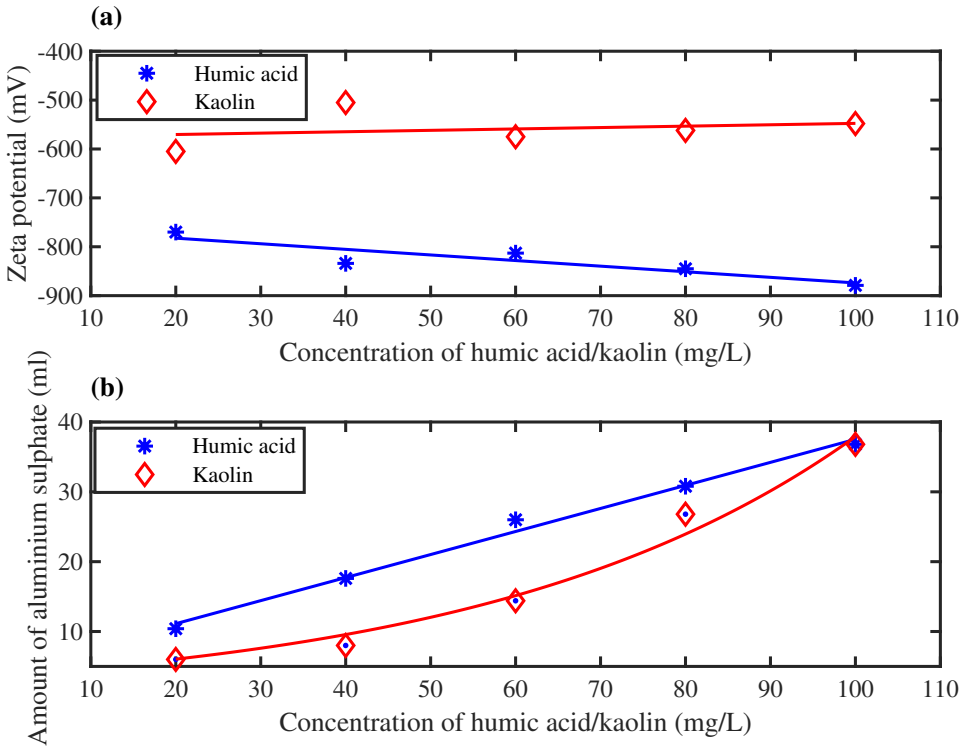

Figure 5.2: (a) Starting zeta potential of the humic and kaolin solutions at different starting concentrations (b) Volume of 1 g/L alum solution required to reduce zeta potential of 400 ml solutions to zero.

5.2.2 Turbidity, pH and particle size measurements

The turbidity of humic acid and kaolin prior to flocculation increased with increasing concentration, as expected (Figure 5.3 (a)). Kaolin had a higher turbidity range from 9.2 to 139 NTU compared to humic acid with 1.1 to 72.9 NTU. This is likely due to the kaolin clay sheet layers hydrating and exfoliating into disc-shaped particles, while humic acid were completely dissolved. The turbidity of the solutions decreased after flocculation, showing a 25% to 82% removal of turbidity for humic acid and a 40% to 72.6% removal for kaolin at concentrations between 60 and 100 mg/L. Using a buffered solution (pH 7) resulted in a much lower removal of kaolin compared to unbuffered solution (pH 4–6.5 —Figure 5.3), and generally, turbidity and pH of the flocculated kaolin solutions increased as fluorescein concentration increased (Figure 5.3 and Figure 5.4).

The pH increase from fluorescein addition is due to the sodium bicarbonate added to the stock fluorescein solution to dissolve fluorescein. Kaolin has an isoelectric point at pH 3–4, and its zeta potential becomes more negative as the pH increases (Dwari and Mishra, 2019), hence more alum is required to flocculate it. In addition, the charge of fluorescein is pH dependent (Le Guern *et al.*, 2020), exhibiting a positive charge at pH 2.1 or less, a neutral charge between pH 2.1 and 4.3, a single negative charge

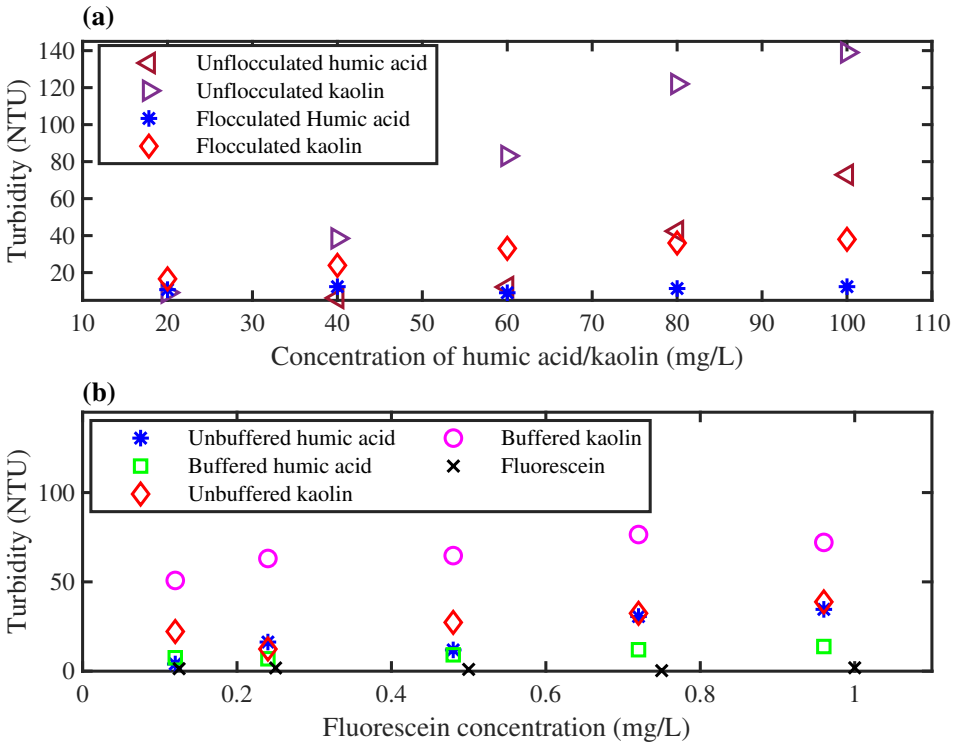

Figure 5.3: Turbidity measured in for (a) flocculated and unflocculated solutions at different concentrations of humic acid and kaolin and 0.48 mg/L fluorescein (b) flocculated solutions of buffered and unbuffered 60 mg/L humic acid and kaolin solutions at different fluorescein concentrations.

between pH 4.3 and 6.4, and two negative charges above pH 6.4. Therefore, as more fluorescein solution was added, the pH charge resulted in a greater negative charge on the fluorescein and kaolin, requiring more alum to neutralise the charge and achieve better flocculation. For humic acid, a buffered solution resulted in lower turbidity than an unbuffered solution. Humic acid also has an isoelectric point between pH 2–4 and becomes more negative as pH increases. However, the structure of humic acid consists of quinone, phenols, catechol, and sugar moieties, similar to the chemical structure of fluorescein; hence, interactions between the aromatic groups of fluorescein and humic acid, as well as hydrogen bonding, will play an important role and appear to be more favourable at pH 6.9 than at the unbuffered pH of 3.97 to 6.24. Figure 5.5 shows the average particle size measured using the Malvern Mastersizer 3000 after flocculation in unbuffered humic acid and kaolin solutions. The particle size generally decreased with increasing concentrations of humic acid and kaolin (Figure 5.5(a)), which corresponds with the increase in turbidity observed under the same conditions in Figure 5.3(a). This trend is partly due to an increase in solution pH (Figure 5.4(a)), leading to a more negative zeta potential for humic acid and kaolin, thereby requiring more alum for effective flocculation. In addition, the ratio of fluorescein to humic acid and kaolin decreases; it appears from Figure 5.5(b) that as fluorescein concentration increases (i.e.

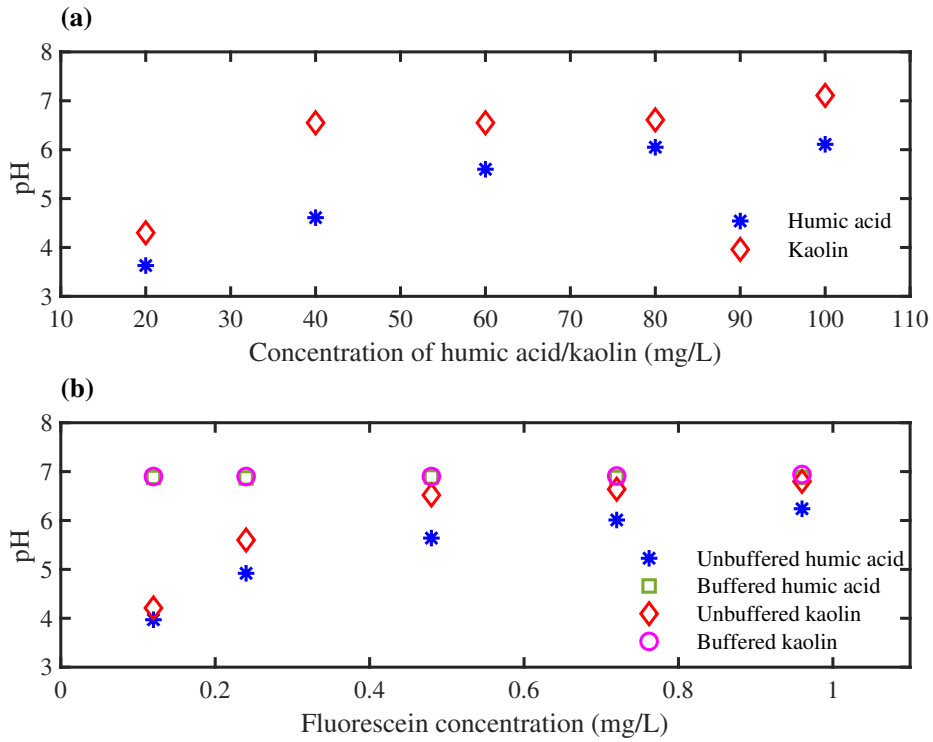

Figure 5.4: pH measurements for (a) flocculated solutions at different concentrations of humic acid and kaolin and 0.48 mg/L fluorescein (b) flocculated solutions of buffered and unbuffered 60 mg/L humic acid and kaolin solutions at different fluorescein concentrations.

the ratio of fluorescein to humic acid and kaolin increases), the particle size increases for kaolin, while humic acid has the largest particle size at a fluorescein concentration of 0.5 to 0.7 mg/L; hence, fluorescein contributes to some extent as a flocculant.

5.2.3 Floc morphology

Observation of the floc particles under a light microscope showed that kaolin floc particles are largely non-spherical and flat, with the one observed in the image 222 to 223 μm in size (Figure 5.6). Humic acid flocs flocculated from 20–40 mg/L humic acid solutions (i.e. a high ratio of fluorescein to humic acid) were non-spherical and flat, while higher concentrations of humic acid (i.e. a low ratio of fluorescein to humic acid) resulted in floc particles with a more dense spherical shape (as shown in Figure 5.7(a,b)). This suggests that fluorescein plays a role in bridging flocs, resulting in larger flocs (as shown in Figure 5.7(c,d)) and a flatter, less spherical appearance. This has important implications for using fluorescein as a fluorophore, as high ratios of fluorescein to particulate and dissolved matter result in morphological changes to the flocs which will impact the interpretation of fluorescence data from floc particles. Ideally, the fluorescein dose needs to be low enough to maintain a floc morphology similar to what would normally occur, but high enough to generate a fluorescence emission signal so that the light penetration

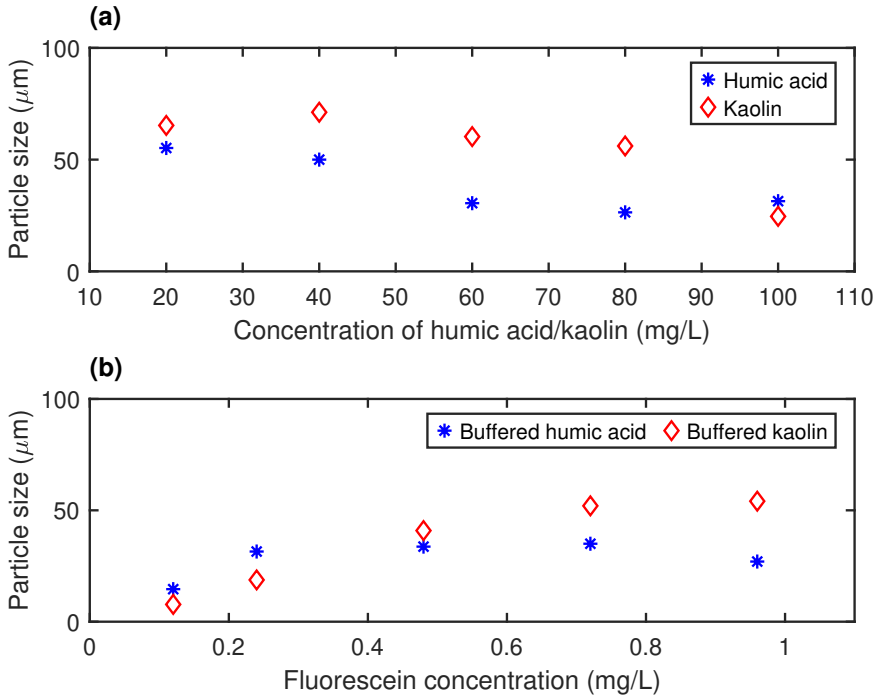

Figure 5.5: Particle size measurements for (a) unbuffered flocculated solutions at different concentrations of humic acid and kaolin and 0.48 mg/L fluorescein (b) buffered flocculated solutions 60 mg/L humic acid and kaolin solutions at different fluorescein concentrations.

of the floc can be accurately measured.

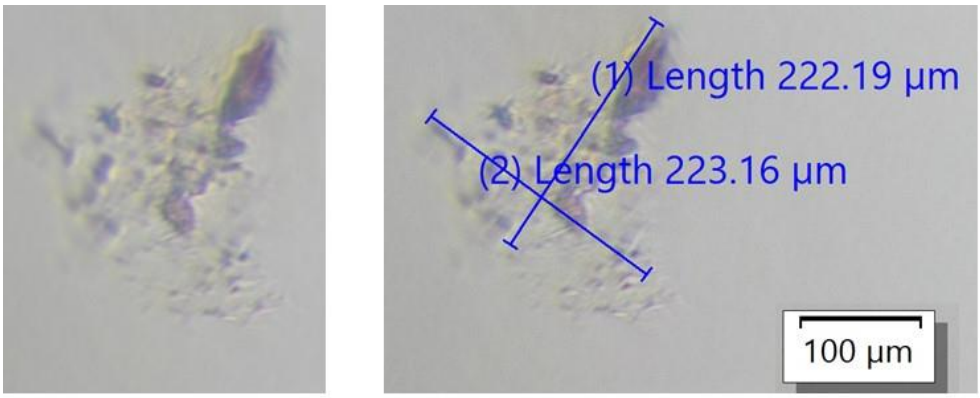

Figure 5.6: Microscope images (20x magnification) of kaolin floc particles from 20 mg/L unbuffered kaolin solutions with 0.48 mg/L fluorescein.

5.2.4 Fluorescence measurements

Fluorescein fluoresces at excitation wavelengths between 250 nm to 330 nm and 450 to 520 nm peaking at the 510 nm emission wavelength, when excited at 260 nm and 490 nm as shown in Figure 4.4.

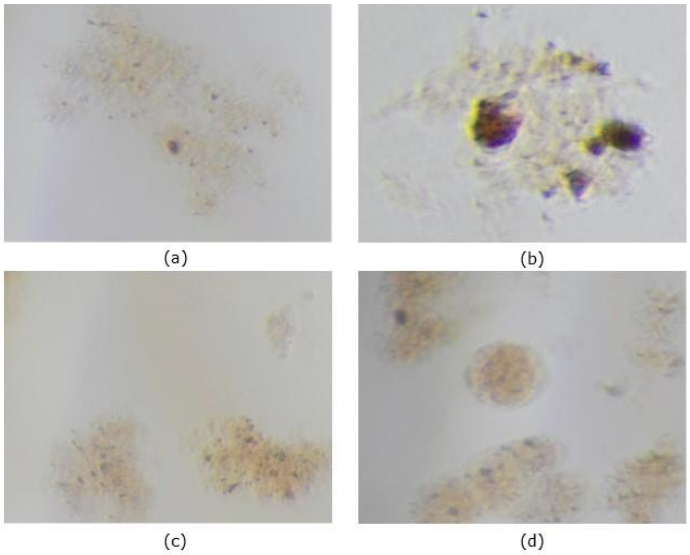

Figure 5.7: Microscope images (20x magnification) of humic acid floc particles from (a) 20 mg/L, (b) 40 mg/L, (c) 60 mg/L and (d) 80 mg/L, unbuffered humic acid solutions with 0.48 mg/L fluorescein.

This shows that fluorescein can be used to measure UV and visible light penetration, and the fluorescence is at a significantly different wavelength to the wavelength used to excite the fluorophore. In addition, the emission from fluorescein when excited at 490 nm is approximately 80% of that emitted when excited at 260 nm; therefore, excitation at visible wavelengths is a reasonable proxy for measuring fluorescence at the wavelengths used for UV disinfection. The accuracy of the measurements will depend on the absorbance spectrum of the material from which the floc is made (in addition, some materials are auto-fluorescing, e.g. chemical and protein structures containing aromatic groups such as porphyrins, tyrosine, and tryptophan), but this can be measured using EEM and corrected for the differences in emission at the different wavelengths.

As kaolin and humic acid concentrations increased, a scattering effect in the fluorescence data was observed, as shown by first- and second-order Rayleigh scattering (Figure 5.8) (Tan *et al.*, 2020), and a reduction in fluorescence emissions. The scattering is due to the flocculated material scattering the light, as observed by the emission wavelength matching the excitation wavelength for the first order, and the second order scattering due to the excitation light diffracting off the monochromator, passing through the sample, and scattering as well, both of which become observable as the fluorescence emission decreases due to the equipment auto-scaling of the signal received. Scattering is stronger with kaolin because it is white and more reflective, while humic acid has a brown/black colour, is more absorbing, and exhibits a fluorescence signal at the 250-280 nm excitation wavelength due to the abundance of aromatic groups in its structure (termed auto-fluorescence, see (Ma *et al.*, 2017)). To examine the effect of fluorescein on fluorescence and scattering, another study was conducted using kaolin (60 mg/L)

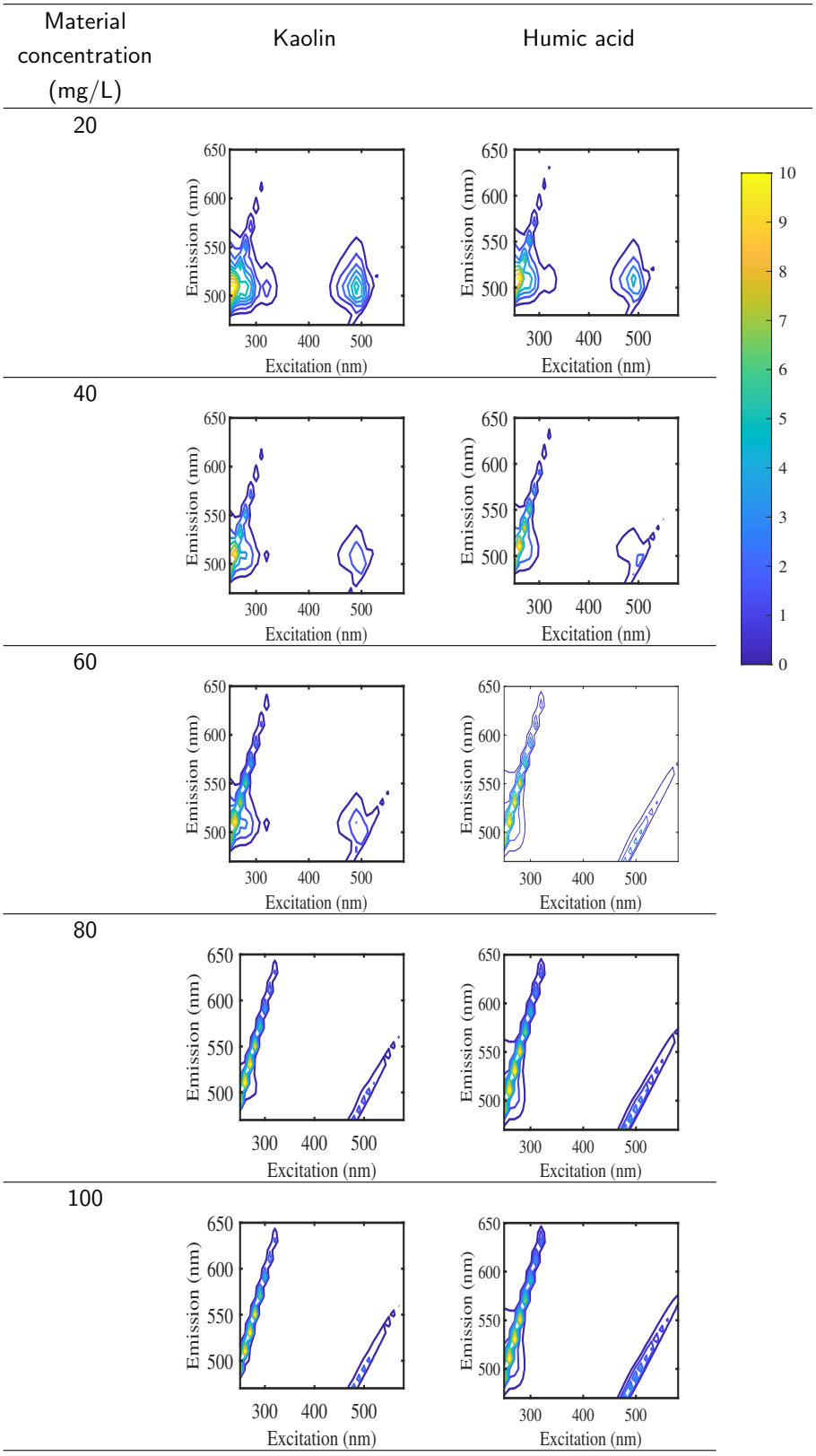

Figure 5.8: Fluorescence emission from flocculated solutions containing 0.5 mg/L fluorescein and different kaolin and humic acid levels.

and humic acid samples at different concentrations of fluorescein.

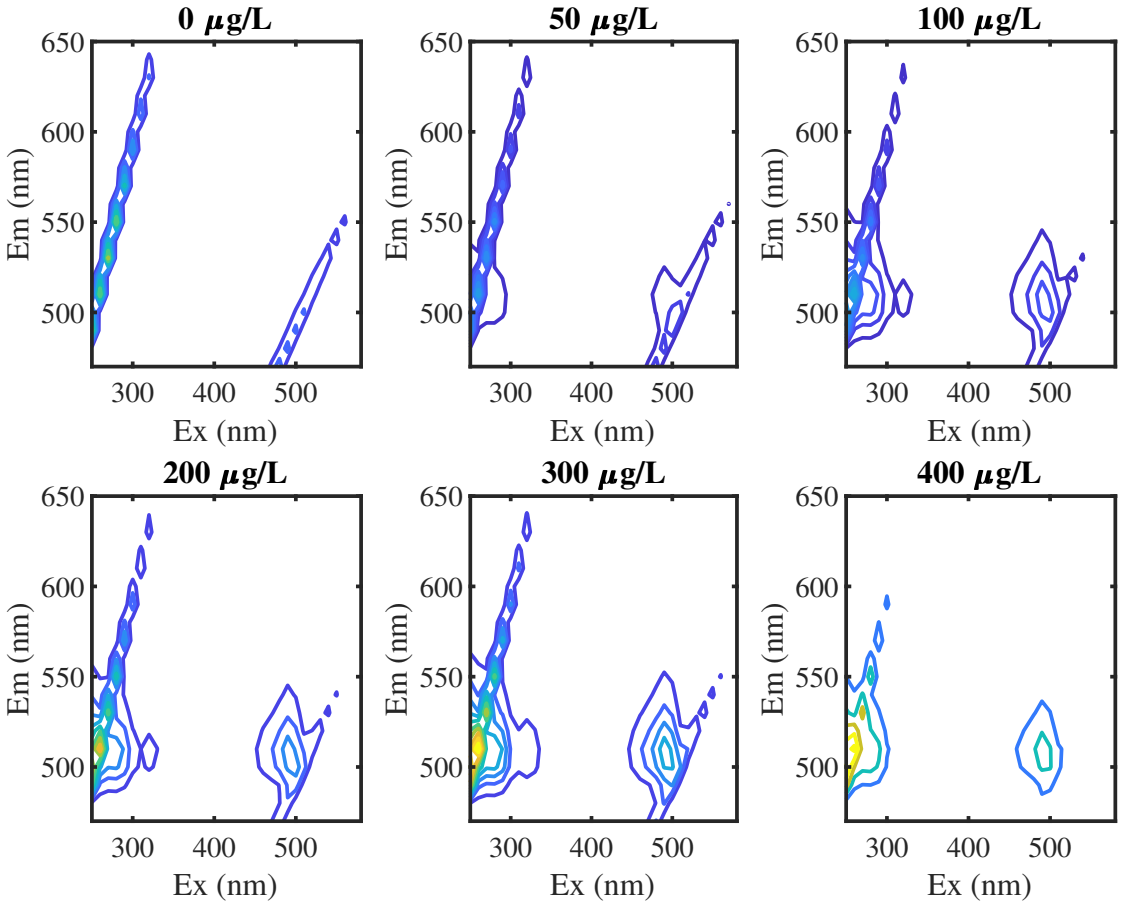

Figure 5.9: Fluorescence emission data for flocculated solutions containing different concentrations of fluorescein in 60 mg/L of kaolin

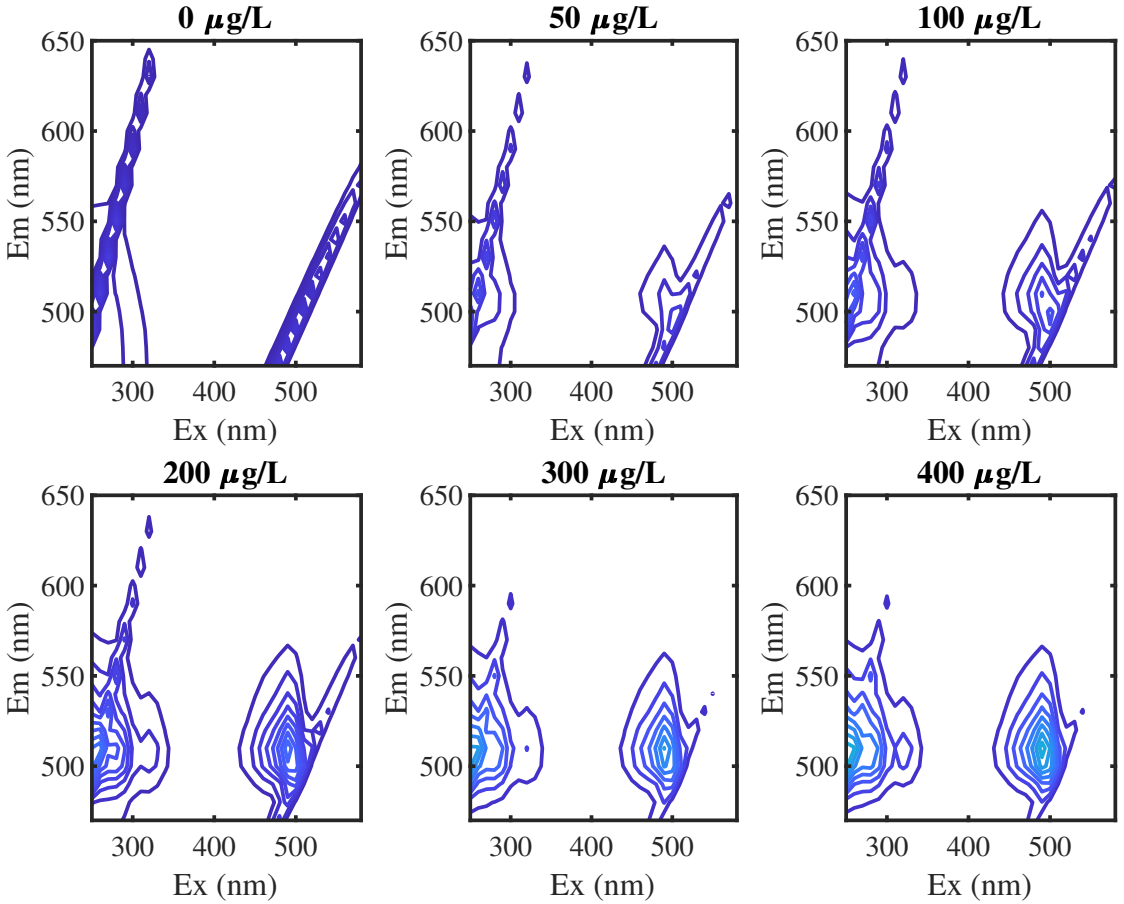

Figure 5.10: Fluorescence emission data for flocculated solutions containing different concentrations of fluorescein in 60 mg/L of humic

As the fluorescein concentration increased, the scattering effect was reduced and was barely observable at a fluorescein concentration of 1 mg/L. The auto-fluorescence of humic acid is observed in Figure 5.10 for the sample with 0 mg/L fluorescein, as the sample does not have fluorescein. To generate a reasonable fluorescence signal, kaolin required at least 1 mg fluorescein per 60 mg of kaolin, while humic acid required 0.72 mg fluorescein per 60 mg humic acid.

5.2.5 Fluorescein adsorption results

The fluorescence of the samples can originate from free fluorescein in the solution and from bound fluorescein in the floc. Ideally, most of the fluorescein should be bound to the floc to generate reliable light penetration data for the floc from fluorescence measurements. To examine the extent of fluorescein adsorption into floc samples of buffered flocculated humic acid and kaolin solutions, the samples were centrifuged to remove the floc particles, and the fluorescence of the supernatant was measured. Fluorescence data were compared against a calibration to determine the fluorescein concentration in the solution, and by mass balance, the concentration of fluorescein in the floc, which was then used to generate adsorption isotherms, as shown in Figure 5.11.

The isotherms were nonlinear and unfavourable; that is, fluorescein had a low affinity for humic acid and kaolin flocs and predominantly resided in solution at low fluorescein concentrations. Fluorescein adsorption was greater on kaolin than on humic acid reaching a concentration of 4 mg/g kaolin and 0.35 mg/g on humic acid. Among the isotherm models applied, the Henry and Langmuir isotherms provided the worst fits, while the Freundlich isotherm:

$$\mathrm{Q} = KC^{1/\mathrm{n}} \tag{5.1}$$

where Q is the adsorbed amount at equilibrium, K is the adsorption capacity, and $1/n$ is the adsorption intensity) provided the best fit for kaolin solutions (Figure 5.11a). Freundlich isotherm model parameters were determined using the least-squares curve fitting method in MATLAB and were found to be $K = 7.094$ and $n = 0.515$. The SIPs isotherm:

$$\mathrm{Q} = \frac{K^{'}C^{\beta}}{1 + \alpha C^{\beta}} \tag{5.2}$$

where Q is the adsorbed amount at equilibrium, β is a model exponent, α and $K^{'}$ are model constants (Kalam *et al.*, 2021), which provided the best fit for humic acid solutions (Figure 5.11b). The SIPS model parameters are $K^{'} = 1.975$, $\alpha = 7.257$, and $\beta = 3.51$.

Ideally, the adsorption isotherm should be Langmuir, that is, fluorescein has a high affinity for humic acid and kaolin and will be present in high concentrations on the floc, even at low concentrations in solution. Based on previous findings for turbidity, pH,

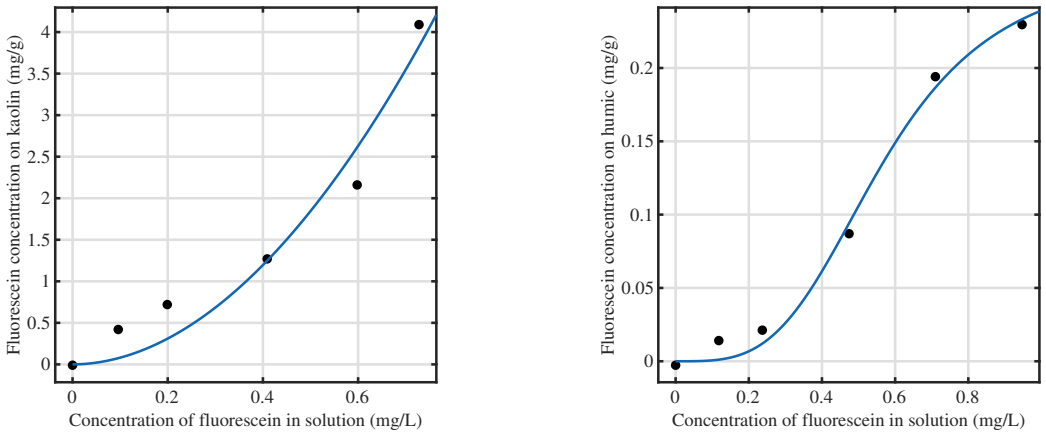

(a) (b)

Figure 5.11: Fluorescein adsorption isotherms for flocculated samples containing (a) 60 mg/L kaolin and (b) 60 mg/L humic acid.

and particle size and the explanations provided, kaolin, humic acid, and fluorescein had a negative charge under the conditions used, and the alum doses used were not high enough to promote good flocculation. The humic acid model demonstrates an excellent fit to the experimental data, with an R^2 of 0.9979 and an adjusted R^2 of 0.9965, indicating that nearly all variability is explained by the model. The low SSE (0.0002) and RMSE (0.0080) confirm high predictive accuracy. In contrast, the kaolin model shows a moderate fit, with an R^2 of 0.7492 and an adjusted R^2 of 0.6865, explaining about 75% of the variability. The higher SSE (5.0843) and RMSE (1.1274) indicate greater prediction error. These results suggest that while the humic acid model is highly reliable, the kaolin model requires refinement or additional data to improve accuracy and parameter stability.

Hence, another trial was conducted by adjusting the amount of alum required to neutralise the potential of fluorescein mixed with either humic acid or kaolin. The same procedure was used to draw the isotherms, as shown in Figure 5.12. This shows that increasing the amount of alum increased the amount of fluorescein attached to the kaolin and humic acid floc. However, this is not sufficient evidence to show that fluorescein is absorbed into the floc.

5.3 Surface charge analysis for particles

The stability of a colloidal dispersion is determined by its surface charge. Similarly charged particles repel each other, preventing sedimentation and aggregation. Surface charge frequently depends on pH, which affects particle behaviour in various pH ranges. Hence, this section focuses on understanding the surface charge variation with different compounds.

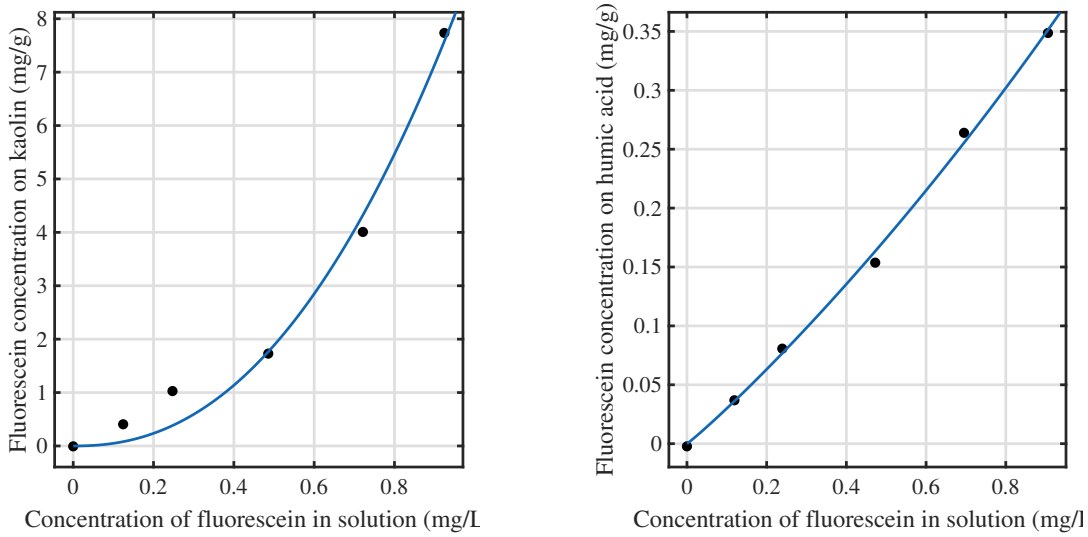

Figure 5.12: Fluorescein adsorption isotherm for flocculated with additional alum in samples using (a) 60 mg/L kaolin and (b) 60 mg/L humic acid.

5.3.1 Solvent behaviour influence surface charge

Surface charge analysis of different particles in water (kaolin, humic acid, and bentonite) was performed using a Mutek Particle Charge Detector (PCD 03). Each solution was tested with a 10 mL volume and a concentration of 60 mg/L.

Buffer behaviour with compounds

A buffered solution was used to maintain the pH of the solution. Figure 5.13 illustrates the behaviour of the surface charge on buffered pH 7, buffered bentonite, and buffered kaolin solutions.

The buffered solution charges became more negative when alum was added to the solution. After reaching the negative peak, it began to neutralise the negative charges. Hence, a buffered solution requires more alum to neutralise the sample. Therefore, maintaining pH using a buffered solution is not suitable for coagulation and flocculation testing. Moreover, tap water is pH-controlled; therefore, tap water is an alternative to buffered solutions.

Tap water behaviour with compounds

A 60 mg/L concentration of kaolin, humic acid, and bentonite solutions with a concentration of 60 mg/L were prepared using tap water treated at the Hamilton water treatment station, New Zealand. These samples were tested along with 0.5 mg/L fluorescein solution to test the surface charge variation with the addition of 1 g/L alum solution.

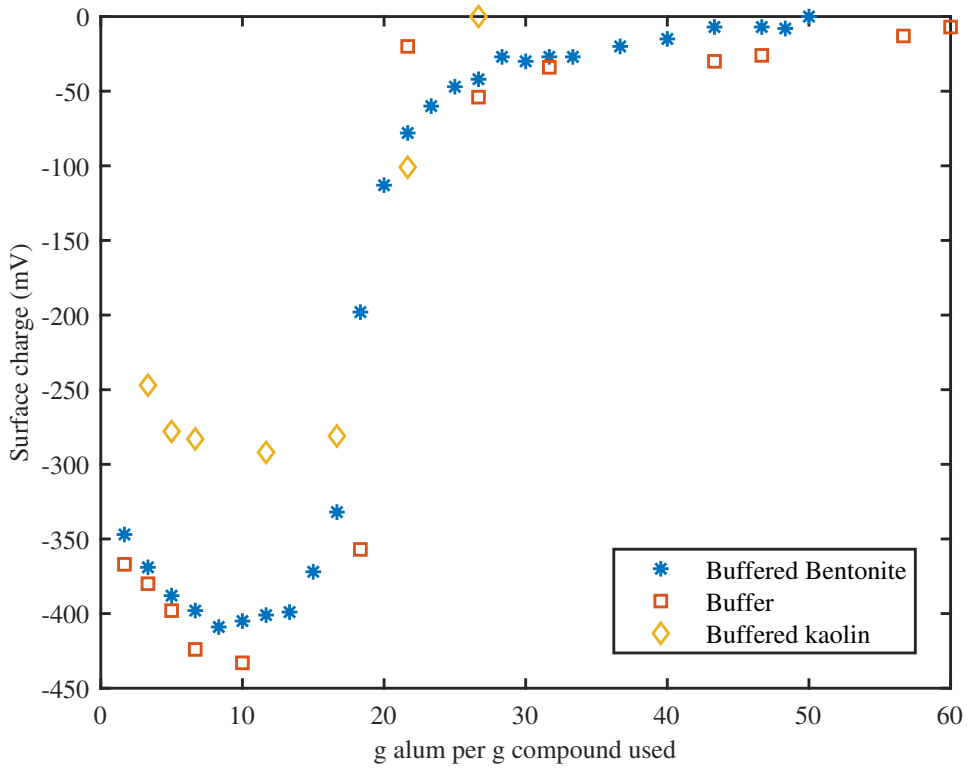

Figure 5.13: Different buffered solutions influence to the surface charge, with solutions of pH 7 buffered 60 mg/L kaolin and humic acid solutions.

Figure 5.14 presents the surface charge variation in the presence of alum, which acts as a coagulant to neutralise the surface charges of the particles.

Humic acid had the highest surface charge among the three compounds, followed by kaolin and bentonite. However, the variations in kaolin and bentonite behave similarly, and the same amount of alum is used to neutralise the negative charges. The behaviour of humic acid is interesting, as it requires more alum until it reaches −350 mV, then gradually neutralises the solution.

Fluorescein influence to the bentonite solution

Surface charge of particles have an influence of absorption or adsorption into another particle. Hence, an experiment was conducted to study the influence of the surface charge of the bentonite solution. A concentration of 60 mg/L was prepared using tap water, and 10 ml of the bentonite solution was used to test the surface charge variation using a PCD 03 when different concentrations of fluorescein were added to the sample (Figure 5.15).

There was a slight increase in the negative surface charge caused by fluorescein. Fluorescein generates negative charge when pH value exceeds 6.5 (Le Guern *et al.*, 2020), which consumes more alum to neutralize the solution.

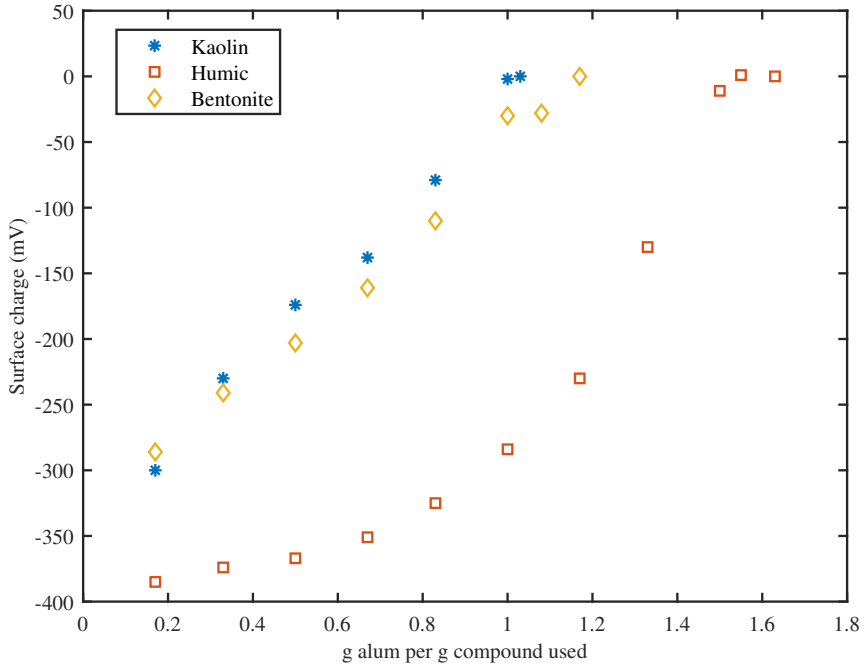

Figure 5.14: The surface charge influence on 60 mg/L kaolin, bentonite and humic acid solutions.

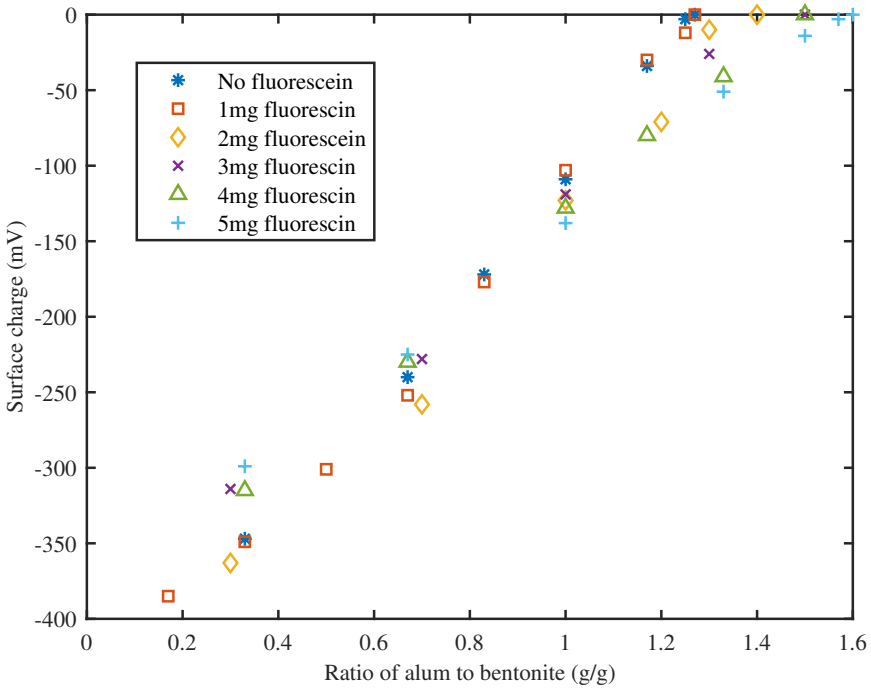

Figure 5.15: Different fluorescein amounts mixed with alum (1 g/L) to bentonite (60 mg/L) ratio to test the influence on the surface charge.

5.4 Summary

Overall, the results indicate that only a small amount of fluorescein attaches to the floc particles, regardless of the compound used to prepare the floc, and fluorescein does not penetrate inside the floc. The negative charge in materials found in water and fluorescein may repel each other, where a third agent is required to form the bond. If this occurs, there is a possibility of testing light penetration via flocs.

Chapter 6

Fluorescence Lifetime Measurements

The use of a single frequency to measure the fluorescence lifetime can lead to accuracy problems when the measured signal is contaminated with the excitation signal or when another fluorophore is present in the sample. A multi-frequency analysis eliminates lifetime analysis errors due to excitation contamination and provides reliable fluorescence lifetime measurements as well as the contamination ratio. This chapter provides the results of the multi-frequency analysis conducted for the floc particle samples produced from humic acid, kaolin, and fluorescein.

6.1 Signal analysis

The optical setup for measuring the fluorescence lifetime was oriented in the scatter orientation to minimise the contamination of the received signal with the excitation light. The laser beam intensity was set to 100 mW and was modulated at frequencies 10–60 MHz. The oscilloscope was set to a sampling rate of 10 GSa/s. The oscilloscope acquisition was triggered by the rising edge of the sinusoidal signal applied to the laser. Ten acquisition samples, each with 5000 acquisition points for each modulation frequency, were extracted from the oscilloscope. Excitation light scattering was determined using a reference sample containing sucrose crystals mixed with water. The transmitted excitation signal was observed via a neutral density (ND) filter of 1, and the scattered signal from the reference sample was measured using a 1.5 ND filter. Subsequently, the reference sample was changed to a sample containing 0.25 mg/L fluorescein in water, and the 1.5 nm ND filter was changed to a 500 nm long-pass filter to filter out the excitation light. The two signals measured using the two detectors were processed to obtain the phase measurements. The signals obtained from the detectors, transmission excitation beam, and fluorescence scatter are shown in Figure 6.1.

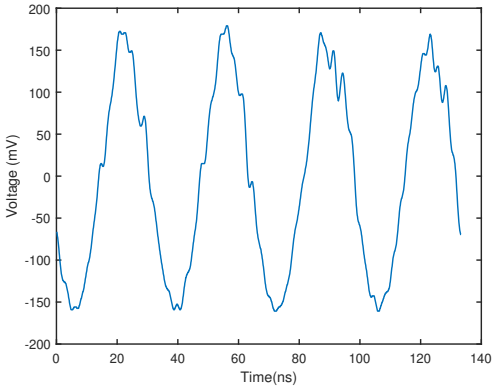

(a)

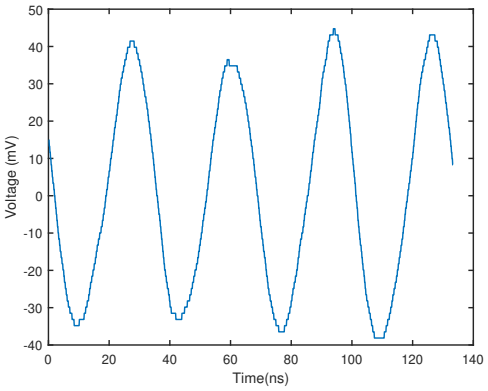

(b)

Figure 6.1: Time domain signals measured at (a) the transmission excitation signal (b) the scattered fluorescence signal modulated at 30 MHz frequency captured with 10 acquisition each having 5000 acquisition points at a sample rate of 10 GSa/s.

Figure 6.2 shows the measured phase difference captured by the two detectors for the reference sample. The phase angle increases with the modulation frequency, which is consistent with the theory discussed in Chapter 3.

Oscilloscope acquisition data were averaged over 10, 100, and 1000 acquisitions using the oscilloscope itself to improve the signal-to-noise ratio (SNR) and observe any reductions in the uncertainty of the measurements (Figure 6.3). Phase angle increased with increased average acquisitions for each modulation frequency from 0.05 rad for 10 to 30 MHz to 0.2 rad for 60 MHz. This change in the phase angle can be attributed to scattering effects, such as Rayleigh or Mie scattering, due to the reference sample containing sucrose crystals (Penkov *et al.*, 2024). A sample containing a non-uniform mixture, such as non-dissolved sucrose crystals, can lead to localised changes in the refractive index due to those regions having a different concentration or different media (e.g. solid sucrose or water).

There was little or no difference between the measured phase angle and the standard

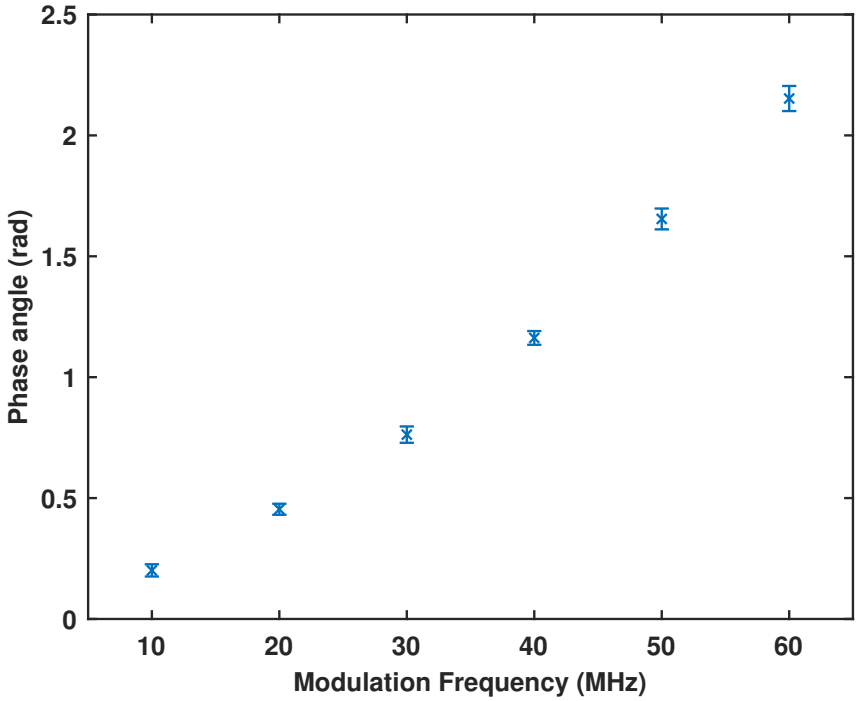

Figure 6.2: Phase angle difference between the two detectors measured with the reference water sample excited with 100 mW laser power and modulated frequencies from 10–60 MHz, extracted 10 acquisition samples each having 5000 acquisition points.

deviation for 100 and 1000 averaged acquisitions (Figure 6.3). However, the acquisition time to collect the data is over 3 min for the 1000 averaged acquisitions compared to less than 30 s for 100 averaged acquisitions; therefore, to prevent photobleaching when fluorescein samples are used, 100 averaged acquisitions were used.

The laser power was increased from 100 mW to 400 mW to observe the effect of increasing light intensity on the phase measurements of the sucrose reference sample (Figure 6.4). When one acquisition was collected, there was little or no difference in phase for each modulation frequency measured at 100 or 400 mW laser power, whereas when the acquisition samples were averaged over 10 or 100 acquisitions, the phase angle for 400 mW laser power was lower than that for 100 mW laser power. This could be due to an increase in signal due to increased light intensity due to scattering.

To analyse the impact of the average acquisition on fluorescence lifetime measurements, the fluorescence lifetime of a sample containing 0.25 mg/L fluorescein in water was measured using 10 acquisition samples from real-time acquisition and 100 averaged acquisitions using multi-frequency analysis to determine the fluorescence lifetime and contamination ratio (Table 6.1). The fluorescence lifetime measured using 100 averaged acquisitions was 4.12, which is very close to the literature values (Roding *et al.*, 2014) and has a much lower standard deviation than that calculated using real-time acquisition. The contamination ratio was low for both acquisitions at between 4–6%. Subsequent

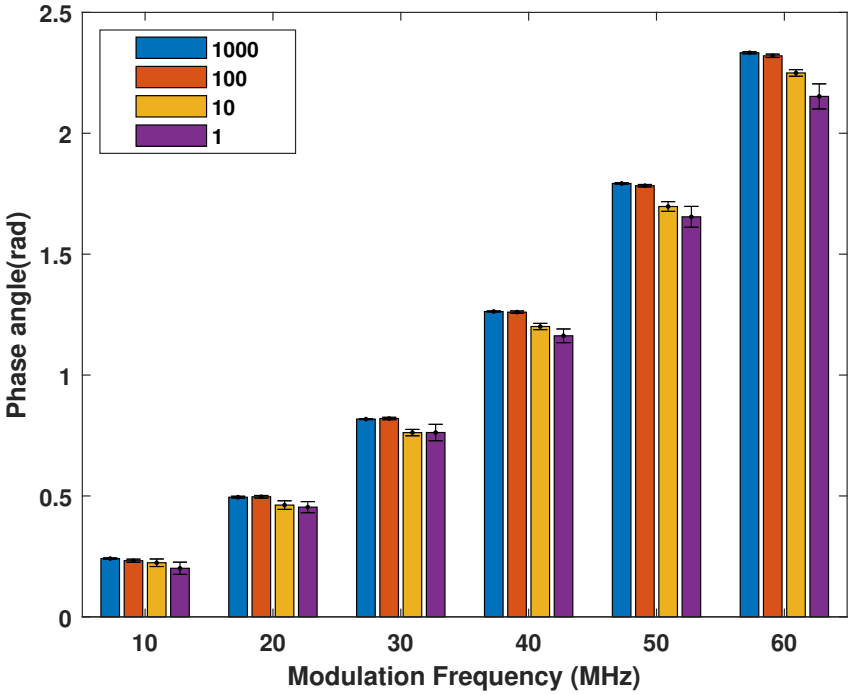

Figure 6.3: Effect on the phase measurements with acquisitions with different averaged acquisitions(1, 10,100,1000) for modulated frequencies from 10–60 MHz. The 10 acquisition samples, with 5000 acquisition points with different averaged acquisitions with a 10 GSa/s sampling rate.

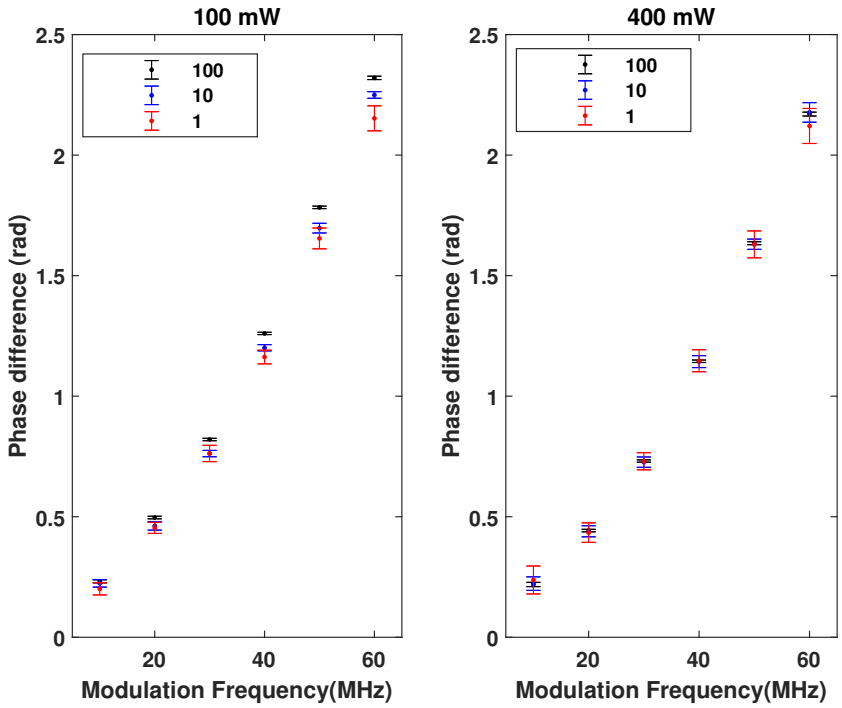

Figure 6.4: Effect on phase measurements at two laser powers and different averaged acquisitions for frequencies from 10–60 MHz. Ten acquisition samples, each with 5000 points, were extracted at a 10 GSa/s sampling rate.

Table 6.1: Multi-frequency analysis to measure fluorescence lifetime and contamination ratio, when the acquisition extracted real time and 100 averaged acquisitions, and laser power was 100 mW.

Averaged acquisition	Fluorescence lifetime (ns)	Contamination ratio
1	3.89 ± 0.62	0.04 ± 0.3
100	4.12 ± 0.16	0.06 ± 0.03

fluorescence lifetime measurements were collected using 100 averaged acquisitions.

6.2 Signal measurement

6.2.1 Sample preparation

Stock solutions of 1 g/L aluminium sulfate ($Al_2(SO_4)_3$), 1 mg/mL fluorescein, 500 mg/L humic acid, and 500 mg/L kaolin were prepared. Humic acid and kaolin stock solutions were used to prepare 60, 120, and 180 mg/L solutions for flocculation with 100 µL of fluorescein and aluminium sulfate. Humic acid and kaolin solutions at each concentration were tested for surface charge and the amount of aluminium sulfate needed to neutralise the charge using a Mutek particle charge detector (PCD03) to achieve the best flocculation, that is, the bulk of the compounds were incorporated into the floc. Humic acid, kaolin and control samples were dosed with fluorescein and flocculated by adding aluminium sulfate solution in a Boltac jar tester. The volumes of each solution are listed in Table 6.2. The flocculation process consisted of 2 min of fast mixing at

Table 6.2: Recipes for each type of flocculated particles and control.

Sample	1	2	3	4	5
Volume of water (mL)	400	400	0	0	0
Volume of humic acid/kaolin solution (mL)	0	0	400	400	400
Concentration of humic acid/kaolin (mg/L) in solution	0	0	60	120	180
Volume of fluorescein (μL)	100	100	100	100	100
Volume of $Al_2(SO_4)_3$solution for humic acid floc (mL)	0	40	40.4	52	64
Volume of $Al_2(SO_4)_3$solution for kaolin floc (mL)	0	30	28	31	30

100 rpm, 5 min of slow mixing at 30 rpm, and 5 min of settling time. Flocculated samples were extracted after 5 min and stored for fluorescence measurements.

6.3 Multi frequency measurements

6.3.1 Measurement procedure

The prototype system was first calibrated with a reference sample, and the phase was calculated using two signals extracted from the detectors using frequency-domain analysis. The phase of each sample was measured at modulation frequencies from 10 to 60 MHz in 10 MHz steps. Each measurement involved one-hundred averaged acquisitions with 5000 acquisition points from the oscilloscope, and the averaged signal was extracted and processed using MATLAB. This was repeated ten times for each sample. The extracted data were stored in computer files. This process was repeated for all fluorescence samples. The data were processed to measure the fluorescence lifetime of fluorescein and contamination, as described in Chapter 4.

6.3.2 Multi frequency analysis

Multi frequency phase measurements and non-linear regression analysis were used to measure the fluorescence lifetime of fluorescein and contamination of excitation (Chapter 4). The particles in a sample either absorb or scatter light, and the same phenomenon can occur due to the presence of floc particles in a sample. Figure 6.5 shows the measured fluorescence lifetime and contamination when the setup is operated at 100 mW and 400 mW laser power. The fluorescence lifetime and contamination in Figure 6.5a and 6.5b indicate a variation with different compounds, such as alum, humic acid, and kaolin in the sample. Three repeats of a sample are represented in the graphs, where a single data point is acquired from 60 phase measurements calculated using the six frequencies. Error bars represent the standard deviation of the measurements. Similarly, Figure 6.6 and 6.7 show the results of the estimated fluorescence lifetime and contamination with 60, 120, and 180 mg/L concentrations of humic acid and kaolin solutions.

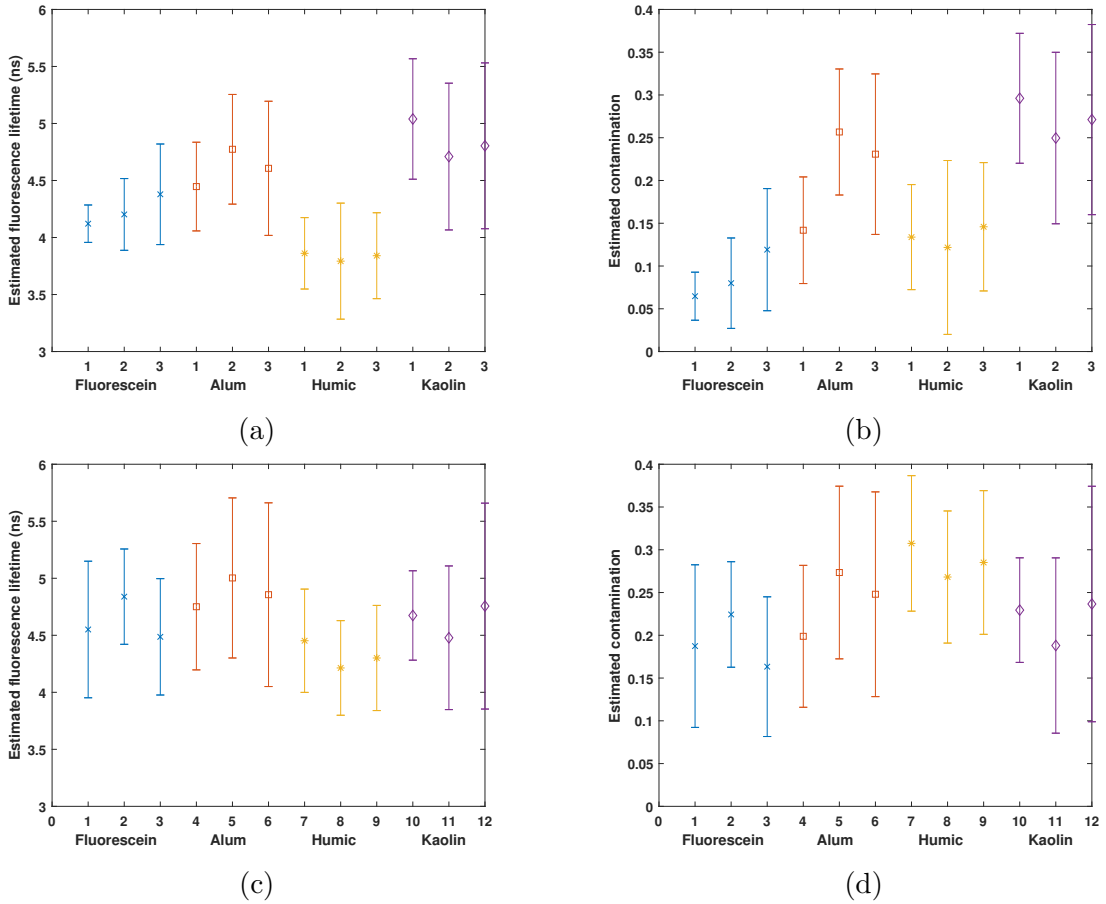

Figure 6.5: Non-linear model processed data for fluorescein, 1 g/L $Al_2(SO_4)_3$, 120 mg/L humic acid, and 120 mg/L kaolin. Measured (a) fluorescein lifetime and (b) contamination at 100 mW, and estimated (c) fluorescein lifetime and (d) contamination at 400 mW. Three repeated data acquisitions were performed for each sample. Error bars represent the standard deviation of the measurement, with each measurement consisting of 60 phase readings

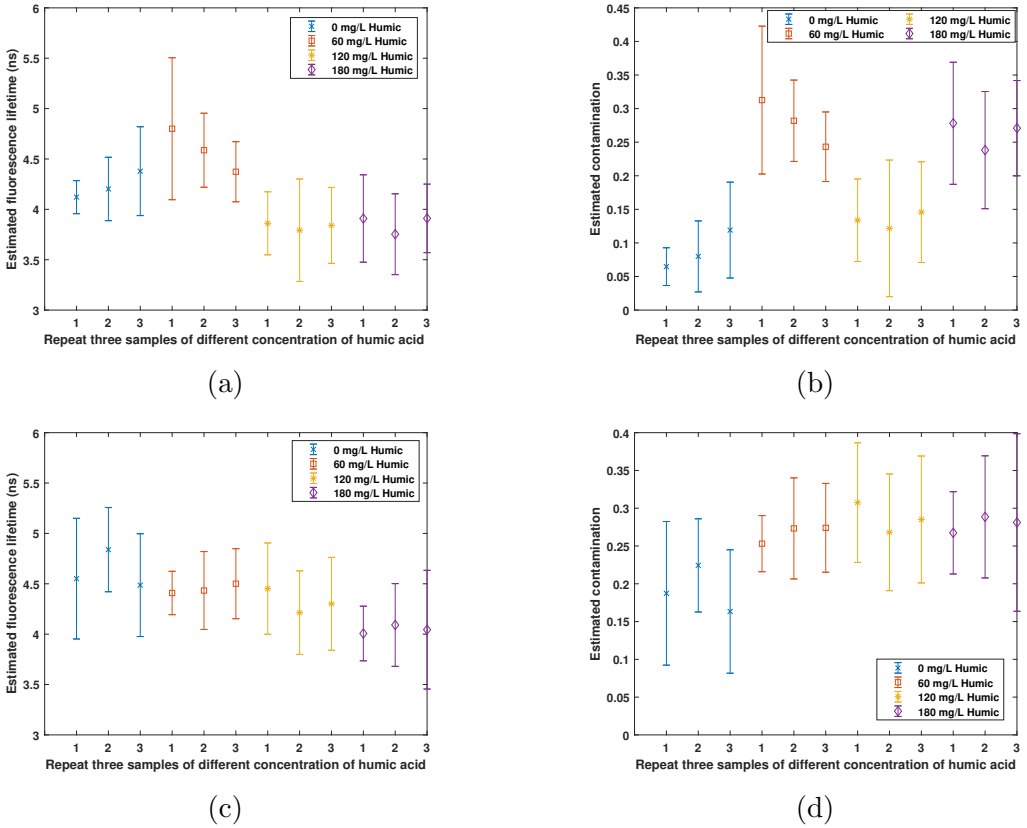

Figure 6.6: Non-linear model processed data for fluorescein, 1 g/L $Al_2(SO_4)_3$, 60 mg/L,120 mg/L, 180 mg/L humic acid measured(a) Fluorescence lifetime and (b) contamination at 100 mW and estimated (c) Fluorescence lifetime and (d) contamination at 400 mW.Three repeat data acquisitions were performed for the same sample. Error bars represent the standard deviation of the measurement and a single measurement consist of 60 phase measurement.

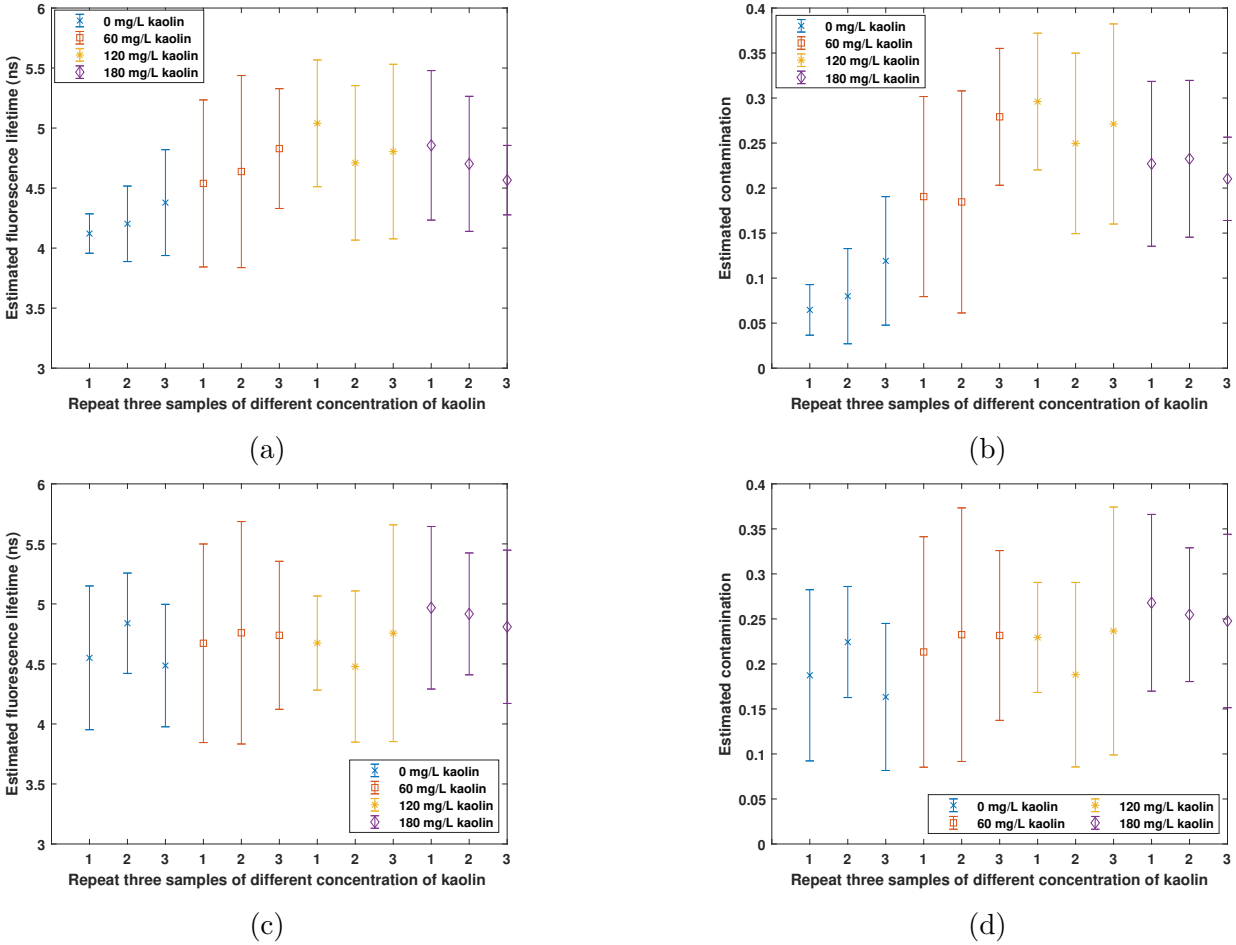

Figure 6.7: Non-linear model processed data for fluorescein, 1 g/L $Al_2(SO_4)_3$, 60 mg/L,120 mg/L, 180 mg/L kaolin measured (a) Fluorescence lifetime and (b) contamination at 100 mW and estimated (c) Fluorescence lifetime and (d) contamination at 400 mW.Three repeat data acquisitions were performed for the same sample. Error bars represent the standard deviation of the measurement and a single measurement consist of 60 phase measurement.

Table 6.3: Averaged measured fluorescence lifetime and contamination with uncertainties with operated laser power of 100 mW and 400 mW laser power.

Laser power (mW)	100				400			
Sample	Lifetime (ns)		Contamination		Lifetime (ns)		Contamination	
	AVG	SD	AVG	SD	AVG	SD	AVG	SD
Fluorescein	4.23	0.32	0.09	0.05	4.62	0.51	0.19	0.08
Alum	4.61	0.49	0.21	0.08	4.87	0.69	0.24	0.10
60 mg/L humic acid	4.59	0.49	0.28	0.08	4.45	0.33	0.27	0.05
120 mg/L humic acid	3.83	0.41	0.13	0.08	4.32	0.44	0.29	0.08
180 mg/L humic acid	3.86	0.39	0.26	0.08	4.05	0.44	0.28	0.09
60 mg/L kaolin	4.67	0.68	0.22	0.10	4.72	0.80	0.22	0.12
120 mg/L kaolin	4.85	0.64	0.27	0.10	4.64	0.67	0.22	0.10
180 mg/L kaolin	4.71	0.51	0.22	0.08	4.90	0.61	0.26	0.09

The literature value for the fluorescence lifetime of fluorescein is 4.14 ± 0.3 ns (Roding *et al.*, 2014) which is comparable to Figure 6.5a and the averaged fluorescence lifetime of fluorescein in Table 6.3 which is 4.2 ± 0.3 ns. When the sample was excited with a 100 mW laser power, samples containing flocculated particles had fluorescence lifetimes between 3.8–4.8 ns. Samples with kaolin particles showed fluorescence lifetimes larger than 4.2 ±0.3 ns when excited using 100 mW laser power and were all significantly different from the sample only containing fluorescein with a probability ≤ 0.01 of being the same (t-test analysis shown in Table 6.4). Fluorescein is strongly coupled to the kaolin, which was confirmed by adsorption isotherm data showing fluorescein is approximately ten times more strongly adsorbed into kaolin floc than into humic acid floc (Chapter 5). This kaolin bonding might be responsible for the increased time taken for fluorescein to absorb or release energy which causes a larger fluorescein lifetime measurement.

The fluorescence lifetimes of the humic acid floc samples containing fluorescein were lower than the fluorescein lifetime (with the exception of the sample made from the 60 mg/L humic acid solution) (Table 6.3). The contamination ratio (Figure 6.6b) for humic acid samples was higher than that for fluorescein without humic acid, indicating light scattering due to the presence of particles. The contamination ratio for fluorescein was 0.09 on average (Table 6.3) and increased to 0.13–0.28 for any sample that contained flocculated particles. It is possible that in solutions containing 60 mg/L humic acid, fluorescein molecules interact with a limited number of binding sites on humic macromolecules, placing them in a less polar and more rigid microenvironment that reduces non-radiative relaxation. This results in a slightly longer fluorescence lifetime

compared with the 120 mg/L and 180 mg/L humic acid solutions.

When the laser power was increased from 100 to 400 mW, the measured fluorescein fluorescence lifetime increased from 4.23 to 4.62 ns, and the contamination ratio increased from 0.09 to 0.19. The fluorescence lifetime also increased for alum and humic acid samples (with the exception of the 60 mg/L humic acid sample), while kaolin fluorescence lifetime remained the same. The contamination ratios for all the flocculated particles were similar regardless of whether the laser power was 100 or 400 mW. The change in contamination for fluorescein could be due to light scattering due to slight misalignments of the sample holder, which is not observable when flocculated particles are present because of the much greater scattering by the particles than that due to refraction and reflection inside the sample holder. The change in the fluorescence lifetime of fluorescein could be due to light saturation at 400 mW laser power compared to 100 mW laser power. The light saturation of fluorophores has been documented to increase the fluorescence lifetime (Lakowicz, 2006). It is possible that, in the case of kaolin samples, the kaolin floc with high light scattering and leafy floc morphology is more protective of fluorescein from light saturation. In the case of humic acid, the floc formed solid spheres; therefore, it is possible that the humic acid floc had a smaller surface area to protect the fluorescein. Thus, in the case of the 120 and 180 mg/L humic acid samples, the fluorescence lifetime increased. Table 6.4 shows the results from student t-tests determining whether the fluorescence lifetime for each flocculated sample containing fluorescein was significantly different from that of the fluorescein reference sample. The dataset for each sample consisted of 10 phase angle measurements at six modulation frequencies, resulting in 60 data points per sample. Thus, when each t-test was conducted, the set of 60 data points for each sample was compared with the set of 60 data points for the fluorescein. Even though the standard deviations for each fluorescence lifetime measurement were high (10% of the measurement) because the sample number was high, almost all of the fluorescence lifetime measurements (with the exception of one) were significantly different from fluorescein at 100 mW laser power. At 400 mW laser power, because the fluorescein fluorescence lifetime increased from 4.23 ns at 100 mW to 4.62 ns due to saturation, nine out of the 21 tests were not significantly different. Therefore, fluorescence lifetime measurements would be better to be conducted at 100 mW to improve the chance of results being significantly different and to avoid fluorescence lifetime increase due to saturation. In Table 6.5, the student t-test results for comparing the contamination ratios for flocculated samples versus fluorescein are shown, and in the majority of cases, the contamination ratios were significantly different for flocculated samples.

Table 6.4: Two lifetime sample t-test analysis to calculate statistical significant from fluorescein sample and other samples extracted under 100 mW and 400 mW laser exposure. Each dataset for each sample consisted of 10 measurements at 6 modulation frequencies, a total 60 data points per condition that was compared against the 60 data points for fluorescein.

Sample	Concentration (mg/L)	Sample no.	Data points	100 mW		400 mW	
				Statistical significant	Probability	Statistical significant	Probability
Alum	1000	1	60	Yes	<0.0001	No	0.0604
		2	60	Yes	<0.0001	No	0.1226
		3	60	Yes	0.018	Yes	0.0033
Humic acid	60	1	60	Yes	<0.0001	No	0.0861
		2	60	Yes	<0.0001	Yes	<0.0001
		3	60	No	0.9335	No	0.8579
	120	1	60	Yes	<0.0001	No	0.3109
		2	60	Yes	<0.0001	Yes	<0.0001
		3	60	Yes	<0.0001	Yes	0.0387
	180	1	60	Yes	0.0006	Yes	<0.0001
		2	60	Yes	<0.0001	Yes	<0.0001
		3	60	Yes	<0.0001	Yes	<0.0001
Kaolin	60	1	60	Yes	<0.0001	No	0.3598
		2	60	Yes	<0.0001	No	0.5467
		3	60	Yes	<0.0001	Yes	0.0163
	120	1	60	Yes	<0.0001	No	0.1859
		2	60	Yes	<0.0001	Yes	0.0003
		3	60	Yes	0.0002	Yes	0.0464
	180	1	60	Yes	<0.0001	Yes	0.0005
		2	60	Yes	<0.0001	No	0.3605
		3	60	Yes	0.0069	Yes	0.0028

Table 6.5: Two contamination sample t-test analysis to calculate statistical significant from fluorescein sample and other samples extracted under 100 mW and 400 mW laser exposure. Each dataset for each sample consisted of 10 measurements at 6 modulation frequencies, a total 60 data points per condition that was compared against the 60 data points for fluorescein.

Sample	Concentration (mg/L)	Sample no.	Data points	100 mW		400 mW	
				Statistical significant	Probability	Statistical significant	Probability
Alum	1000	1	60	Yes	<0.0001	No	0.4416
		2	60	Yes	<0.0001	Yes	0.0034
		3	60	Yes	<0.0001	Yes	< 0.0001
Humic acid	60	1	60	Yes	<0.0001	Yes	< 0.0001
		2	60	Yes	<0.0001	Yes	0.0003
		3	60	Yes	<0.0001	Yes	< 0.0001
	120	1	60	Yes	<0.0001	Yes	< 0.0001
		2	60	Yes	0.0056	Yes	0.0024
		3	60	Yes	0.0477	Yes	< 0.0001
	180	1	60	Yes	<0.0001	Yes	< 0.0001
		2	60	Yes	<0.0001	Yes	<0.0001
		3	60	Yes	<0.0001	Yes	< 0.0001
Kaolin	60	1	60	Yes	<0.0001	No	0.1848
		2	60	Yes	<0.0001	No	0.6951
		3	60	Yes	<0.0001	Yes	< 0.0001
	120	1	60	Yes	<0.0001	Yes	0.0015
		2	60	Yes	<0.0001	Yes	0.0304
		3	60	Yes	<0.0001	Yes	0.0006
	180	1	60	Yes	<0.0001	Yes	< 0.0001
		2	60	Yes	<0.0001	Yes	0.0303
		3	60	Yes	<0.0001	Yes	< 0.0001

6.4 Summary

Floc composition affects the fluorescence lifetime of fluorescein. The presence of particulates increases excitation light contamination due to scattering, which can be corrected using multi-frequency analysis by measuring phase changes between the laser excitation and fluorescence signals at different modulation frequencies. This effect is more pronounced at a low laser power of 100 mW compared to 400 mW, where the higher laser power saturates fluorescein, resulting in a longer fluorescence lifetime that makes it difficult to distinguish from flocculated samples. Increasing the laser power generally increased the fluorescence lifetime for all samples except kaolin. Kaolin flocs appear to protect fluorescein from saturation, likely due to their leafy morphology, whereas humic acid flocs are more spherical and do not produce the same effect. Therefore, avoiding fluorophore saturation is important in fluorescence lifetime analysis, and both the composition and morphology of the flocs must be considered.

Chapter 7

Conclusion and Recommendations

UV disinfection is used to inactivate pathogens, such as viruses, bacteria, and protozoa, that are not removed during water treatment. These pathogens can be shielded by floc particles that are not separated during the clarification and filtration stages of water treatment. In this study, a technique using frequency domain fluorescence fluorometry (FDFF) was developed that could be used to infer information about what was in the floc and the extent of light penetration into the floc. This study was divided into two parts: 1) development and testing of the equipment and 2) use of the equipment to test the fluorescence lifetime of fluorescein embedded in floc particles made from kaolin and humic acid. The second part involved understanding the floc properties and fluorescein adsorption to the floc.

7.1 Equipment development

Fluorescein is excellent as a fluorophore for fluorescence lifetime measurements. It has a high quantum yield compared to graphene quantum dots (GQD), is 1000 fold cheaper than GQD, can be readily incorporated into floc particles or made into solutions, and is non-toxic. This is important for the large-scale implementation of FDFF, for example, in water treatment plants, which would require a relatively cheap, non-toxic fluorophore. Furthermore, fluorescein fluoresces at UV wavelengths as well as in the visible range, meaning that it could be readily tested in the lab without requiring a UV laser which is not currently available. In addition, because the quantum yield is high, less fluorescein is needed to generate a fluorescence signal compared to GQD. If GQD are used, the signal is poor, and a more sensitive detector is required.

An intensity modulated 450 nm laser light source operated at 100 mW and 400 mW was required to excite the fluorophore between 10–60 MHz so fluorescence lifetime could be measured using the change in phase between the excitation light and fluorescence emission. To compensate for changes in the signal phase due to impedance and light travel, a reference signal was collected, as well as a fluorescence signal. The ideal sample

collection rate was 10 GSa/s, collecting a total of 5000 acquisition points, using an average of 100 acquisition points to smooth the signal. Fast Fourier transform was used to analyse the signal and extract frequency and phase data. An analysis of the signal-to-noise ratio showed that at least 5000 acquisition points were required to achieve a good fluorescence signal-to-noise ratio; at 1000 acquisition points, the fluorescence signal was barely visible relative to the noise. At 10,000 acquisition points, photobleaching of fluorescein could occur, but was not observed. Avalanche photo detectors were used to measure the fluorescence, and the emitted light was concentrated through a condenser lens to improve the signal. A 500 nm long-pass filter was used to eliminate wavelengths below 500 nm. A collimator lens was used to collimate the laser beam on the sample, and a beam splitter was installed between the collimator and the sample to collect the reference signal. Operating the laser at 400 mW resulted in excessive excitation light contamination of the fluorescence light signal due to light scattering, and as a consequence, accurate fluorescence lifetime data could not be obtained; therefore, operating the laser at low power was more conducive to obtaining good lifetime data.

7.2 Fluorescein adsorption to floc

Floc particles were made using humic acid and kaolin to mimic what is naturally found in raw water sources, aluminium sulphate as the flocculant, and fluorescein. Fluorescein more strongly adsorbs to kaolin compared to humic acid. Kaolin consists of clay platelets with a negatively charged surface and positively charged edges held together by cations, whereas humic acid has a large structure of phenyl, carboxyl, and carbonyl groups. Fluorescein consists of two phenyl rings, a carboxyl group, and an OH group, and is negatively charged at pH greater than 6.5; therefore, adsorption to kaolin and humic acid would be primarily due to charge neutralisation by the aluminium cation. The addition of fluorescein increased the floc particle size and changed the floc morphology from spherical to flat leaf-like structures. Therefore, it is important to keep fluorescein to a minimum to ensure that the floc properties are as similar as possible to those of flocs without fluorescein.

7.3 Fluorescence lifetime of the floc

The addition of fluorescein to humic acid did not change the fluorescence lifetime, but light scattering increased. In the case of kaolin, the fluorescence lifetime of fluorescein changed by 0.6 ns compared to 4.2 $\pm$ 0.3 ns for fluorescein (which is within the uncertainty measurement provided with the time correlated single photon counting (TCSPC) technique used (Roding *et al.*, 2014)). In principle, based on these data, kaolin and humic acid can be distinguished from each other in the floc.

7.4 Future work

The developed system used a quartz cuvette in which the sample was placed to measure the fluorescence lifetime. For a system to be implemented in a water treatment plant, a flow-through cell must be developed and tested. The effects of flow and particle concentration on fluorescence lifetime measurements must be evaluated, particularly the effect of particles moving past the laser at a frequency dictated by the particle concentration and flow velocity. Microfluidic flow channels can be explored, but these can be easily blocked by flocs larger than the channels.

This study involved the use of floc particles in a clean solution, whereas in water treatment, raw water has organic and mineral contaminants that impart colour and turbidity. Therefore, the effects of colour and turbidity on fluorescence lifetime measurements must be evaluated to determine the maximum colour or turbidity that can be tolerated.

This study used flocs made of either kaolin or humic acid. Future studies could explore the effects of kaolin and humic acid ratios and other materials on fluorescence lifetime measurements and fluorescence intensity.

The effect of particle size on light penetration and fluorescence should be explored in future studies.

In this study, a sinusoidal signal was used to excite fluorescein and measure its lifetime. The use of different harmonics, such as a square wave or pulse-width-modulated signal, could be tested to observe whether this has any improvement in lifetime measurements. Square waves generate higher harmonic components, which may increase the complexity of the lifetime analysis. In addition, machine learning algorithms can be tested to improve the accuracy of the measurements and differentiate the compounds in a sample.

While fluorescein has a high quantum yield, it does change floc properties; therefore, other fluorophores could be explored that either preferentially adsorb to particular compounds making up the floc or have a significant change in fluorescence lifetime when adsorbed to a particular material compared to other materials. Further work could be conducted to determine whether the concentrations of these components can be reliably determined using fluorescence intensity and lifetime.

References

Alimova, A., A. Katz, M. Siddique, G. Minko, H. E. Savage, M. K. Shah, R. B. Rosen, and R. R. Alfano. Native fluorescence changes induced by bactericidal agents. *IEEE Sensors Journal*, **5(4)**, pp. 704–711 (2005).

Altintas, Z., M. Akgun, G. Kokturk, and Y. Uludag. A fully automated microfluidic-based electrochemical sensor for real-time bacteria detection. *Biosensors and Bioelectronics*, **100**, pp. 541–548 (2018).

Ayres, J., R. Harrison, G. Nichols, and R. M. CBE. Section D: Diseases related to the ingestion of infectious agents. In: *Environmental Medicine*, pp. 371–416. CRC Press (2010).

Baghvand, A., A. D. Zand, N. Mehrdadi, and A. Karbassi. Optimizing coagulation process for low to high turbidity. *Journal of Materials and Environmental Science*, **6(5)**, pp. 442–448 (2010).

Baker, M., M. Prickett, F. Pourzand, J. Kerr, and S. Hales. Queenstown outbreak highlights future challenges for clean drinking water. *Public Health Expert Briefing* (2023).

Baldursson, S. and P. Karanis. Waterborne transmission of protozoan parasites: review of worldwide outbreaks–an update 2004–2010. *Water research*, **45(20)**, pp. 6603–6614 (2011).

Bargellini, A., I. Marchesi, E. Righi, A. Ferrari, S. Cencetti, P. Borella, and S. Rovesti. Parameters predictive of Legionella contamination in hot water systems: association with trace elements and heterotrophic plate counts. *Water research*, **45(6)**, pp. 2315–2321 (2011).

Becker, W. Fluorescence lifetime imaging–techniques and applications. *Journal of microscopy*, **247(2)**, pp. 119–136 (2012).

Benedict, K. M., H. Reses, M. Vigar, D. M. Roth, V. A. Roberts, M. Mattioli, L. A. Cooley, E. D. Hilborn, T. J. Wade, K. E. Fullerton, *et al.* Surveillance for water-

borne disease outbreaks associated with drinking water—United States, 2013–2014. *Morbidity and Mortality Weekly Report*, **66(44)**, p. 1216 (2017).

Berezin, M. Y. and S. Achilefu. Fluorescence lifetime measurements and biological imaging. *Chemical reviews*, **110(5)**, pp. 2641–2684 (2010).

Bitton, A., J. Sambrano, S. Valentino, and J. P. Houston. A review of new high-throughput methods designed for fluorescence lifetime sensing from cells and tissues. *Frontiers in Physics*, **9**, p. 648553 (2021).

Blackburn, K. and D. Green. The potential effects of microplastics on human health: What is known and what is unknown. *Ambio*, **51(3)**, pp. 518–530 (2022).

Boens, N., W. Qin, N. Basarić, J. Hofkens, M. Ameloot, J. Pouget, J.-P. Lefevre, B. Valeur, E. Gratton, M. VandeVen, *et al.* Fluorescence lifetime standards for time and frequency domain fluorescence spectroscopy. *Analytical chemistry*, **79(5)**, pp. 2137–2149 (2007).

Bratby, J. *Coagulation and flocculation in water and wastewater treatment*. IWA publishing, second edition (2016).

Bui, D. A. and P. C. Hauser. Analytical devices based on light-emitting diodes–a review of the state-of-the-art. *Analytica chimica acta*, **853**, pp. 46–58 (2015).

Cabral, J. P. Water microbiology. Bacterial pathogens and water. *International journal of environmental research and public health*, **7(10)**, pp. 3657–3703 (2010).

Cantwell, R. E. and R. Hofmann. Inactivation of indigenous coliform bacteria in unfiltered surface water by ultraviolet light. *Water research*, **42(10-11)**, pp. 2729–2735 (2008).

Chalmers, R. M., G. Robinson, K. Elwin, and R. Elson. Analysis of the *Cryptosporidium spp.* and gp60 subtypes linked to human outbreaks of cryptosporidiosis in England and Wales, 2009 to 2017. *Parasites & vectors*, **12(1)**, pp. 1–13 (2019).

Chang, Q., Z. Murtaza, J. R. Lakowicz, and G. Rao. A fluorescence lifetime-based solid sensor for water. *Analytica chimica acta*, **350(1-2)**, pp. 97–104 (1997).

Chauhan, A., P. Goyal, A. Varma, and T. Jindal. Microbiological evaluation of drinking water sold by roadside vendors of Delhi, India. *Applied Water Science*, **7**, pp. 1635–1644 (2017).

Chhetri, B. K., E. Galanis, S. Sobie, J. Brubacher, R. Balshaw, M. Otterstatter, S. Mak, M. Lem, M. Lysyshyn, T. Murdock, *et al.* Projected local rain events due to climate change and the impacts on waterborne diseases in Vancouver, British Columbia, Canada. *Environmental Health*, **18(1)**, pp. 1–9 (2019).

Chiou, C. Contaminant sorption to soils and natural solids. *Partition and adsorption of organic contaminants in environmental systems. John Wiley & Sons Ltd* (2002).

Clark, C. D., J. Jimenez-Morais, G. Jones II, E. Zanardi-Lamardo, C. A. Moore, and R. G. Zika. A time-resolved fluorescence study of dissolved organic matter in a riverine to marine transition zone. *Marine Chemistry*, **78(2-3)**, pp. 121–135 (2002).

Daly, E., S. Roy, D. Blaney, J. Manning, V. Hill, L. Xiao, and J. Stull. Outbreak of giardiasis associated with a community drinking-water source. *Epidemiology and Infection*, **138(4)**, pp. 491–500 (2010).

Dandin, M., P. Abshire, and E. Smela. Optical filtering technologies for integrated fluorescence sensors. *Lab on a Chip*, **7(8)**, pp. 955–977 (2007).

Danopoulos, E., M. Twiddy, and J. M. Rotchell. Microplastic contamination of drinking water: A systematic review. *PloS one*, **15(7)**, p. e0236838 (2020).

De Jong, E. P. and C. A. Lucy. Spectral filtering of light-emitting diodes for fluorescence detection. *Analytica chimica acta*, **546(1)**, pp. 37–45 (2005).

De Silva, M., S. Schafer, M. K. Scott, B. Robinson, A. Hills, G. Buser, K. Salis, J. Gargano, J. Yoder, V. Hill, *et al.* Communitywide cryptosporidiosis outbreak associated with a surface water-supplied municipal water system–baker city, oregon, 2013. *Epidemiology & Infection*, **144(2)**, pp. 274–284 (2016).

Draxler, S. and M. E. Lippitsch. pH sensors using fluorescence decay time. *Sensors and Actuators B: Chemical*, **29(1-3)**, pp. 199–203 (1995).

Droppo, I. G. Rethinking what constitutes suspended sediment. *Hydrological processes*, **15(9)**, pp. 1551–1564 (2001).

Dwari, R. and B. Mishra. Evaluation of flocculation characteristics of kaolinite dispersion system using guar gum: a green flocculant. *International Journal of Mining Science and Technology*, **29(5)**, pp. 745–755 (2019).

Eerkes-Medrano, D., H. A. Leslie, and B. Quinn. Microplastics in drinking water: A review and assessment. *Current Opinion in Environmental Science & Health*, **7**, pp. 69–75 (2019).

Efstratiou, A., J. E. Ongerth, and P. Karanis. Waterborne transmission of protozoan parasites: review of worldwide outbreaks-an update 2011 – 2016. *Water research*, **114**, pp. 14–22 (2017).

Elmer, P. Avalanche Photodiodes: A User's Guide. *Technical information, PerkinElmer Optoelectronics* (2006).

Emerick, R. W., F. J. Loge, T. Ginn, and J. L. Darby. Modeling the inactivation of particle-associated coliform bacteria. *Water Environment Research*, **72(4)**, pp. 432–438 (2000).

Esposito, A. Beyond range: innovating fluorescence microscopy. *Remote Sensing*, **4(1)**, pp. 111–119 (2012).

Esteban, G. F. and T. M. Fenchel. Ecology of protozoa. *The Biology of Free-living Phagotrophic Protists: Springer International Publishing, Cham, Switzerland* (2020).

Esteban, G. F., B. J. Finlay, and A. Warren. Free-living protozoa. In: *Thorp and Covich's Freshwater Invertebrates*, pp. 113–132. Elsevier (2015).

European Centre for Disease Prevention and Control. Cyclospora infections in European travellers to Mexico - 21 July 2017 . `https://www.ecdc.europa.eu/sites/default/files/documents/rapid-risk-assessment-cyclospora-infections-in-travellers-to-Mexico-21-july-2017.pdf` (2019).

Favreau, P., C. Hernandez, A. S. Lindsey, D. F. Alvarez, T. Rich, P. Prabhat, and S. J. Leavesley. Thin-film tunable filters for hyperspectral fluorescence microscopy. *Journal of biomedical optics*, **19(1)**, pp. 011017–011017 (2014).

Forterre, P. and D. Prangishvili. The origin of viruses. *Research in Microbiology*, **160(7)**, pp. 466–472 (2009).

Franch, N., O. Alonso, J. Canals, A. Vilà, and A. Dieguez. A low cost fluorescence lifetime measurement system based on SPAD detectors and FPGA processing. *Journal of Instrumentation*, **12(02)**, p. C02070 (2017).

Fukasawa, R. Terahertz imaging: Widespread industrial application in non-destructive inspection and chemical analysis. *IEEE Transactions on Terahertz Science and Technology*, **5(6)**, pp. 1121–1127 (2015).

Gerritsen, H. C., M. Asselbergs, A. Agronskaia, and W. Van Sark. Fluorescence lifetime imaging in scanning microscopes: acquisition speed, photon economy and lifetime resolution. *Journal of microscopy*, **206(3)**, pp. 218–224 (2002).

Gertler, M., M. Dürr, P. Renner, S. Poppert, M. Askar, J. Breidenbach, C. Frank, K. Preußel, A. Schielke, D. Werber, *et al.* Outbreak of *Cryptosporidium hominis* following river flooding in the city of Halle (Saale), Germany, August 2013. *BMC infectious diseases*, **15**, pp. 1–10 (2015).

Gharpure, R., A. Perez, A. D. Miller, M. E. Wikswo, R. Silver, and M. C. Hlavsa. Cryptosporidiosis outbreaks—United states, 2009–2017 (2019).

Gill, A. The importance of bacterial culture to food microbiology in the age of genomics. *Frontiers in microbiology*, **8**, p. 777 (2017).

Gilpin, B. J., T. Walker, S. Paine, J. Sherwood, G. Mackereth, T. Wood, T. Hambling, C. Hewison, A. Brounts, M. Wilson, *et al.* A large scale waterborne *campylobacteriosis* outbreak, Havelock North, New Zealand. *Journal of Infection*, **81(3)**, pp. 390–395 (2020).

Girones, R., M. A. Ferrús, J. L. Alonso, J. Rodriguez-Manzano, B. Calgua, A. de Abreu Corrêa, A. Hundesa, A. Carratala, and S. Bofill-Mas. Molecular detection of pathogens in water–the pros and cons of molecular techniques. *Water research*, **44(15)**, pp. 4325–4339 (2010).

Gratton, E., M. Limkeman, J. Lakowicz, B. Maliwal, H. Cherek, and G. Laczko. Resolution of mixtures of fluorophores using variable-frequency phase and modulation data. *Biophysical journal*, **46(4)**, pp. 479–486 (1984).

Greaves, J. How are coagulants and flocculants used in water and wastewater treatment? `https://www.wcs-group.co.uk/wcs-blog/coagulants-flocculants-wastewater-treatment` (2022). Accessed: 16.01.2024.

Gregory, J. J. *Particles in water properties and processes*. IWA Pub. ; Taylor & Francis, London : Boca Raton, FL (2005). ISBN 0-429-21162-7.

Guliy, O. I., S. S. Evstigneeva, and L. A. Dykman. Recombinant antibodies by phage display for bioanalytical applications. *Biosensors and Bioelectronics*, **222**, p. 114909 (2023).

Guo, J., J. Zhang, S. Thomas, and S. Sonkusale. CMOS Fluorometer for Oxygen Sensing. *IEEE Sensors Journal*, **12(7)**, pp. 2506–2507 (2012).

Gupta, A., S. K. Bhardwaj, A. L. Sharma, K.-H. Kim, and A. Deep. Development of an advanced electrochemical biosensing platform for *E. coli* using hybrid metal-organic framework/polyaniline composite. *Environmental research*, **171**, pp. 395–402 (2019).

Harris, L. and K. McFarlane. Small systems, big challenges: Review of small drinking water system governance. *Environmental Reviews*, **26(4)**, pp. 378–395 (2018).

Hassan, A. H. A., J. F. Bergua, E. Morales-Narváez, and A. Mekoçi. Validity of a single antibody-based lateral flow immunoassay depending on graphene oxide for highly sensitive determination of *E. coli* O157: H7 in minced beef and river water. *Food chemistry*, **297**, p. 124965 (2019).

Health Protection Surveillance Centre. Epidemiology of Cryptosporidiosis in Ireland, 2014. https://www.hpsc.ie/a-z/gastroenteric/cryptosporidiosis/publications/epidemiologyofcryptosporidiosisinirelandannualreports/ (2014).

Health Protection Surveillance Centre. Epidemiology of Cryptosporidiosis in Ireland, 2014. https://www.hpsc.ie/a-z/gastroenteric/cryptosporidiosis/publications/epidemiologyofcryptosporidiosisinirelandannualreports/ (2015).

Health Protection Surveillance Centre. Epidemiology of Cryptosporidiosis in Ireland, 2019 a. https://www.hpsc.ie/a-z/gastroenteric/cryptosporidiosis/publications/epidemiologyofcryptosporidiosisinirelandannualreports/ (2019).

Heijnen, L. and G. Medema. Method for rapid detection of viable *Escherichia coli* in water using real-time NASBA. *Water research*, **43(12)**, pp. 3124–3132 (2009a).

Heijnen, L. and G. Medema. Method for rapid detection of viable *Escherichia coli* in water using real-time NASBA. *Water research*, **43(12)**, pp. 3124–3132 (2009b).

Hijjawi, N., A. Zahedi, M. Kazaleh, and U. Ryan. Prevalence of *Cryptosporidium* species and subtypes in paediatric oncology and non-oncology patients with diarrhoea in Jordan. *Infection, Genetics and Evolution*, **55**, pp. 127–130 (2017).

Houssin, T., J. Follet, A. Follet, E. Dei-Cas, and V. Senez. Label-free analysis of water-polluting parasite by electrochemical impedance spectroscopy. *Biosensors and bioelectronics*, **25(5)**, pp. 1122–1129 (2010).

Hrudey, S. and E. Hrudey. Common themes contributing to recent drinking water disease outbreaks in affluent nations. *Water supply*, **19(6)**, pp. 1767–1777 (2019).

Hui, Y., C. Xiong, C. Bian, S. Gui, J. Tong, Y. Li, C. Gao, Y. Huang, W. C. Tang, and S. Xia. Temperature-controlled ionic liquid dispersive liquid–liquid microextraction combined with fluorescence detection of ultra-trace Hg 2+ in water. *Analytical methods*, **11(20)**, pp. 2669–2676 (2019).

Ibekwe, A. and C. Grieve. Detection and quantification of *Escherichia coli* O157: H7 in environmental samples by real-time PCR. *Journal of applied microbiology*, **94(3)**, pp. 421–431 (2003).

Institute of Environmental Science and Research,New Zealand. Annual Summary of Outbreaks in New Zealand . https://www.esr.cri.nz/assets/1Reports/Corporate-publications/ESR-Annual-Report-2013.pdf (2013).

Institute of Environmental Science and Research,New Zealand. Annual Summary of Outbreaks in New Zealand. https://sacnzs.org.nz/assets/1Reports/Corporate-publications/ESR-Annual-Report-2014.pdf (2014).

Institute of Environmental Science and Research,New Zealand. Annual Summary of Outbreaks in New Zealand. https://www.esr.cri.nz/assets/1Reports/Corporate-publications/esr-annual-report-2018.pdf (2018).

Institute of Environmental Science and Research,New Zealand. Annual Summary of Outbreaks in New Zealand. https://www.esr.cri.nz/assets/1Reports/Corporate-publications/esr-annual-report-2019.pdf (2019).

Islam, M. S., M. Hassan-uz Zaman, M. S. Islam, J. D. Clemens, and N. Ahmed. Waterborne pathogens: Review of outbreaks in developing nations. *Waterborne Pathogens*, pp. 43–56 (2020).

Iwata, T. Proposal for Fourier-transform phase-modulation fluorometer. *Optical review*, **10(1)**, pp. 31–37 (2003).

Iwata, T., T. Kamada, and T. Araki. Phase-modulation fluorometer using an ultraviolet light-emitting diode. *Optical Review*, **7(6)**, pp. 495–498 (2000).

Iwata, T., H. Shibata, and T. Araki. Construction of a Fourier-transform phase-modulation fluorometer. *Measurement Science and Technology*, **16(11)**, p. 2351 (2005).

Jain, S., T. G. C. Melo, S. S. Dolabella, and J. Liu. Current and emerging tools for detecting protozoan cysts and oocysts in water. *TrAC Trends in Analytical Chemistry*, p. 115695 (2019).

Jares-Erijman, E. A. and T. M. Jovin. FRET imaging. *Nature biotechnology*, **21(11)**, pp. 1387–1395 (2003).

Jenkins, A. *Conditions Contributing to Poor Coagulation and Sedimentation Performance in Municipal Water Treatment*. Master's thesis, Graduate school, Auburn University (2006).

Jyoti, A., S. Ram, P. Vajpayee, G. Singh, P. D. Dwivedi, S. K. Jain, and R. Shanker. Contamination of surface and potable water in South Asia by Salmonellae: Culture-independent quantification with molecular beacon real-time PCR. *Science of the total environment*, **408(6)**, pp. 1256–1263 (2010).

Kalam, S., S. A. Abu-Khamsin, M. S. Kamal, and S. Patil. Surfactant adsorption isotherms: A review. *ACS omega*, **6(48)**, pp. 32342–32348 (2021).

Kaufmann, K. Photomultipliers: Low-Light, High-Speed Specialists (2004).

Key, J. A., S. Koh, Q. K. Timerghazin, A. Brown, and C. W. Cairo. Photophysical characterization of triazole-substituted coumarin fluorophores. *Dyes and Pigments*, **82(2)**, pp. 196–203 (2009).

Khan, S., S. Ajmal, T. Hussain, and M. U. Rahman. Clay-based materials for enhanced water treatment: adsorption mechanisms, challenges, and future directions. *Journal of Umm Al-Qura University for Applied Sciences*, pp. 1–16 (2023).

Khurana, S. and P. Chaudhary. Laboratory diagnosis of cryptosporidiosis. *Tropical parasitology*, **8(1)**, p. 2 (2018).

Kissinger, J. and D. Wilson. Portable fluorescence lifetime detection for chlorophyll analysis in marine environments. *IEEE Sensors Journal*, **11(2)**, pp. 288–295 (2010).

Koenraad, P., F. Rombouts, and S. Notermans. Epidemiological aspects of thermophilic *Campylobacter* in water-related environments: a review. *Water environment research*, **69(1)**, pp. 52–63 (1997).

Kollu, K. and B. Örmeci. Effect of particles and bioflocculation on ultraviolet disinfection of *Escherichia coli*. *Water research*, **46(3)**, pp. 750–760 (2012).

Kordbacheh, F. and G. Heidari. Water pollutants and approaches for their removal. *Materials Chemistry Horizons*, **2(2)**, pp. 139–153 (2023).

Kuhn, R. C., C. M. Rock, and K. H. Oshima. Effects of pH and magnetic material on immunomagnetic separation of *Cryptosporidium oocysts* from concentrated water samples. *Appl. Environ. Microbiol.*, **68(4)**, pp. 2066–2070 (2002).

Kumar, A. T., S. B. Raymond, B. J. Bacskai, and D. A. Boas. Comparison of frequency-domain and time-domain fluorescence lifetime tomography. *Optics letters*, **33(5)**, pp. 470–472 (2008).

Kuo, J. S., C. L. Kuyper, P. B. Allen, G. S. Fiorini, and D. T. Chiu. High-power blue/UV light-emitting diodes as excitation sources for sensitive detection. *Electrophoresis*, **25(21-22)**, pp. 3796–3804 (2004).

Kuwana, E. and E. M. Sevick-Muraca. Fluorescence lifetime spectroscopy for pH sensing in scattering media. *Analytical chemistry*, **75(16)**, pp. 4325–4329 (2003).

Lakowicz, J. R. *Principles of fluorescence spectroscopy*. Springer (2006).

Lakowicz, J. R., I. Gryczynski, Z. Gryczynski, and M. L. Johnson. Background suppression in frequency-domain fluorometry. *Analytical Biochemistry*, **277(1)**, pp. 74–85 (2000).

Landgraf, S. Semiconductor lights sources in modulation fluorometry using digital storage oscilloscopes. In: *Reviews in Fluorescence 2004*, pp. 341–363. Springer (2004).

Lawrence, W. G., G. Varadi, G. Entine, E. Podniesinski, and P. K. Wallace. A comparison of avalanche photodiode and photomultiplier tube detectors for flow cytometry. In: *Imaging, Manipulation, and Analysis of Biomolecules, Cells, and Tissues VI*, volume 6859, pp. 128–138. SPIE (2008).

Le Guern, F., V. Mussard, A. Gaucher, M. Rottman, and D. Prim. Fluorescein derivatives as fluorescent probes for pH monitoring along recent biological applications. *International Journal of Molecular Sciences*, **21(23)**, p. 9217 (2020).

Li, B., Q. Yu, and Y. Duan. Fluorescent labels in biosensors for pathogen detection. *Critical reviews in biotechnology*, **35(1)**, pp. 82–93 (2015).

Li, W., W. Qi, J. Chen, W. Zhou, Y. Li, Y. Sun, and K. Ding. Effective removal of fluorescent microparticles as *Cryptosporidium* parvum surrogates in drinking water treatment by metallic membrane. *Journal of Membrane Science*, p. 117434 (2019).

Lieske, T., W. Uhring, N. Dumas, J. Leonard, and D. Fey. Embedded fluorescence lifetime determination for high throughput real-time droplet sorting with microfluidics. In: *2017 Conference on design and architectures for signal and image processing (DASIP)*, pp. 1–6. IEEE (2017).

van der Linden, F. H., E. K. Mahlandt, J. J. Arts, J. Beumer, J. Puschhof, S. M. de Man, A. O. Chertkova, B. Ponsioen, H. Clevers, J. D. van Buul, *et al.* A turquoise fluorescence lifetime-based biosensor for quantitative imaging of intracellular calcium. *Nature Communications*, **12(1)**, p. 7159 (2021).

Luka, G., A. Ahmadi, H. Najjaran, E. Alocilja, M. DeRosa, K. Wolthers, A. Malki, H. Aziz, A. Althani, and M. Hoorfar. Microfluidics integrated biosensors: A leading technology towards lab-on-a-chip and sensing applications. *Sensors*, **15(12)**, pp. 30011–30031 (2015).

Luka, G., E. Samiei, S. Dehghani, T. Johnson, H. Najjaran, and M. Hoorfar. Label-Free Capacitive Biosensor for Detection of *Cryptosporidium*. *Sensors*, **19(2)**, p. 258 (2019).

Lun, J., D. Liu, T. Liu, S. Zhang, Y. Dong, C. Li, Y. Zhang, and Z. Hu. Evaluation of outer membrane protein U (OmpU) as a novel capture target of Vibrio parahaemolyticus and rapid detection of acute hepatopancreatic necrosis disease (AHPND) using PCR combined with immunomagnetic separation. *Aquaculture*, **485**, pp. 225–232 (2018).

Ma, J., K. Fu, L. Jiang, L. Ding, Q. Guan, S. Zhang, H. Zhang, J. Shi, and X. Fu. Flocculation performance of cationic polyacrylamide with high cationic degree in humic acid synthetic water treatment and effect of kaolin particles. *Separation and Purification Technology*, **181**, pp. 201–212 (2017).

Ma, J.-Y., M.-Y. Li, Z.-Z. Qi, M. Fu, T.-F. Sun, H. M. Elsheikha, and W. Cong. Waterborne protozoan outbreaks: An update on the global, regional, and national prevalence from 2017 to 2020 and sources of contamination. *Science of the Total Environment*, **806**, p. 150562 (2022).

Makuei, M. S. and N. M. Peleato. Factors affecting particle-microorganism association and UV disinfection: Effect of source water, organics, and particle characteristics. *Journal of Water Process Engineering*, **56**, p. 104335 (2023).

Mao, X.-J., H.-Z. Zheng, Y.-J. Long, J. Du, J.-Y. Hao, L.-L. Wang, and D.-B. Zhou. Study on the fluorescence characteristics of carbon dots. *Spectrochimica Acta Part A: Molecular and Biomolecular Spectroscopy*, **75(2)**, pp. 553–557 (2010).

Marcu, L. Fluorescence lifetime techniques in medical applications. *Annals of biomedical engineering*, **40**, pp. 304–331 (2012).

Masago, Y., K. Oguma, H. Katayama, and S. Ohgaki. Quantification and genotyping of *Cryptosporidium spp.* in river water by quenching probe PCR and denaturing gradient gel electrophoresis. *Water science and technology*, **54(3)**, pp. 119–126 (2006).

Medina-Rodríguez, S., A. De La Torre-Vega, J. Fernández-Sánchez, and A. Fernández-Gutiérrez. An open and low-cost optical-fiber measurement system for the optical detection of oxygen using a multifrequency phase-resolved method. *Sensors and Actuators B: Chemical*, **176**, pp. 1110–1120 (2013).

de Melo, B. A. G., F. L. Motta, and M. H. A. Santana. Humic acids: structural properties and multiple functionalities for novel technological developments. *Materials Science and Engineering: C*, **62**, pp. 967–974 (2016).

Ministry of Health. Drinking-water Standards for New Zealand 2005 (revised 2018). Standard, Ministry of Health, Wlellington, New Zealand (2018).

Ministry of Health NZ. Ministry of health drinking water quality guidelines for new zealand. `https://www.taumataarowai.govt.nz/assets/Uploads/Guidance/Ministry-of-Health-Drinking-Water-Quality-Guidelines-for-New-Zealand.pdf` (2021). Accessed: 16.01.2024.

Minnesota Rural Water Association. Filtration. `https://www.mrwa.com/WaterWorksMnl/Chapter%2018%20Filtration.pdf` (2012). Accessed: 20.01.2024.

Minuzzi, C. E., F. D. Fernandes, L. P. Portella, P. Bräunig, D. A. F. Sturza, L. Giacomini, E. Salvagni, J. d. S. Ribeiro, C. R. Silva, C. M. Difante, *et al.* Contaminated water confirmed as source of infection by bioassay in an outbreak of toxoplasmosis in South Brazil. *Transboundary and Emerging Diseases*, **68(2)**, pp. 767–772 (2021).

Mondal, D., R. Binish, S. Samanta, D. Paul, and S. Mukherji. Detection of total bacterial load in water samples using a disposable impedimetric sensor. *IEEE Sensors Journal*, **20(4)**, pp. 1712–1720 (2019).

MW Le Chevallier, K.-K. A. Water Treatment and Pathogen Control: Process efficiency in achieving safe drinking water. `https://iris.who.int/bitstream/handle/10665/42796/9241562552.pdf?sequence=1` (2004). Accessed: 15.01.2024.

National Center for Biotechnology Information. Pubchem compound summary for cid 56841936 (2012).

Nokes, C. Water standards to drinking water contaminants, treatment and management. `https://environment.govt.nz/assets/Publications/Files/introduction-users-nes-human-drinking-water-jun08.pdf` (2008).

Obeidat, S., B. Bai, G. D. Rayson, D. M. Anderson, A. D. Puscheck, S. Y. Landau, and T. Glasser. A multi-source portable light emitting diode spectrofluorometer. *Applied Spectroscopy*, **62(3)**, pp. 327–332 (2008).

Pacheco-Linan, P. J., A. Garzon, J. Tolosa, I. Bravo, J. Canales-Vazquez, J. Rodriguez-Lopez, J. Albaladejo, and J. C. Garcia-Martinez. pH-sensitive fluorescence lifetime molecular probes based on functionalized tristyrylbenzene. *The Journal of Physical Chemistry C*, **120(33)**, pp. 18771–18779 (2016).

Palmer, C. and E. G. Loewen. *Diffraction grating handbook*. Newport Corporation New York (2005).

Pancheri, L., N. Massari, and D. Stoppa. SPAD image sensor with analog counting pixel for time-resolved fluorescence detection. *IEEE Transactions on Electron Devices*, **60(10)**, pp. 3442–3449 (2013).

Pandey, C. M., I. Tiwari, V. N. Singh, K. Sood, G. Sumana, and B. D. Malhotra. Highly sensitive electrochemical immunosensor based on graphene-wrapped copper oxide-cysteine hierarchical structure for detection of pathogenic bacteria. *Sensors and Actuators B: Chemical*, **238**, pp. 1060–1069 (2017).

Pang, L., U. Nowostawska, J. Ryan, W. Williamson, G. Walshe, and K. Hunter. Modifying the surface charge of pathogen-sized microspheres for studying pathogen transport in groundwater. *Journal of Environmental Quality*, **38(6)**, pp. 2210–2217 (2009).

Paviolo, C., A. Clayton, S. Mcarthur, and P. Stoddart. Temperature measurement in the microscopic regime: a comparison between fluorescence lifetime-and intensity-based methods. *Journal of microscopy*, **250(3)**, pp. 179–188 (2013).

Penkov, N., V. Zhmurin, A. Kobelev, E. Fesenko, and N. Penkova. Dispersed, optical and concentration characteristics of submicron heterogeneities in aqueous solutions of sugars. *Journal of Molecular Liquids*, **398**, p. 124281 (2024).

Pickup, J. C., F. Hussain, N. D. Evans, O. J. Rolinski, and D. J. Birch. Fluorescence-based glucose sensors. *Biosensors and Bioelectronics*, **20(12)**, pp. 2555–2565 (2005).

Pinon, A. and M. Vialette. Survival of viruses in water. *Intervirology*, **61(5)**, pp. 214–222 (2019).

Pires, N. M. M. and T. Dong. A cascade-like silicon filter for improved recovery of oocysts from environmental waters. *Environmental technology*, **35(6)**, pp. 781–790 (2014).

Public Health England(PHE). PHE Gastrointestinal Infections Data. `https://assets.publishing.service.gov.uk/media/5a806e56e5274a2e8ab501ae/eFOSS_surveillance_tables_for_Web.pdf` (2015).

Rae, B. R., J. Yang, J. McKendry, Z. Gong, D. Renshaw, J. M. Girkin, E. Gu, M. D. Dawson, and R. K. Henderson. A vertically integrated CMOS microsystem for time-resolved fluorescence analysis. *IEEE Transactions on Biomedical Circuits and Systems*, **4(6)**, pp. 437–444 (2010).

Randtke, S. J. and M. B. Horsley. *Water treatment plant design*. McGraw-Hill (2012).

Raza, S., M. Folga, M. Łoś, Z. Foltynowicz, and J. Paczesny. The effect of zero-Valent iron nanoparticles (nZVI) on bacteriophages. *Viruses*, **14(5)**, p. 867 (2022).

Redford, G. I. and R. M. Clegg. Polar plot representation for frequency-domain analysis of fluorescence lifetimes. *Journal of fluorescence*, **15(5)**, p. 805 (2005).

Reinhart, G. D., P. Marzola, D. M. Jameson, and E. Gratton. A method for on-line background subtraction in frequency domain fluorometry. *Journal of fluorescence*, **1(3)**, pp. 153–162 (1991).

Roding, M., S. J. Bradley, M. Nydén, and T. Nann. Fluorescence lifetime analysis of graphene quantum dots. *The Journal of Physical Chemistry C*, **118(51)**, pp. 30282–30290 (2014).

Rosenthal, M., M. Taylor, K. S. Anderson III, and K. K. Carter. Gastroenteritis Associated With Rafting the Middle Fork of the Salmon River—Idaho, 2013. *Journal of Environmental Health*, **80(1)**, pp. 14–21 (2017).

Rossi, L., N. Chèvre, R. Fankhauser, J. Margot, R. Curdy, M. Babut, and D. A. Barry. Sediment contamination assessment in urban areas based on total suspended solids. *Water research*, **47(1)**, pp. 339–350 (2013).

Rossle, N. F. and B. Latif. Cryptosporidiosis as threatening health problem: a review. *Asian Pacific journal of tropical biomedicine*, **3(11)**, pp. 916–924 (2013).

Saito Nogueira, M., A. Cosci, R. G. Teixeira Rosa, A. G. Salvio, S. Pratavieira, and C. Kurachi. Portable fluorescence lifetime spectroscopy system for in-situ interrogation of biological tissues. *Journal of Biomedical Optics*, **22(12)**, pp. 121608–121608 (2017).

San Park, T. and J.-Y. Yoon. Smartphone detection of *Escherichia coli* from field water samples on paper microfluidics. *IEEE Sensors Journal*, **15(3)**, pp. 1902–1907 (2014).

Saritha, V., N. Srinivas, and N. Srikanth Vuppala. Analysis and optimization of coagulation and flocculation process. *Applied Water Science*, **7**, pp. 451–460 (2017).

Scarcella, C., A. Tosi, F. Villa, S. Tisa, and F. Zappa. Low-noise low-jitter 32-pixels CMOS single-photon avalanche diodes array for single-photon counting from 300 nm to 900 nm. *Review of Scientific Instruments*, **84(12)** (2013).

Shah, J., A. Židonis, and G. Aggidis. State of the art of UV water treatment technologies and hydraulic design optimisation using computational modelling. *Journal of Water Process Engineering*, **41**, p. 102099 (2021).

Simmons, O. D., M. D. Sobsey, C. D. Heaney, F. W. Schaefer, and D. S. Francy. Concentration and detection of *Cryptosporidium oocysts* in surface water samples by method 1622 using ultrafiltration and capsule filtration. *Appl. Environ. Microbiol.*, **67(3)**, pp. 1123–1127 (2001).

Singh, P., R. Gupta, M. Sinha, R. Kumar, and V. Bhalla. MoS 2 based digital response platform for aptamer based fluorescent detection of pathogens. *Microchimica Acta*, **183**, pp. 1501–1506 (2016).

Smith, H. V. and R. A. Nichols. *Cryptosporidium*: detection in water and food. *Experimental parasitology*, **124(1)**, pp. 61–79 (2010).

Soleimanpour Makuei, M., F. Ketabchi, and N. Peleato. Impact of water characteristics on UV disinfection of unfiltered water. *Water Quality Research Journal*, **57(4)**, pp. 247–261 (2022).

Štefl, M., N. G. James, J. A. Ross, and D. M. Jameson. Applications of phasors to in vitro time-resolved fluorescence measurements. *Analytical biochemistry*, **410(1)**, pp. 62–69 (2011).

Subhash, H. M. and R. K. Wang. Optical coherence tomography: technical aspects. *Biomedical Optical Imaging Technologies: Design and Applications*, pp. 163–212 (2013).

Sun, H. *Laser diode beam basics, manipulations and characterizations*. Springer Science & Business Media (2012).

Szmacinski, H. and J. R. Lakowicz. Fluorescence lifetime-based sensing and imaging. *Sensors and Actuators B: Chemical*, **29(1)**, pp. 16–24 (1995). Proceedings of the 2nd European Conference on Optical Chemical Sensors and Biosensors.

Szmacinski, H. and J. R. Lakowicz. Frequency-domain lifetime measurements and sensing in highly scattering media. *Sensors and Actuators B: Chemical*, **30(3)**, pp. 207–215 (1996).

Tan, L., W. Du, Y. Zhang, L.-J. Tang, J.-H. Jiang, and R.-Q. Yu. Rayleigh scattering correction for fluorescence spectroscopy analysis. *Chemometrics and Intelligent Laboratory Systems*, **203**, p. 104028 (2020).

Templeton, M., R. Hofmann, and R. Andrews. UV inactivation of humic-coated bacteriophages MS2 and T4 in water. *Journal of Environmental Engineering and Science*, **5(6)**, pp. 537–543 (2006).

Thompson, R. B., B. P. Maliwal, and C. A. Fierke. Selectivity and sensitivity of fluorescence lifetime-based metal ion biosensing using a carbonic anhydrase transducer. *Analytical Biochemistry*, **267(1)**, pp. 185–195 (1999).

Thorlabs. *Beamsplitter Guide*. Thorlabs (1999-2024). Accessed: 2024-25-09.

Tilton, L., G. Das, X. Yang, N. Wisuthiphaet, I. M. Kennedy, and N. Nitin. Nanophotonic device in combination with bacteriophages for enhancing detection sensitivity of *Escherichia coli* in simulated wash water. *Analytical Letters*, **52(14)**, pp. 2203–2213 (2019).

USEPA. Long Term 2 Enhanced Surface Water Treatment Rule. Standard, U.S. Environmental Protection Agency, Washington, DC 20460-0001 (2010).

Varga, G. The structure of kaolinite and metakaolinite. *Epitoanyag*, **59(1)**, pp. 6–9 (2007).

Vikesland, P. J. and K. R. Wigginton. Nanomaterial enabled biosensors for pathogen monitoring-a review. *Environmental science & technology*, **44(10)**, pp. 3656–3669 (2010a).

Vikesland, P. J. and K. R. Wigginton. Nanomaterial enabled biosensors for pathogen monitoring-a review. *Environmental science & technology*, **44(10)**, pp. 3656–3669 (2010b).

Villa, F., R. Lussana, D. Bronzi, S. Tisa, A. Tosi, F. Zappa, A. Dalla Mora, D. Contini, D. Durini, S. Weyers, *et al.* CMOS imager with 1024 SPADs and TDCs for single-photon timing and 3-D time-of-flight. *IEEE journal of selected topics in quantum electronics*, **20(6)**, pp. 364–373 (2014).

Villa, F., B. Markovic, S. Bellisai, D. Bronzi, A. Tosi, F. Zappa, S. Tisa, D. Durini, S. Weyers, U. Paschen, *et al.* SPAD smart pixel for time-of-flight and time-correlated single-photon counting measurements. *IEEE Photonics Journal*, **4(3)**, pp. 795–804 (2012).

Vishwanath, K., B. Pogue, and M.-A. Mycek. Quantitative fluorescence lifetime spectroscopy in turbid media: comparison of theoretical, experimental and computational methods. *Physics in Medicine & Biology*, **47(18)**, p. 3387 (2002).

Vitta, P., I. Reklaitis, and A. Žukauskas. Frequency-domain fluorometry in the presence of high in-phase background. *Measurement Science and Technology*, **23(3)**, p. 035502 (2012).

Vryzas, Z. Pesticide fate in soil-sediment-water environment in relation to contamination preventing actions. *Current Opinion in Environmental Science & Health*, **4**, pp. 5–9 (2018).

Wagner, E. G. and R. G. Pinheiro. Upgrading Water Treatment Plants. `https://www.ircwash.org/sites/default/files/Wagner-2001-Upgrading.pdf` (2001). Accessed: 16.01.2024.

Wang, H., Y. Qi, T. Mountziaris, and C. D. Salthouse. A portable time-domain LED fluorimeter for nanosecond fluorescence lifetime measurements. *Review of Scientific Instruments*, **85(5)**, p. 055003 (2014).

Wang, Y. and A. Hu. Carbon quantum dots: synthesis, properties and applications. *Journal of Materials Chemistry C*, **2(34)**, pp. 6921–6939 (2014).

WaterTreatment. An Introduction to Drinking Water Contaminants, Treatment and Management 2008. Standard, Ministry for the Environment, Wlellington, New Zealand (2008).

Wei, L., W. Yan, and D. Ho. Recent advances in fluorescence lifetime analytical microsystems: Contact optics and CMOS time-resolved electronics. *Sensors*, **17(12)**, p. 2800 (2017).

Wenbo, W., H. Dengxin, L. Jing, and L. Meixia. Laser induced chlorophyll fluorescence lifetime measurement and characteristic analysis for plant drought-stress. In: *2013 IEEE 11th International Conference on Electronic Measurement & Instruments*, volume 2, pp. 574–578. IEEE (2013).

Wöll, D. and C. Flors. Super-resolution Fluorescence Imaging for Materials Science. *Small Methods*, **1(10)**, p. 1700191 (2017).

Wong, J. I., L. Wang, Y. Shi, T. Palacios, J. Kong, X. Dong, and H. Ying Yang. Real-time, sensitive electrical detection of *Cryptosporidium parvum* oocysts based on chemical vapor deposition-grown graphene. *Applied Physics Letters*, **104(6)**, p. 063705 (2014).

Wu, H.-M., T.-A. Lee, P.-L. Ko, W.-H. Liao, T.-H. Hsieh, and Y.-C. Tung. Widefield frequency domain fluorescence lifetime imaging microscopy (FD-FLIM) for accurate measurement of oxygen gradients within microfluidic devices. *Analyst*, **144(11)**, pp. 3494–3504 (2019).

Yahav, G., S. Gershanov, M. Salmon-Divon, H. Ben-Zvi, G. Mircus, N. Goldenberg-Cohen, and D. Fixler. Pathogen detection using frequency domain fluorescent lifetime measurements. *IEEE Transactions on Biomedical Engineering*, **65(12)**, pp. 2731–2741 (2018).

Yu, C., X. Li, F. Zeng, F. Zheng, and S. Wu. Carbon-dot-based ratiometric fluorescent sensor for detecting hydrogen sulfide in aqueous media and inside live cells. *Chemical Communications*, **49(4)**, p. 403 – 405 (2013). Cited by: 424.

Zhang, H., X. Zhang, S. Zhang, B. Wei, Q. Jiang, and X. Yu. Detecting *Cryptosporidium* parvum and Giardia lamblia by coagulation concentration and real-time PCR quantification. *Frontiers of Environmental Science & Engineering*, **7(1)**, pp. 49–54 (2013).

Zhang, J. and S.-H. Yu. Carbon dots: large-scale synthesis, sensing and bioimaging. *Materials Today*, **19(7)**, pp. 382–393 (2016).

Zhang, X., M. Li, B. Zhang, K. Chen, and K. He. Development of a Sandwich ELISA for EHEC O157: H7 Intimin γ1. *PLoS One*, **11(9)**, p. e0162274 (2016).

Appendix A

MATLAB Scripts

A.1 Data acquisition

This section is corresponding to the Chapter 4 that presented the data acquisition program to extract data from the oscilloscope in real time.

A.1.1 Communicate with instruments and data extraction

```
1
2  % checking and creating an object for function generator
3  fg = instrfind('Type', 'gpib', 'BoardIndex', 7, 'PrimaryAddress', 20, 'Tag', '')
       ;
4  % Create the GPIB object if it does not exist
5  % otherwise use the object that was found.
6  if isempty(fg)
7      fg = gpib('KEYSIGHT', 7, 20);
8  else
9      fclose(fg);
10     fg = fg(1);
11 end
12
13 % checking and creating an object for oscilloscope
14 %create scope(oscilloscope) object
15 scope= instrfind('Type','visa-usb', RsrcName','USB0::0x2A8D::0x9045::MY58150122
       ::0::INSTR','Tag','');
16 if isempty(scope)
17 scope = visa('KEYSIGHT', 'USB0::0x2A8D::0x9045::MY58150122::0::INSTR');
18 else
19     fclose(scope);
20     scope = scope(1);
21 end
22 set(scope, 'InputBufferSize', 250000);
23
24 % Configure instrument object, scope
25
26 set(scope, 'OutputBufferSize', 20000);
27 fopen(fg);
28 fopen(scope);
29 for i =1:length(frq)
```

```
    folder = sprintf('ref%i', i);
    frq =[10 20 30 40 50 60]*1e6;
    for i =1:6
   Lfrq = frq(i);
      [Vin,Rfrq,shape] = writereadfg(fg,3 ,Lfrq);
   pause(3);
   Ndir = num2str(Lfrq/1e6);
   mkdir(folder, Ndir)
   Mpath = folder
   Dpat = sprintf('%d',Lfrq/1e6)
   mypath = [Mpath filesep Dpat]
    for j=1:20
    [time,Volts2]=readscope(scope,2);
    [time2,Volts3]=readscope(scope,3);
    if (time == time2)
        time = time2 ;
    else
        sprintf("time error")
    end
array = [time,Volts2,Volts3];
pat = sprintf('%d.txt',j);
 fullpath = [mypath filesep pat]
 fid = fopen(fullpath,'w+');
    for j =1: length(array)
    fprintf(fid,'%g ', array(j,1:end-1));
    fprintf(fid,'%g\n', array(j,end));
    end
fclose(fid);
end
end
end

fclose(fg);
fclose(scope);
}
```

A.2 Phase measurement

This program is used to calculate the phase measurement for a sample measured.

```
 a = ['C:'] % path of the data folder
freqs=[10 20 30 40 50 60];
    for j =1:6
    f = freqs(j);
    dd = [a filesep num2str(f)];
    files = dir(dd);
    fprintf('Freq %d MHz:\n', f);

    k = 0;
    for dk = 1:length(files)
        if files(dk).name(1) == '.';
            continue;
    end
    k = k + 1;
        ff = [dd filesep files(dk).name];
```

```
    y = analone(ff, f,0,5000);
    mag(k,:) = abs(y);
        phase(k,:) = angle(y);
        fprintf('   %2d: Analysed %s with phase %g %g %g.\n', k, ff, ...
        phase(k,:));
    uwphase(k,:) = phase(k,:);

%%%%phase unwrapping
if k>1
  for i =1:2
  ephase(k,i) = (uwphase(k-1,i) - phase(k,i))/(2*pi);
    if phase(k,i)<0
    ephase(k,i) = phase(k,i) - ephase(k,i);
    elseif phase(k,i)>0
        ephase(k,i) = phase(k,i) + ephase(k,i);
    end
    if ephase(k,i) > pi +(pi/10)
    uwphase(k,i) = phase(k,i)- (2*pi);
    elseif ephase(k,i) < -pi -(pi/10)
    uwphase(k,i) = phase(k,i)+ (2*pi);
    end
 end

end
  end
 y = sign(uwphase);
 for i=1:2
     for k = 1:9
        if(y(k+1,i) == y(1,i))
        uwphase(k,i) = uwphase(k,i);
        elseif (y(k+1,i) > y(1,i))
        uwphase(k+1,i) = uwphase(k+1,i)- (2*pi);
        else
         uwphase(k,i) = uwphase(k,i)+(2*pi);
        end
        end
        end

    difphase(:,j) = uwphase(:,2)-uwphase(:,1);

    mmag(j,:) = mean(mag);
    smag(j,:) = std(mag);
    mphase(j,:) = mean(uwphase);
    sphase(j,:) = std(uwphase);

    if (mphase(j,2) - mphase(j,1)) > pi
        mphase(j,2) = mphase(j,2) - 2 * pi;
     if (mphase(j,2) - mphase(j,1)) < -pi
        mphase(j,2) = mphase(j,2) + 2 * pi;
    end
    end
   dmphase(j,:) = mphase(j,1)- mphase(j,2);
   dsmphase(j,:) = hypot(sphase(j,2),sphase(j,1));
   acqsam = dk -2;
end
```

A.3 Multi-frequency analysis

Following program is used to measure the fluorescence lifetime and contamination ratio using multi frequency non-linear analysis.

```
function[y, beta,ci] =nonlinearfit(c,sd_c)
f =[10 20 30 40 50 60];
w = 2*pi*f*1e6;
%%%%%%%%%%%%%%%  non-linear fit %%%%%%%%%%%%%%%%%%%%%%%
beta0 =[0 4.1e-9];
myfun = @(A,w)(atan(sin(atan(w.*A(2))./(A(1)+cos(atan(w.*A(2)))))));
[beta,R,J] = nlinfit(w,c,myfun,beta0);
ci = nlparci(beta,R,'jacobian',J);
%%%%%%%%%%%%%% re-calculating using estimaed values %%%%%%%%%%%%%%%%%%%%%
B= beta(1);
LT=beta(2);

y = atan(sin(atan(w.*beta(2))./(beta(1)+cos(atan(w.*beta(2))))));
```